PRODUCTION OF HETEROCYST GLYCOLIPIDS AND GLYCEROL DIALKYL GLYCEROL TETRAETHER MEMBRANE LIPIDS IN THE WATER COLUMN OF A STRATIFIED TROPICAL LAKE, MALAWI, AFRICA

by

Dervla Meegan Kumar

B.Sc. Geological Sciences, SUNY Binghamton, 2013

Submitted to the Graduate Faculty of the

Kenneth P. Dietrich School of Arts and Sciences in partial fulfillment

of the requirements for the degree of

Master of Science

University of Pittsburgh

2017

UNIVERSITY OF PITTSBURGH

KENNETH P. DIETIRCH SCHOOL OF ARTS AND SCIENCES

This thesis was presented

by

Dervla Meegan Kumar

It was defended on

July 6, 2017

and approved by

Dr. Daniel J. Bain, Ph.D., Assistant Professor

Dr. Emily M. Elliott, Ph.D., Associate Professor

Committee Chair: Dr. Josef P. Werne, Ph.D., Professor

ABSTRACT

PRODUCTION OF HETEROCYST GLYCOLIPIDS AND GLYCEROL DIALKYL GLYCEROL TETRAETHER MEMBRANE LIPIDS IN THE WATER COLUMN OF A STRATIFIED TROPICAL LAKE, MALAWI, AFRICA

Dervla Meegan Kumar, M.Sc.

University of Pittsburgh, 2017

Temperature is a critical component of paleoenvironmental reconstructions, yet it is notoriously difficult to measure in terrestrial archives. Presented here is an investigation of the sources and distributions of archaeal and bacterial glycerol dialkyl glycerol tetraethers (GDGTs) and cyanobacterial heterocyst glycolipids (HGs) in Lake Malawi. The study aims to evaluate the potential for these lipids to function as paleotemperature proxies in tropical lacustrine environments. GDGTs and HGs were extracted from settling particulate matter (SPM) collected at bi-monthly intervals from 2011 – 2013. Sediment traps used to collect SPM were moored in both the north and south basins of Lake Malawi in order to evaluate spatial trends, in addition to temporal trends, in lipid production and export across the lake.

Distributions of isoprenoid GDGTs indicate that Thaumarchaeota are the dominant GDGT-producing archaea in the surface waters of Lake Malawi. However, TEX_{86}-based temperatures do not track lake surface temperatures at either the northern or southern sediment trap locations. TEX_{86} in the north basin instead reflects surface water temperatures at the time of maximum Thaumarchaeota activity, while TEX_{86} in the south basin records patterns in seasonal upwelling that possibly drive shifts in the membrane composition of Thaumarchaeota or in the dominant planktonic archaeal community. Branched GDGTs are likely produced by distinct

groups of bacteria within the water column, complicating the interpretation of temperatures reconstructed from their distributions. The inability of available branched GDGT calibrations to produce reasonable temperatures underscores the need for comprehensive studies of autochthonous branched GDGT production in lakes. Bulk sedimentation is the primary driver of branched and isoprenoid GDGT export in the metalimnion.

HGs are present throughout the time-series, but maximum fluxes occur in December. HGs in SPM are sourced from actively living cyanobacteria populations, indicating rapid export of the lipids through the water column. Temperatures reconstructed with published HG-based indices do not match the seasonal variability in surface temperatures, however the fractional abundances of HG diols with C_{26} and C_{28} side chains do appear related to lake temperatures in this system. The production of C_{28} HG keto-ols may also be associated with heterocyst differentiation.

ACKNOWLEDGEMENTS

The Lake Malawi sediment trap study described in this thesis is the product of many individuals' contributions. I could not have carried it to completion without those who helped with the planning and execution of the project in its early stages nor without those who guided me along the way. I want to thank Maxon Ngochera, Tom Johnson, Stephanie Guildford, and Robert Hecky for their contributions in organizing the fieldwork, in addition to Melissa Berke, April Abbott, Messias Maccuiane, Martijn Woltering, and the captain and crew of the *R.V. Ndumduma* for their help with sample collection. I also want to give a special thank you to Ellen Hopmans, Denise Dorhout, Jort Ossebaar, Julia Halbur, and Elisabeth Svensson for their assistance with the lipid analyses. Jay Austin and his group contributed the temperature data, an essential component of the project. This work was funded by grants from the National Geographic Society Committee for Research and Exploration (#8098-06) and the University of Minnesota Grant-in-Aid of Research (#20607) to Josef Werne, and the University of Minnesota Office of International Programs to Stephanie Guildford, Josef Werne, and others. The Geological Society of America, the National Science Foundation, the University of Pittsburgh, and the European Association of Organic Geochemists provided me with additional support that enabled me to conduct this work independently.

It was an immense pleasure to work on this project at both the University of Pittsburgh and the Royal NIOZ. I'm grateful for all the wonderful scientists I have met through these experiences, and for the many adventures I've been fortunate enough to partake in throughout my Master's studies. I owe much appreciation to: my committee, for their help in putting this thesis together; my advisor, Dr. Josef Werne, who provided me with this opportunity and introduced me to organic geochemistry; and to a long-time mentor, Dr. Marcus Bursik, who taught me how to be a real geologist and inspired me to pursue a career in the field. Most of all, thank you to my lab mates and friends, Molly O'Beirne, Troy Ferland, and Nick Weidhaas IV, who shared this unique journey with me. I know our friendship will extend far beyond the walls of the SRCC.

TABLE OF CONTENTS

LIST OF TABLES

LIST OF FIGURES

LIST OF ACRONYMS

APCI	Atmospheric Pressure Chemical Ionization
BDE	Blight-Dyer Extract
BIT	Branched Isoprenoid Tetraether Index
brGDGT	Branched Glycerol Dialkyl Glycerol Tetraether
CB	Central Basin
CBT	Cyclization of Branched Tetraethers Index
CL	Core Lipid
DCM	Dichloromethane
DH	Dihexose
ESI	Electrospray Ionization
FA	Fractional Abundance
GDGT	Glycerol Dialkyl Glycerol Tetraether
HDI	Heterocyst Diol Index
HG	Heterocyst Glycolipid
HPH	Hexose-Phosphohexose
HTI	Heterocyst Triol Index
IPA	Isopropanol
IPL	Intact Polar Lipid
isoGDGT	Isoprenoid Glycerol Dialkyl Glycerol Tetraether
ITCZ	Intertropical Convergence Zone
LC_{CN}	Liquid Chromatography with a Cyano column
LC_{Si}	Liquid Chromatography with 2 Silica columns
LST	Lake Surface Temperature
MAT	Mean Annual Temperature

MBT	Methylation of Branched Tetraethers Index
MeOH	Methanol
MH	Monohexose
MS	Mass Spectrometry
NB	North Basin
NIOZ	Royal Netherlands Institute for Sea Research
NST	North Sediment Trap
OM	Organic Matter
PB	Phosphate Buffer
POM	Particulate Organic Matter
RMSE	Root Mean Square Error
RRF	Relative Response Factor
SB	South Basin
SIM	Scanning Ion Mode
SPM	Settling Particulate Matter
SRM	Selective Reaction Mode
SST-D	Deep South Sediment Trap
SST-S	Shallow South Sediment Trap
TEX_{86}	Tetraether Index with 86 carbon atoms
TOC	Total Organic Carbon
TON	Total Organic Nitrogen
UHPLC	Ultra-High Pressure Liquid Chromatography
UMD	University of Minnesota Duluth

1. INTRODUCTION

1.1 CONSTRUCTING TERRESTRIAL PALEOTEMPERATURE RECORDS

Current strategies for mitigating anthropogenic climate change focus heavily on limiting warming caused by greenhouse gas emissions to a global average of 1.5°C. Temperature is simple to measure with modern instrumentation, thus such a benchmark provides a tangible goal for world leaders. Though the concept of a 1.5°C increase in global average temperature is easy to digest and to communicate, the effects of anthropogenic climate change will be inherently local, and the extent of regional responses to an increase in global temperatures of this magnitude is still poorly understood (Blöschl, 2006; Blöschl et al., 2007; Verdon-Kidd and Kiem, 2010). Under the RCP 4.5 scenario, which involves an increase in radiative forcing due to greenhouse gas concentrations that is equivalent to a 2.4°C temperature anomaly (Clarke et al., 2007; Rogelj et al., 2012; Smith and Wigley 2006; Wise et al. 2009), global climate models (GCM) project widespread expansions of drought in South America, Central America, much of North America, and Europe, while some regions, including Siberia, Northern Canada/Alaska, India, Indonesia, and East Africa, may potentially become wetter (Dai, 2012). The heterogeneity of GCM predictions underscores the need for a deeper understanding of regional climate change. These models are limited in their inability to resolve climatic details, such as the timing and duration of seasonal precipitation or shifts in vegetation community composition, that are critical to natural resource management (Oscar Kisaka et al. ,2015; Yang et al., 2015).

Paleoclimate records reconstruct ecological changes a region has actually experienced under variable climatic regimes, thus providing a valuable perspective for understanding potential future changes. Shifts in precipitation/evaporation and vegetation can be measured using biological and chemical indicators such as pollen assemblages, calcium carbonate oxygen isotopic composition, or leaf wax carbon isotopic composition. Contemporaneous temperature

reconstructions provide context for these shifts that will enable us to more accurately anticipate how modern systems will respond to anthropogenic warming. Moreover, the comparison of local paleotemperature records extracted from terrestrial archives and global paleotemperature records generated from marine archives can create a picture of the spatial variability of continental temperature change relative to global averages. Both of these tasks have been difficult to execute, however, due to the limited number of terrestrial paleotemperature records, especially in tropical regions. Lake sediments are ideal archives for terrestrial paleoclimate reconstructions due to their geographic distribution, ability to integrate watershed-scale signals, high sediment accumulation rates that allow for high-resolution analyses, and potential for long-term temporal extent. The lack of quantitative paleotemperature proxies that are applicable to lacustrine environments, however, is limiting the development of these archives for paleoclimate analysis.

The organic geochemical community is striving to fill this knowledge gap by evaluating the ability of various microbial lipids to serve as paleotemperature proxies in lake sediment archives (e.g. D'Andrea and Huang, 2005; Blaga et al., 2009; Tierney et al., 2010; Rampen et al., 2014; Bauersachs et al., 2015). Microorganisms adapt quickly to changes in their growth habitat to optimize the biochemical composition of their membranes -- which operate as barriers to limit solute and gas entry into the cell -- to ambient environmental conditions. Membrane lipids are relatively recalcitrant and survive degradation in the water column and in surface sediments following cell death, allowing for their accumulation in sediments, in which they can be preserved for millions of years (Brassell 1992). Lipids associated with specific groups of organisms are called biomarkers. Biomarkers are ideal for paleoclimate studies as variability in the environmental relationship due to differing sources over time can be discounted. By analyzing changes in the structures or composition of biomarkers preserved in lake sediment archives, it is then possible to produce a record of the biotic response to environmental factors. Investigating the production of biomarkers in modern environments where climate variables are known enables us to determine the validity of the biomarker-based proxy for recording environmental change, in addition to providing insights into potential nuances of the proxy, such as seasonal biases, that aids in interpretation of the record. Three classes of membrane lipids that have shown particular promise in recording lake surface water temperatures are isoprenoid glycerol dialkyl glycerol tetraethers (isoGDGTs), branched glycerol dialkyl glycerol tetraethers (brGDGTs), and heterocyst glycolipids (HGs), and will be discussed in detail below.

1.2 GDGT-MEMBRANE LIPIDS & GDGT-BASED PROXIES

1.2.1 IsoGDGTs: Sources and structural diversity

To fully understand the genesis of isoGDGT-based proxies, it is critical to examine how knowledge of their archaeal source has developed over time. The first organisms identified within the Archaea domain (previously Archaebacteria) were restricted to extremophilic groups of methanogens (e.g. Balch et al., 1979; Fox et al., 1980; Fox et al., 1977) halophiles (Magrum et al., 1978), thermoacidophiles (e.g. Smith et al., 1973), and sulfate-reducing symbionts (e.g. (Langworthy et al., 1974). The domain was organized into two phylum-level subgroups – Crenarchaeota, to which the hyperthermophiles belonged, and Euryarchaeota, which encompasses the remaining groups (Woese et al., 1990). Later examinations of environmental 16s rRNA material revealed that archaea are actually widespread in the pelagic ocean (DeLong, 1992; Fuhrman et al., 1993; Karner et al., 2000), and even in terrestrial environments such as lakes and soils (e.g. Hershberger et al., 1996; Keough et al., 2003). Comparative 16s rRNA analyses placed the mesophilic archaea formed phylogenetic clusters into two groups, the first closely related to Crenarchaeota, deemed Group I, aka mesophilic Crenarchaeota, (Könneke et al., 2005), and the second was related to Euryarchaeota, Group II (DeLong 1992; López-García et al., 2004). While Group II archaea represent a distinct branch within the Euryarchaeota lineage, Brochier-Armanet et al. (2008) importantly established that Group I archaea branched from their hyperthermophilic Crenarchaeota ancestors much deeper in the evolutionary tree, and thus suggested the group's reclassification into the unique phylum Thaumarchaeota. A key trait that is common amongst Thaumarchaeota is their ability to oxidize ammonia to nitrite, and, in fact, Thaumarchaeota are the only archaea capable of aerobic nitrification in archaea (Könneke et al., 2005). For water-dwelling Thaumarchaeota, this may explain their preferred depth of habitat near the oxic-anoxic boundary, which has been observed in both marine (Ingalls et al., 2006; Karner et al., 2001; Massana et al, 1997; Wuchter et al., 2004) and lacustrine water columns (Llirós et al., 2010; Schouten et al., 2012; Sinninghe Damsté et al., 2009; Woltering et al., 2012).

Analyses of archaeal lipids have added to our functional understanding of the biology and ecology of the domain. Carbon isotopic values of some Archaean rocks suggests that Archaea

have inhabited Earth since at least 2.7 Ga (Hayes, 1994). Lipid concentrations and distributions can serve as taxonomic indicators when genetic material is not analyzed or not available, such as in samples from deep geologic time (Buckles et al., 2013; Gibson et al., 2013; Pitcher et al., 2009; De Rosa et al., 1986; Schouten et al., 2000). Moreover, as the membrane serves as the cell's buffer and protection from its surroundings, the molecular structure of membrane lipids can also provide excellent insights into the source organisms' environment. The unique structural characteristics of archaeal lipids enabled them to inhabit the extreme environments of early Earth. Bipolar, membrane-spanning structures with di- and tetraether glycerol bonds are more stable than the acyl ester lipids characteristic from bacteria (De Rosa et al., 1986; P. F. Smith et al., 1973; Woese et al., 1978). Furthermore, archaeal lipids consist of isoprenoid chains rather than fatty acids; the methyl branches of isoprene units can be cyclized into cyclopentane rings for added membrane stability for organisms that occupy high temperature or high salinity environments (Mathai et al., 2001; De Rosa et al., 1980). These traits are the same that allow modern archaea to thrive in harsh settings such as hot springs, salt flats, and hydrothermal vents. Despite inhabiting less extreme environments, mesophilic archaea produce membrane lipids that are very similar to their ancestors. Some notable differences include that mesophilic archaeal lipids do not have quite as many rings and have additional kinks, such as larger cyclohexane rings, that allow for a more fluid membrane that is more suitable to normal environments (Schouten et al., 1998; Sinninghe Damsté et al., 2002).

Some of the most common lipids in both extremophilic and mesophilic archaea are GDGTs. Like other archaeal lipids, archaeal GDGTs are constructed from isoprene units and are thus called isoprenoid GDGTs (isoGDGTs, Figure 1.1). Isoprene is constructed into two C_{40} biphytanyl chains that are bound by four glycerol ether linkages (Schouten et al., 1998). Cyclization of methyl branches along the biphytanyl chain can form up to eight cyclopentane moieties (Hopmans et al., 2000), 0 to 4 cyclopentane rings most common within the mesophilic archaea. GDGT-0, also known as caldarchaeol, has no cyclization. Crenarchaeol is a GDGT exclusively produced by Thaumarchaeota. Crenarchaeol has four cyclopentane rings and one cyclohexyl ring, while its regioisomer has an identical structure but a parallel configuration (Sinninghe Damsté et al., 2002).

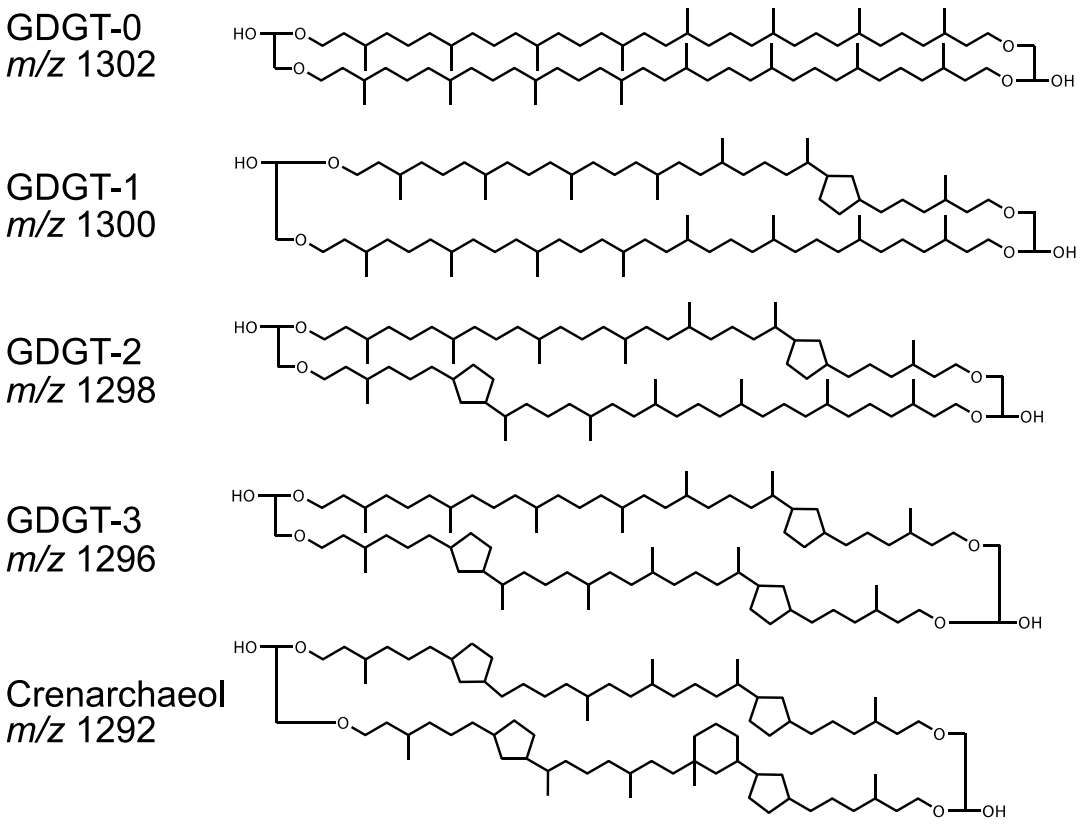

Figure 1.1: Molecular structures of isoGDGT membrane lipids, after Hopmans et al. (2000). Cren' is the regio isomer of crenarchaeol.

1.2.2 The TEX_{86} Proxy

The relationship between isoGDGT cyclization and temperature was first observed in thermophilic archaea (De Rosa et al., 1980). Schouten et al. (2002) sought to determine if Thaumarchaeota adjust the structures of their membrane lipids in response to growth temperature in a similar manner as their thermophilic ancestors despite inhabiting mesophilic environments. In their analysis of isoGDGTs preserved in marine surface sediments, the authors did in fact find a significant correlation between isoGDGT cyclization and sea surface temperatures. In particular, the authors found the best fit with sea surface temperature was based on the relative abundances of GDGTs with 1 – 3 rings and the regio-isomer of crenarchaeol, which they quantified in the TEX_{86} ratio (TetraEther indeX of tetraethers with 86 carbon atoms,).

Incubation experiments conducted by Wuchter et al. (2004) and Schouten et al. (2007) confirmed the direct relationship between growth temperature and GDGT cyclization in Thaumarchaeota. TEX_{86}-paleotemperature reconstructions from marine sediments have since become widespread due to the fairly consistent relationship between the proxy and sea surface temperature throughout the oceans (Kim et al. 2010b; Schouten et al., 2013 and references therin).

Application of the proxy in lake sediment archives, however, has been unreliable. Powers et al. (2004) first explored the possibility and found that the isoGDGTs needed for calculation of TEX_{86} were in sufficient abundance in the four large lakes they sampled. Attempts to expand upon this by Blaga et al. (2009) and Powers et al. (2005, 2010) ultimately revealed the limitations in applying the proxy to sedimentary lacustrine archives. These studies sampled both large and small lakes, and found that in the small lakes TEX_{86} values were significantly influenced by soil-derived isoGDGTs, thus the lake surface temperature relationship did not hold. The proxy has been successfully applied in very large lakes, however, including Lake Malawi (Johnson et al., 2016; Powers et al., 2005; Woltering et al., 2011) and several others located in East Africa, such as Lake Tanganyika (Tierney et al., 2008), Lake Challa (Sinninghe Damsté et al., 2012), Lake Turkana (Morrissey et al., 2017)**,** Lake Albert (Berke et al., 2014), and Lake Victoria (Berke et al., 2012).

1.2.3 BrGDGTs: Potential sources and structural diversity

BrGDGTs were first identified in terrestrial samples alongside isoGDGTs (e.g. Hopmans et al., 2004; Schouten et al., 2000). While the archaeal source of the latter was clear, the mix of archaeal and bacterial traits in brGDGTs made their origins unclear. BrGDGTs are similar to isoGDGTs in that both have membrane-spanning carbon chains with tetraether linkages to their glycerol backbones, and because the core lipids can cyclize into up to two cyclopentane moieties (Schouten et al., 2000; Weijers et al., 2006a) (Figure 1.2). The two groups of lipids differ, however, in that brGDGTs are made of non-isoprenoidal alkyl chains with only 4-6 methyl branches, hence the nomenclature branched GDGTs (Hopmans et al., 2004; Schouten et al., 2000; Weijers et al., 2006) (Figure 1.2). Though a few strains of thermophilic and sulfate-reducing bacteria have been reported to produce mono- and diether membrane lipids (Huber et al., 1996; Huber et al., 1992; Langworthy et al., 1983; Pancost et al., 2001), and one thermophilic

bacteria, *Thermotoga maritime*, has been identified as a producer of membrane spanning lipids (Carballeira et al., 1997), the combination of these features was believed to be unique to archaea until the landmark study by Weijers et al. (2006). By establishing that brGDGTs have a 1,2-di-*O*-alkyl-*sn*-glycerol stereoconfiguration rather than the 2,3-di-*O*-alykl-*sn*-glycerol stereoconfiguration characteristic of archaeal lipids, Weijers et al. (2006) confirmed earlier suggestions by Schouten et al. (2000) and Sinninghe Damsté et al. (2000) that brGDGTs are produced by bacteria despite having the aforementioned archaeal traits. The difference in stereochemistry of membrane lipids between Bacteria and Archaea is one of the primary biochemical factors that distinguish the two domains (Kates, 1977), therefore it is highly unlikely that a lipid with such a stereoconfiguration could be sourced from Archaea (Weijers et al., 2006).

Initial surveys of brGDGTs in terrestrial environments found that the lipids are ubiquitous in soils and peat, though they were in especially high abundances in the catotelm of peat bogs, leading to the suggestion that the bacterial sources of the lipids are likely widespread anaerobes (Weijers et al., 2006a; Weijers et al., 2006b). A metagenomic analysis in a northern peat bog targeted this hypothesis and found that Acidobacteria 16s rRNA abundances co-varied with brGDGT concentrations, with both increasing with depth (Weijers et al., 2009). Acidobacteria is a highly diverse phylum, with 26 identified subgroups (Barns et al., 2007), many of which include anaerobic or microaerophilic strains (Kielak et al., 2016 and references therein), and is one of the most abundant in soils worldwide (Janssen, 2006). The ubiquity of Acidobacteria thus provides a likely explanation for the presence of brGDGTs in globally distributed soils (De Jonge et al., 2014; Peterse et al., 2012; Weijers et al., 2007). Moreover, abundances of Acidobacteria 16s rRNA material has a significant negative correlation with soil pH (Jones et al., 2009; Lauber et al., 2009), a relationship identical to that found between pH and soil-derived brGDGTs (Peterse et al., 2010; Weijers et al., 2007). Alternatively, Mueller-Niggemann et al. (2016) suggested that brGDGT producers could also be denitrifiers after observing a correlation between brGDGT abundance and nirK gene abundances in a rice-paddy soil. A few strains of Acidobacteria have been shown to possess similar genes that encode for the enzymes necessary to perform nitrate/nitrite reduction (Männistö et al., 2012; Ward et al., 2009), however this ability is generally rare within the phylum (Kielak et al., 2016). Overall, ample circumstantial evidence that Acidobacteria are a primary source of brGDGTs in soils has been put forth. The first concrete evidence to support this theory came in 2011 when Sinninghe

Damsté et al. (2014) isolated GDGT Ia (Figure 1.2) from two strains of subdivision 1 Acidobacteria. Although a variety of brGDGT-precursor molecules (e.g. *iso*-diabolic acid) have also been identified in some strains of Acidobacteria (Sinninghe Damsté et al., 2011, 2014), culture studies have yet to detect the full suite of brGDGTs found in environmental samples (i.e. I – III, Figure 1.2) in living organisms.

As research on brGDGTs expanded, it became clear that these lipids are abundant across terrestrial environments, including rivers (e.g. Tierney & Russell, 2009; De Jonge et al., 2014a; Ajioka et al., 2014; De Jonge et al., 2015a; De Jonge et al., 2015b; Kim et al., 2015), lakes (e.g. Blaga et al., 2010, 2009; Pearson et al., 2011; Sun et al., 2011; Tierney et al., 2012; Schoon et al., 2013; Foster et al., 2016) , hot springs (Peterse et al., 2009a; Schouten et al., 2007b), and coastal and open marine settings (Bendle et al., 2010; Huguet et al., 2008; Kim et al., 2010a; Lincoln et al., 2013; Sanchi et al., 2014). Initially the brGDGTs in these aquatic environments were believed to be delivered through soil erosion (Hopmans et al., 2004). However, in 2009 two studies were published that compared the distributions of brGDGTs in lakes to those in the watershed soils (Sinninghe Damsté et al., 2009; Tierney and Russell, 2009). Both found that the fractional abundances of soil-brGDGTs were significantly different from those in the lake, likely indicating that there are both allochthonous and autochthonous sources of the lipids to lake sediments (Sinninghe Damsté et al., 2009; Tierney and Russell, 2009). A pattern has since emerged in low temperature aquatic environments where GDGT II and III are more abundant compared to in soils, where GDGT I is generally the dominant compound (Ajioka et al. 2014; Buckles et al. 2014; Naeher et al. 2014; Peterse et al., 2015; Sun et al. 2011; Tierney et al. 2010).

A recent advance in the instrumental analysis of brGDGTs has further illuminated the differences in brGDGT structural diversity between soils and aquatic environments. De Jonge et al. (2013) enhanced the chromatography of brGDGTs by using multiple columns with a different stationary phase to enable the separation of closely related isomers that co-eluted in older versions of the method (Liu et al., 2012). These isomers vary in the positioning of the additional methyl branches, where 6-methyl isomers have a branch located at the C6 or C6' location instead of the originally described C5 and C5' positions, which are the so-called 5-methyl structures (Figure 1.2). Subsequent studies have shown that brGDGTs in aquatic environments have a high degree of isomerization (Ding et al., 2016; De Jonge et al., 2015a; De Jonge et al. 2015b; Weber et al., 2015). An isomer of IIIa that has so far been exclusively found in aquatic environments

contains methyl branches at both the C5 and C6' position (Ding et al., 2016; Weber et al., 2015), As there is no apparent environmental advantage of positioning methyl groups at a C5 vs. C6 position, this may be a taxonomic indicator and a potential biomarker for autochthonous brGDGTs in lakes.

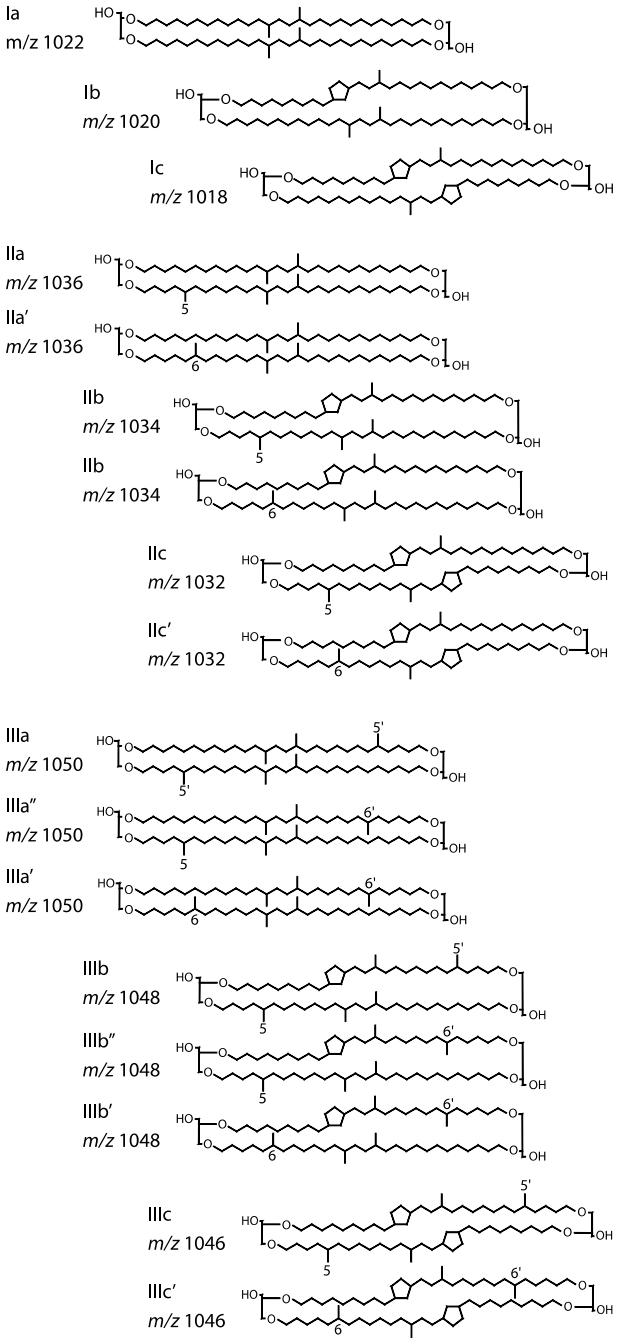

Figure 1.2: Molecular structures of brGDGT membrane lipids, after De Jonge et al. (2014) and Weber et al. (2015).

1.2.4 BrGDGT-based proxies

Weijers et al. (2007) defined the first two indices used to describe the distributions of brGDGTs in environmental samples: MBT (Methylation of Branched Tetraethers), which describes the relative abundance of tetramethylated structures in the total brGDGT pool, and CBT (Cyclization of Branched Tetraethers), which describes the proportion of cyclized structures to non-cyclized structures. Using a dataset of 134 globally distributed soils, the authors demonstrated that the CBT was influenced by soil pH, while MBT showed a strong, significant relationship with both mean annual temperature (MAT) and soil pH. Combined as the MBT/CBT proxy, the indices have been used to reconstruct MAT. Even in its refined form as the MBT'/CBT, which was calculated from an expanded dataset of 278 soils (Peterse et al., 2012), the proxy has met only variable success (e.g. Contreras et al. 2016; Schreuder et al., 2016; Fawcett et al. 2011). This is particularly true for its attempted application in paleolimnological studies. Due to the dual sources of brGDGTs to lake sediments, soil-based MBT/CBT calibrations consistently underestimate lake surface temperatures (LST) (Blaga et al., 2010; Sun et al., 2011; Tierney et al., 2010; Tierney & Russell, 2009). Regional calibrations of the proxy generated using lake surface sediments have yet to disentangle *in situ* vs. soil-derived sources, complicating interpretations of the sedimentary records where lake levels have varied drastically.

Greater insight into the sources of brGDGTs in environmental samples has come following the discovery of the 5- and 6-methyl brGDGT isomers. De Jonge et al. (2014) performed a re-analysis of the soils used in the global MBT/CBT and MBT'/CBT calibrations by Weijers et al. (2007) and Peterse et al. (2012), respectively, showed that the abundances of 5-methyl isomers is strongly controlled by temperature whereas that of 6-methyl isomers is related to soil pH. Calculating MAT using only 5-methyl fractional abundances then substantially improved the RMSE of soil-based calibrations (De Jonge et al. 2014). These results have been confirmed in other soil-based studies (Dang et al. 2016; Yang et al. 2015), but has not yet been applied to lacustrine surface sediment datasets. As such, how the isomerization of brGDGTs produced by aquatic organisms relates to environmental conditions is still not well-understood for lacustrine environments.

1.3 HGS & HG-BASED PROXIES

1.3.1 Nitrogen-fixing cyanobacteria and the heterocyst

Diazotrophic cyanobacteria have adapted to thrive in nitrogen-depleted environments because of their ability to fix atmospheric N_2. The nitrogenase enzyme mediates the process of microbial nitrogen fixation into ammonia, which is a biologically available form. Exposure to oxygen permanently inhibits the reductive power of nitrogenase, however, posing a biological challenge for phototrophic cyanobacteria (Fay & Cox, 1967). Two groups of filamentous cyanobacteria – *Nostocales* and *Stigonematales* – isolate nitrogenase from the toxic byproducts of photosynthesis by forming specialized heterocyst cells designated exclusively for nitrogen fixation (Wolk, 1973). The heterocysts have a thick wall made of an inner laminated glycolipid layer and an outer homogenous polysaccharide layer (Gambacorta et al., 1998; Nichols & Wood, 1968; Winkenbach et al., 1972). Heterocyst glycolipids (HGs) contain a sugar head group glycosidically bound to an alkyl side chain. The alkyl chain varies in length, from 26 to 32 carbons (i.e. C26 – C32), and in the number and type of functional groups, with possible combinations of 1 – 3 hydroxyl groups and 0 – 1 ketone groups (Figure 1.3; Soriente et al., 1992; Bauersachs et al., 2009a). HGs have only been detected in these cyanobacterial heterocysts and are therefore excellent biomarkers for heterocystous cyanobacteria. Distributions of specific HGs provide additional chemotaxonomic information. Marine endosymbiotic diazotrophs produce HGs with a C5 head group (Bale et al., 2015) while HGs from freshwater heterocystous cyanobacteria have a C6 sugar head (Bauersachs et al., 2009). Culture studies have further demonstrated that the degree of hydroxylation (i.e. diol vs. triol) and the number of carbon atoms in the alkyl side chain correspond to family level classifications of heterocystous cyanobacteria (Bauersachs et al. 2009b, 2011).

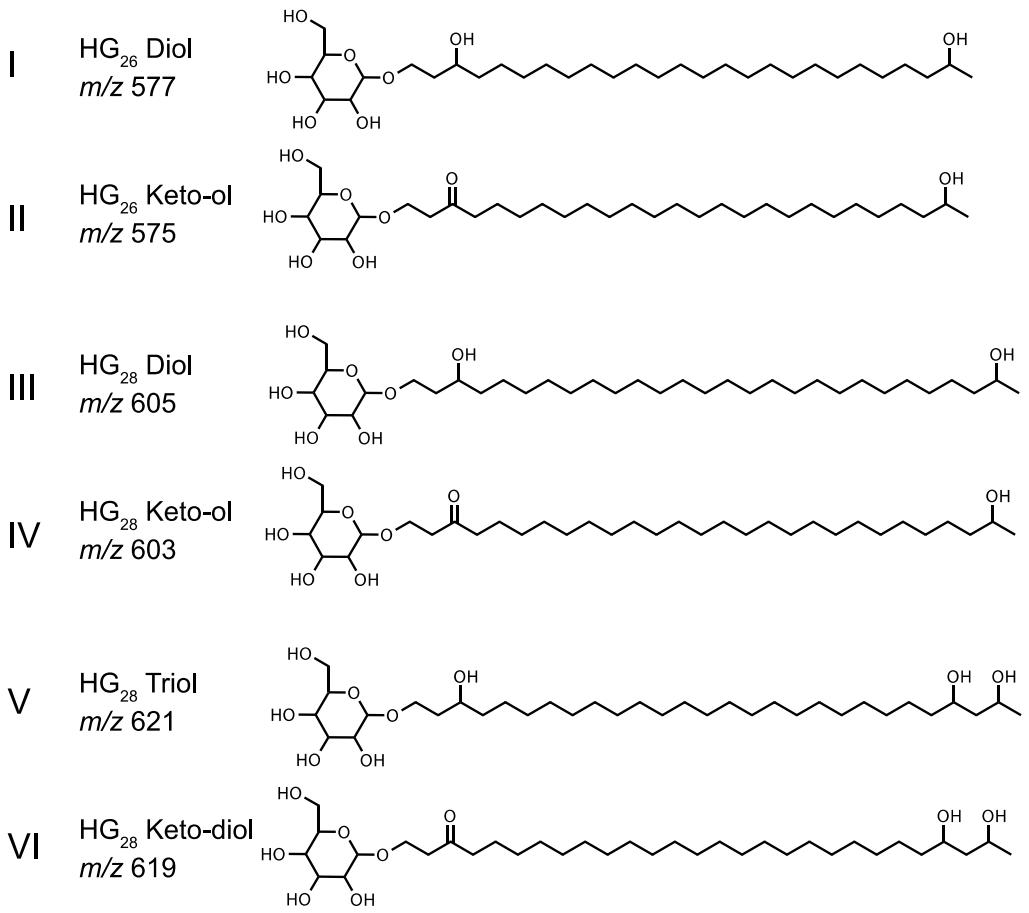

Figure 1.3: Molecular structures of HGs analyzed in Lake Malawi SPM samples. Roman numerals used to indicate HG structures follow Bauersachs et al. (2015).

1.3.2 HGs and temperature

The heterocyst wall serves a dual role as a gas diffusion barrier – to protect the sensitive nitrogenase enzyme from excess O_2 in addition to regulating the inflow of N_2 so that sufficient levels are available for conversion to NH_3. It is hypothesized that cyanobacteria adjust the composition of the glycolipid layer to maintain the optimum ratio of incoming O_2:N_2 in response to changing environmental conditions (Kangatharalingam et al., 1992; Staal et al., 2003; Walsby, 1985)**.** Early examinations of heterocystous cyanobacteria cultures suggested that elevated ambient oxygen concentrations instigated a thickening of the glycolipid envelope to enhance the physical limitation of gas diffusion into the cell (Kangatharalingam et al., 1992). As gas diffusion rates increase with warming temperatures, under this reasoning, heterocyst walls

should thicken in response. Staal et al. (2003) was the first to put forth a contrary hypothesis after taking both the passive regulation of oxygen by the heterocyst wall and the active scavenging of oxygen through respiration into account. According to his calculations, heterocystous cyanobacteria would actually increase the permeability of the glycolipid envelope under warming conditions to permit maximal flows of N_2 into the cell while enhanced respiratory rates account for the excess O_2 flowing in. The first empirical evidence for this theory came from Bauersachs et al. (2009), who found that *Anabaena* and *Nostoc* strains grown in warmer incubation temperatures produced less hydroxyketone HGs; such an adaption would create a thinner and more permeable membrane (Bauersachs et al., 2009; Bauersachs et al., 2014). Analyses of HGs isolated from water column filtrates in lakes further demonstrated that the relative proportions of ketone-bearing and non-ketone-bearing HGs were related to *in situ* temperatures (Bauersachs et al., 2014; Wörmer et al., 2012). Bauersachs et al. (2014) quantified the relative proportions of ketone-bearing and non-ketone-bearing HGs as the HDI_n (Heterocyst Diol Index of *n* carbon atoms, where *n* is 26 or 28) and HTI_n (Heterocyst Triol Index of *n* carbon atoms, where *n* is 28, 30, or 32). A subsequent study by (Bauersachs et al., 2015) found that the HDI_{26}, and to a lesser extent the HDI_{28}, of HGs from water column filtrates from a temperate lake tracked seasonal changes in LST. Along with these findings, the ubiquity of HGs in freshwater environments and the persistence of these lipids in the geologic record (Bauersachs et al., 2010) make HG-based proxies potentially well suited for widespread continental paleotemperature reconstructions.

1.4 STUDY SITE: LAKE MALAWI

1.4.1 Climatology, physiology, and limnology

Lake Malawi is the southernmost of the East African rift lakes, spanning from 9.5°S to 14.5°S, and is situated at ~500 m ASL (Figure 1.4**)**. The lake is 560 km long by 75 km wide with a maximum depth of ~700 m (Eccles, 1974). There is a single-basin with the depocenter located along the western shore, just north of Nkhata Bay (Figure 1.4). The meromictic lake is

permanently anoxic below ~250m due to basin morphology that inhibits complete overturning and gradients in temperature and dissolved species that sustain stratification (Vollmer et al., 1999; Wüest et al., 1996). Catchment relief also varies by latitude; fault-block mountains reaching over 2000 m border the northern end of the lake while lakeshore plains surround the southern end (Figure 1.4). Spatial variations in topography and rainfall generate higher terrestrial runoff into the north basin of the lake (Kingdon et al., 1999). The Shire River at the southern tip of Lake Malawi is the only outflow. Overall, riverine inputs and outputs are small given the large surface area of the lake, thus lake level is primarily dictated by changes in precipitation and evaporation (Bootsma & Hecky, 2003).

The climatology of the region is driven by the seasonal migration of the Intertropical Convergence Zone (ITCZ). While there is slightly more seasonal variability in solar radiation at Lake Malawi compared to the other equatorial African Lakes, the seasons are primarily defined by changes in precipitation and wind patterns (Nicholson & Yin, 1996). Located at the southern reach of the ITCZ, there is one dry season and one wet season each year (Eccles, 1974). The rainy season lasts from December to March and is more intense at the northern end of the lake. Weak northerly winds are prevalent at this time that allow for heating of surface waters and the development of shallow stratification, with thermocline depths reaching ~40 m to 60 m by February (Guildford et al., 2007). As the ITCZ moves northward during the onset of austral winter, southeasterly trade winds move in. The winter winds are much stronger than summer winds and prevail throughout the dry season, which lasts from April until August. The combination of the wind stress and cooler surface water temperatures promote mixing of the epilimnion down to ~100 m water depth (Eccles, 1974; Hamblin et al., 2003; Vollmer et al., 2005), though the mixed layer has been reported to extend as deep as 230 m (Patterson & Kachinjika, 1995). Upwelling is common at the southern end of the lake at this time and the seasonal mixing can even drive complete overturning in the shallow southern arms (Eccles, 1974). The lake is permanently anoxic below ~250 m, but the interaction between internal waves that propagate at mid-depths carrying nutrient-rich metalimnetic waters and cooled, sinking epilimnetic water masses can lead to localized entrainment and upwelling in central and northern regions. Conditions remain dry for the remainder of the year, September – November, but slackened winds and warming temperatures promote the beginning of summer stratification (Eccles, 1974; Guildford et al., 2007).

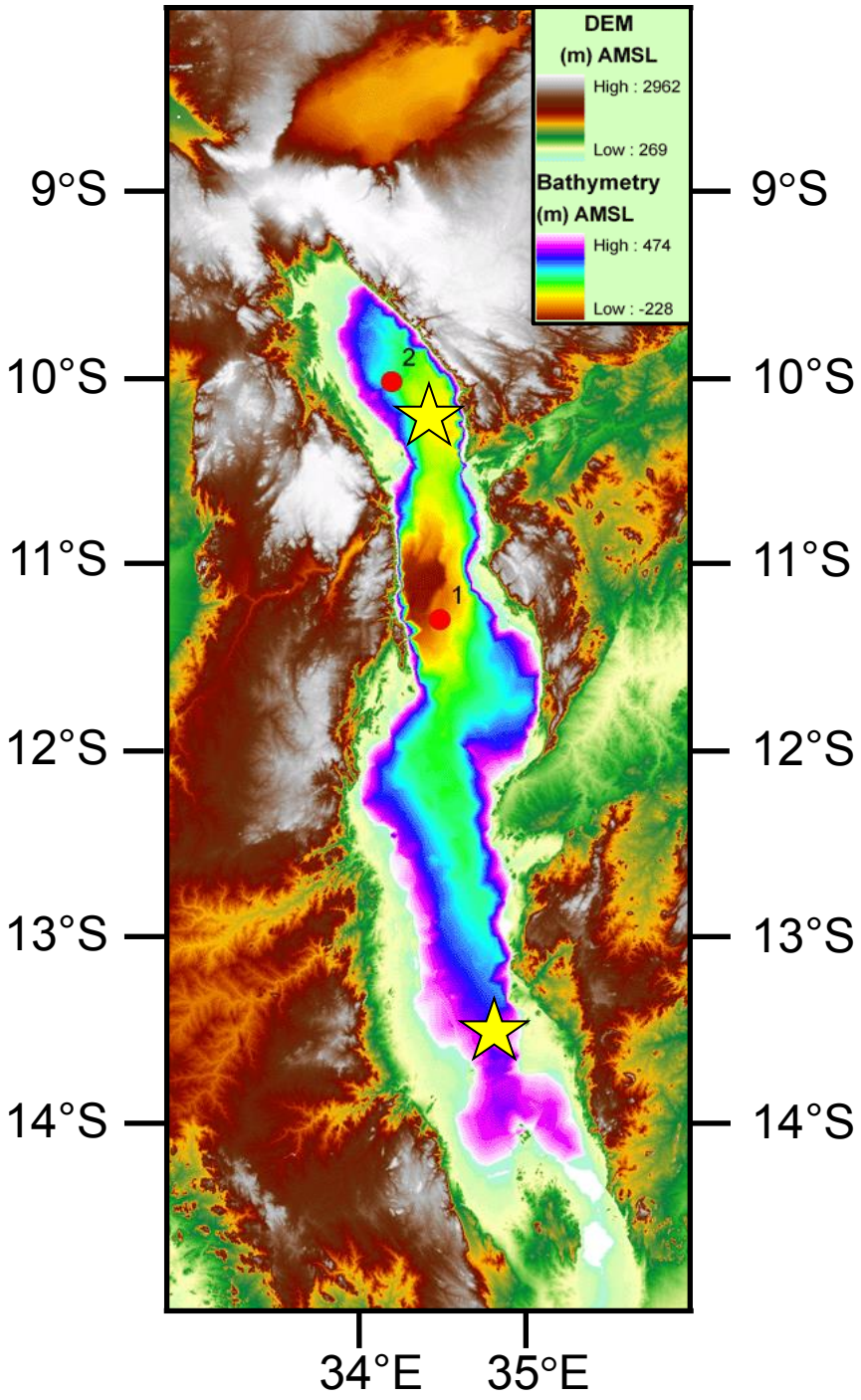

Figure 1.4: Digital elevation model (DEM) of the catchment of Lake Malawi and bathymetric map of the basin adapted from Scholz (Syracuse University, http://malawi.icdp-online.org). Red dots indicate drilling locations of the International Continental Drilling Project – Lake Malawi Drilling Project. Yellow stars indicate the location of sediment traps in this study.

1.4.2 Phytoplankton microbial diversity

The phytoplankton community of Lake Malawi is similar to that of other large tropical lakes that experience seasonal stratification (*cf.* Hecky and Kling 1987). Diatoms (e.g. *Aulacoseira, Nitzschia, Stephanodiscus, Cyclostephanos;* (Bootsma, 1993; Hecky, Kling, Johnson, Bootsma, & Wilkinson, 1999; Patterson & Kachinjika, 1995), cyanobacteria (e.g. *Anabaena, Microcystis, Synechococcus, Planktolyngbya;* Hecky et al. 1999), green algae (e.g. *Botryococcus, Closterium, Staurastrum, Mougeotia/Oedogonium;* Northern Rhodesian Joint Fisheries Research Organization, 1958-1961; Hecky and Kling 1987; Bootsma 1993; Hecky et al. 1999**)** and dinoflagellates (*Peridinium*; Hecky et al. 1999) are the most populous taxa, but their relative abundances are strongly influenced by seasonal changes in climate and lake water chemistry (Bootsma 1993; Patterson and Kachinjika 1995**)**. Deep mixing, elevated nutrient levels, and high turbidity characteristic of the dry season favor diatom assemblages, consistent with observations of peak diatom abundance in Lake Malawi from June – September (Bootsma 1993 Hecky and Kling 1987**)**. Peak cyanobacterial blooms typically follow the winter diatom bloom, with maximum cyanobacterial biomass typically detected in November – December (e.g. Northern Rhodesian Fisheries reports 1958-1961; Bootsma 1993; Hecky et al. 1999; Patterson and Kachinjika 1995). This is likely due to high irradiance, low wind stress, and low nutrient concentrations that develop during the dry stratified season and are favorable for cyanobacterial growth (Bootsma, 1993). Chlorophytes are generally the dominant taxa for the duration of the wet season (Bootsma, 1993), though blooms of the heterocystous cyanobacteria *Anabaena* have been observed in March – April and may be linked to phosphorus enrichment from riverine inputs during the rainy season (Hecky et al. 1999). This is just one example of how phytoplankton biodiversity is shifting in Lake Malawi in response to environmental factors such as warming temperatures (Verburg et al., 2003; Vollmer et al. 2005) and land-use change in the catchment that has led to significant increases (up to 50%) in sediment and nutrient loadings (Hecky et al., 2003) that will likely continue to alter the phytoplankton populations in the lake.

1.5 SCOPE OF THIS THESIS

The aim of this thesis is to investigate the production of the three classes of lipids discussed above – isoGDGTs, brGDGTs, and HGs – in the modern water column of Lake Malawi, Africa in order to determine their suitability as terrestrial paleotemperature proxies in a tropical environment. The lipids were extracted from settling particulate matter (SPM), as this material is likely most representative of the lipids reaching the sediment floor. SPM was collected in the lake at bi-monthly intervals over a three year time series. This study is the first to characterize the annual variability of brGDGT distributions in a lacustrine environment since the development of the method for the separate quantification of 5- and 6-methyl brGDGT isomers. This is also the first study to evaluate the production of HGs in a natural environment over a continuous multi-year period, in addition to being the first to analyze the HG content of SPM. Through the comparison of lipid distributions with environmental properties, this research provides insights into the sources of these paleotemperature-relevant lipids to SPM and the environmental and ecological factors that may dictate their structure.

2. MATERIALS AND METHODS

2.1 SEDIMENT TRAP SAMPLING

Sediment traps (PARFLUX Mark 78H-21, McLane Research Laboratories Ltd., East Falmouth, MA, USA) were installed in the north basin (NB) (10°25.018 S, 34°20.630 E; NST) and south basin (SB) (13°28.150 S, 34°43.718 E; SST-D) of Lake Malawi in January 2011 (Figure 2.1). The northern sediment trap (NST) was moored at 170m below lake surface and deployed until January 2013. The deep south sediment trap (SST-D) was moored at 125m below lake surface and deployed until January 2013. In January 2013, both traps were installed at the south basin location, moored at 50m (SST-S) and 115m (SST-D) below lake surface, and deployed until January 2014 (Figure 2.1). Thermistors (Brancker Research TR-1050) were placed along the mooring lines to record hourly changes in water column temperature over the course of the study. NST thermistors were located at 7m, 20m, 40m, 60m, 80m, 100m, 200m, 300m, and 395m water depths. SST thermistors were located at 7m, 20m, 40m, 60m, 80m, 100m, and 165m water depths from January 2011 to January 2013 and at 7m, 20m, 40m, 60m, 80m, 100m, and 170m water depths from January 2013 to January 2014. The traps were outfitted with 21 pre-labeled 500 mL polyethylene collection cups filled with de-ionized water. Each cup collected a 17-day interval of SPM. The naming scheme for samples uses the abbreviated sediment trap acronym and year followed by the sample number in that year. For example, sample 1 collected from the north sediment trap in 2011 is NST11-1. The traps were emptied and re-deployed annually in January with the Malawi Department of Fisheries, Monkey Bay Research/Fishing Vessel, *R/V Ndunduma*. Recovered samples were refrigerated during transport to the Large Lakes Observatory (LLO) at the University of Minnesota Duluth (UMD). Samples were stored at the LLO at 4°C until analysis.

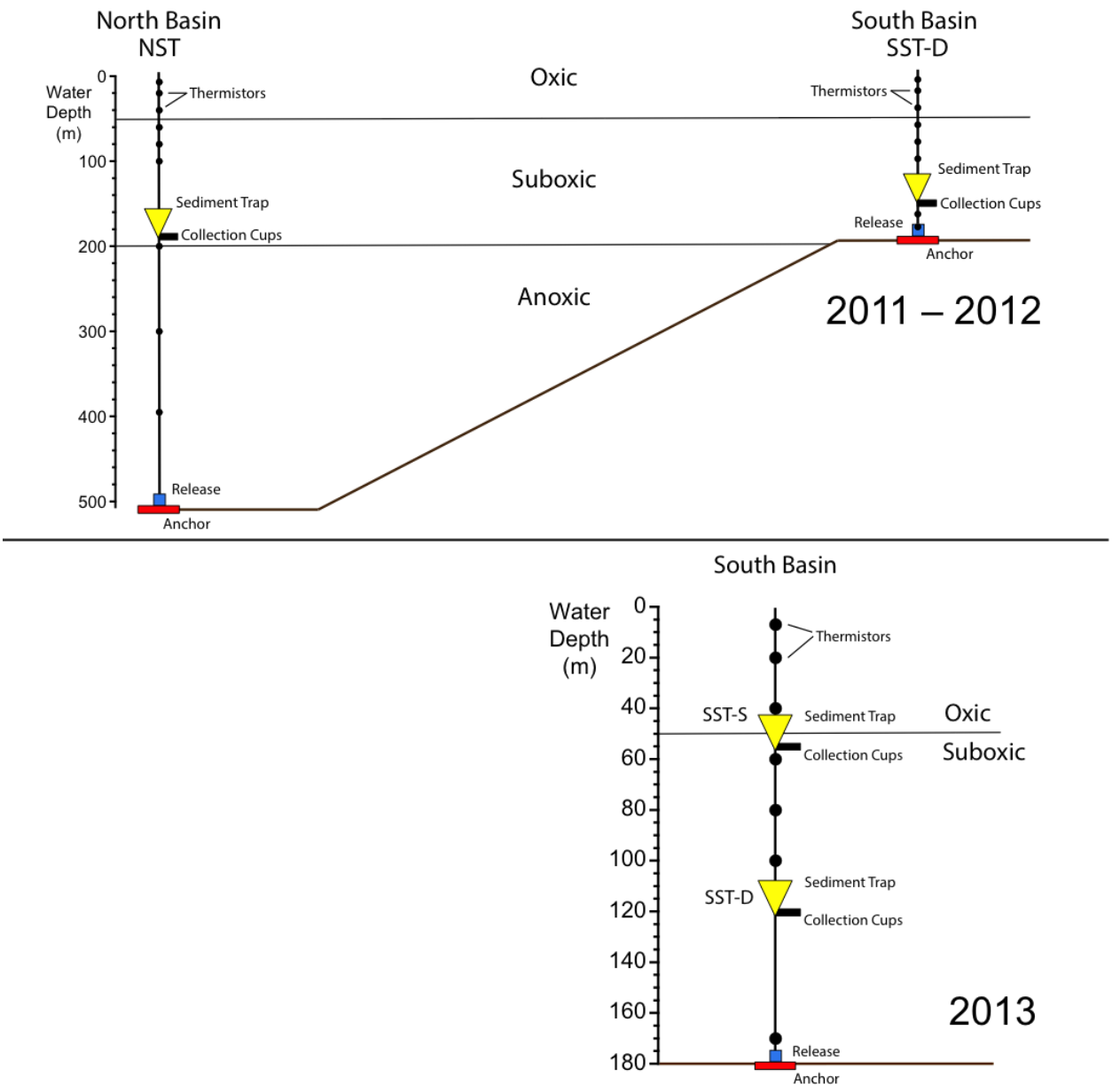

Figure 2.1: Simplified schematic of the mooring set-ups used for the sediment trap sampling. From January 2011 – January 2013 one sediment trap was in each the NB and SB while from January 2013 – January 2014 both traps were positioned along the same mooring in the SB. Sediment floor is at 507 m in the NB and 180 m in the SB. Location of the oxic/suboxic and suboxic/anoxic boundaries are approximate. Figures are not to scale.

2.2 LIPID ANALYSES

2.2.1 Sediment processing and extraction

SPM samples with enough available material were split into 10 fractions with a WSD-10 sediment splitter (McLane Research Laboratories Ltd., East Falmouth, MA, USA) at UMD for various proxy analyses. The amount of material collected in SST12-2, SST12-5, SST12-12 – SST12-21, SST13-S-9, and SST13-D-14 – SST13-D-21 was extremely low, therefore these samples were not split and instead used exclusively for bulk measurements. Due to a trap malfunction, no material was collected from SST11-13 – SST11-21. All sediment fractions for lipid analyses were freeze-dried **(**FreeZone Freeze Dryer, LABCONCO, Kansas City, MO, USA**)** and homogenized with a mortar and pestle at UMD prior to extraction. The dry weight of fractions designated for lipid analyses ranged from 0.12 g - 7.87 g. Fractions from NST11-1 – NST11-21 and SST11-1 – SST11-12 were extracted at UMD in 2012. Fractions from NST12-1 – NST12-21, SST12-1 – SST12-12, SST13-S-1 – SST13-S-21, and SST13-D-1 – SST13-D-13 were shipped to the University of Pittsburgh in 2014 and extracted there in February/March 2016.

All samples were extracted using a modified Bligh-Dyer procedure according to Sturt et al. (2004) to ensure maximum preservation of lipids during extraction. Sediment was ultrasonicated for 10 minutes in a mixture of dichloromethane (DCM), methanol (MeOH), and phosphate buffer, pH 7.4 (PB) at a ratio of 2:1:0.8 (v:v:v). The supernatant was transferred to a solvent-rinsed centrifuge tube and this step was repeated twice for a total of three extractions, sonicating for each of the subsequent extractions. The combined supernatant was adjusted to a new ratio of DCM/MeOH/PB at 1:1:0.9 (v:v:v:) with additional DCM and PB, then centrifuged to achieve phase separation. The lipid-containing organic phase was pipetted off and the remaining aqueous phase was washed twice with DCM. The combined organic phase constitutes the Bligh-Dyer Extract (BDE). Excess solvent was evaporated under a gentle stream of N_2 to near-dryness and transferred to pre-weighed 4 mL vials. It was then dried completely with N_2 and weighed. The dry BDE was re-dissolved in DCM/MeOH (1:1, v:v) and split volumetrically into two aliquots - one for GDGT analysis and one for HG analysis. For samples collected in

2011, a portion of the GDGT aliquot was also reserved for the analysis of isoGDGT intact polar lipids (IPL). BDE aliquots reserved for HG and IPL analyses were dried under N_2 and stored frozen (-20°C) until analysis.

2.2.2 GDGT purification

BDE aliquots for core lipid (CL) GDGT analysis were further purified using alumina column chromatography. Columns were constructed from 5.25" Pasteur pipets plugged with extracted cotton wool and filled with activated aluminum oxide (Al_2O_3). The BDE was dissolved in a small amount of hexane/DCM (9:1, v:v) and loaded onto a saturated column. Compounds were separated based on polarity and collected in pre-weighed 4 mL vials. The apolar fraction eluted with hexane/DCM (9:1, v:v). The polar fractions eluted second with DCM/MeOH (1:1, v:v). Fractions were dried under N_2 gas and weighed. A known amount of C_{46} internal standard (Appendix A; Huguet et al. 2006) was added to the polar fractions and dried under N_2.

2.2.3 Filtration

Filtration of samples prior to high-pressure liquid chromatography (HPLC) analysis is necessary to remove clay, flocculants, and other fine particles that can interfere with the chromatography. The spiked polar fractions for GDGT analysis were dissolved in chromatography-grade hexane/isopropanol (IPA) (99:1, v:v) and filtered over 0.45 μm PTFE filters (Whatman, Maidstone, UK) and dried under N_2. The BDE fractions for HG and IPL analyses were dissolved in a mixture of hexane/IPA/H_2O (72:27:1, v:v) and filtered over 0.45 μm regenerated cellulose syringe filters (Grace Alltech, Deerfield, IL, USA) and dried under N_2.

2.3 HPLC/MS ANALYSIS

2.3.1 IPL GDGT HPLC/ESI-MS^2 Analysis

The IPL analyses were performed at the Royal Netherlands Institute for Sea Research (NIOZ) in 2013. Analysis of crenarchaeol-based IPLs was conducted with HPLC/Electrospray Ionizaton (ESI)-MS^2. An Agilent 1100 series LC coupled to a Thermo TSQ Quantum Ultra EM triple quadrupole mass spectrometer with an Ion Max source and ESI probe was operated in selected reaction monitoring mode according Schouten et al. (2008) and Pitcher et al. (2011b), as modified from Sturt et al. (2004). Chromatographic separation of IPLs was achieved using an Inertsil diol column (250 x 2.1 mm, 5 μm; Alltech Inc., Deerfield, IL) maintained at 30°C and an elution gradient of mobile phases A: hexane/IPA/formic acid/14.8 $NH_{3(aq)}$ (79:20:0.12:0.04, v/v/v/v), and B: IPA/H_2O/formic acid/14.8 $NH_{3(aq)}$ (88:10:0.12:0.04, v/v/v/v). A flow rate of 0.2 mL min^{-1} was held throughout the analysis, which used a linear gradient of 100% A to 35% A/65% B in 45 minutes, maintained for 20 minutes, followed by a return to 100% A that is maintained for 20 minutes to requilibrate the column. SRM transitions used for the detection of crenarchaeol-hexose (MH), crenarchaeol-dihexose (DH), and crenarchaeol-hexose-phosphohexose (HPH) were based on the IPLs extracted from *Ca. Nitrososphaera gargensis* biomass as described by Pitcher et al. (2011b). No direct crenarchaeol IPL standard was available for quantification so results are listed as peak area units.

2.3.2 CL GDGT HPLC/APCI-MS Analysis

All filtered polar fractions were re-dissolved in hexane/IPA (99:1, v:v) to a concentration of 2mg/mL prior to analysis. Analysis of CL GDGTs via high performance liquid chromatography/positive ion atmospheric pressure chemical ionization mass spectrometry (HPLC/APCI-MS) was conducted at NIOZ in 2013 and 2017.

Samples NST11-1 – NST11-21 and SST11-D-1 – SST11-D-12 were analyzed in 2013 according to Hopmans et al. (2000) and Schouten et al. (2007). HPLC/APCI-MS was performed on an Agilent 1100 HPLC connected to an MSD SL mass detector. Separation was achieved

using a Prevail Cyano column (2.1 x 150mm, 3 μm; Alltech, Deerfield, IL, USA) maintained at 30°C and the following elution program: isocratic elution with 99% A/1% B for 5 minutes, then a linear gradient to 98.2% A/1.8% B in 45 minutes, followed by a 10-minute back-flush with 90% A/10% B. Total run time was 60 minutes. Eluent A is hexane and eluent B is IPA. Flow rate was 0.2 mL min^{-1}. Injection volumes were 5 μL. GDGTs were detected in single ion monitoring (SIM) mode, targeting [M + H]+ ions of *m/z* 1302, 1300, 1298, 1296, 1292, 1050, 1036, 1022, and 744. Note that only the major, non-cyclized brGDGTs were screened for in this assay.

The remaining samples were analyzed in March 2017 according to Hopmans et al. (2016). This method utilizes improved chromatography that allows for the separation of brGDGT isomers. Analysis was performed on an Agilent 1260 UHPLC coupled to a 6130 quadrupole MSD operated in positive ion mode. Two UHPLC silica columns (BEH HILIC columns, 2.1 x 150mm, 1.7 μm; Waters) connected in series and maintained at 30°C were used to achieve the enhanced chromatography. Injection volumes were 5 μL. Elution protocol was as follows: isocratic elution with 82% A/18% B for 25 minutes, a linear gradient to 65% A/35% B in 25 minutes, a second linear gradient to 100% B in 30 minutes, and last equilibration at 90% A/10% B for 20 minutes**.** Total run time is 100 minutes. Flow rate was 0.2 mL min^{-1}. Solvents A and B are the same as above. Detection of GDGTs was performed in SIM mode. Targeting [M + H]+ ions of *m/z* 1302, 1300, 1298, 1296, 1292, 1050, 1048, 1046, 1036, 1034, 1032, 1022, 1020, 1018, and 744 allowed for the detection of the full suite of brGDGTs and all major isoGDGTs.

Integrated peak areas for each GDGT were compared to the peak area of the internal standard (*m/z* 744) in individual samples to calculate lipid abundance. The relative response factor (RRF) of crenarchaeol and the C_{46} internal standard was determined in advance and corrected for after analysis (Huguet et al., 2006).

2.3.3 HG HPLC/MS Analysis

Filtered BDE for HG analysis was re-dissolved in hexane/IPA/H_2O (72:27:1, v:v) to a concentration of 5-10 mg/mL prior to analysis. Analysis of HGs via HPLC/ESI-MS^2 was also conducted at NIOZ. Samples NST11-1 – NST11-21 and SST11-D-1 – SST11-D-12 were analyzed in 2012 while the remaining samples were analyzed in March 2017. The

instrumentation for all HG analyses was the same except for the type of column used due to a manufacturer discontinuation.

HG analysis was performed on an Agilent 1100 series LC coupled to a Thermo TSQ Quantum ultra EM triple quadrupole mass spectrometer with an Ion Max Source and ESI probe operated in positive ion mode. The methodology followed Bauersachs et al. (2010) and Bale et al. (2015). Samples analyzed in 2012 were separated over a LiChrospher Diol column (250 mm x 2.1 mm, 5 μm; Alltech, Deerfield, IL, USA). Samples analyzed in 2017 were separated over an YMC-pack Diol-120-NP column (250 x 2.1 mm, 5 um; YMC Separation Technology, YMC Europe GmbH). Chromatography and abundance of HGs is not impacted by the change of column (Hopmans, *personal communication*). Column temperatures were maintained at 30°C. Injection volumes were 10uL. Elution of HGs was achieved at a flow rate of 0.2 mL min^{-1} with the following protocol: linear gradient from 90% A/10% B to 70% A/30% B in 10 minutes, isocratic elution at 70% A/30% B for 20 minutes, a second linear gradient to 35% A/65% B in 15 minutes, isocratic elution at 35% A/65% B for an additional 15 minutes, finally returning to 90% A/10% B in 1 minute, maintaining this mixture for 20 minutes to re-equilibrate the column. Eluent A was hexane/IPA/formic acid/14.8 M $NH_{3(aq)}$ (79:20:0.12:0.04, v/v/v/v) and eluent B was IPA/H_2O/formic acid/14.8 M $NH_{3(aq)}$ (88:10:0.12:0.04, v/v/v/v). Total run-time was 81 minutes. Detection of HGs was performed in selective reaction monitoring (SRM) mode targeting [M + H]+ ions of *m/z* 577.5, 577.5, 605.4, 603.5, 621.6, and 619.6.

The abundances of individual HGs were quantified via integration. No internal standard for HGs was available at the time of analysis, thus mass concentrations could not be calculated and results are reported using peak areas. As several years passed in-between the analysis of the 2011 and the 2012-2013 samples, peak areas for the latter group were ~2 orders of magnitude greater. Select samples from 2011 were re-run along with the 2012-2013 set and showed comparable distributions to the first analyses, however also showed a two order of magnitude increase in peak area. This is likely due to changes in the MS detection and do not reflect any actual change in concentration of HGs in the samples (*cf* Huguet et al., 2006), though the lack of measurement of an HG standard prevents the determination of changes the RRF of an MS for HGs over time.

2.4 STATISTICAL ANALYSES

Correlation coefficients (*r*) were calculated with least squares regressions of linear curve fits. Significance values (*p*) were calculated with a one-way analysis of variance (ANOVA) test (Zar, 1999). Statistical analyses were performed in Kaleidagraph (version 4.5.2, Synergy Software 2014).

2.5 CALCULATION OF LIPID RATIOS AND PROXIES

In the following equations, integers refer to the isoGDGT containing that number of cyclopentane moieties (Figure 1.1) and roman numerals refer to brGDGTs (Figure 1.2). Accents are used to denote the isomer of a structure.

TEX_{86} was calculated according to Schouten et al. (2007):

$$\mathrm{TEX}_{86} = \frac{[2] + [3] + [\mathrm{Crenarchaeol}']}{[1] + [2] + [3] + [\mathrm{Crenarchaeol}']}$$

TEX_{86}-based water temperatures were calculated using the calibration from Powers et al. (2010). This lake-specific calibration was generated from a set of 20 globally distributed lake surface sediments that included three samples from tropical east African lakes:

$$\mathrm{LST} = -10.4 + 50.8 \times \mathrm{TEX}_{86} \qquad R^2 = 0.68, \mathrm{RMSE} = 5.6°\mathrm{C}$$

BIT index values were calculated using the equation from Hopmans et al. (2004), as modified by De Jonge et al. (2014a):

$$\mathrm{BIT} = \frac{[\mathrm{Ia}] + [\mathrm{IIa}] + [\mathrm{IIa}'] + [\mathrm{IIIa}] + [\mathrm{IIIa}']}{[\mathrm{Crenarchaeol}] + [\mathrm{Ia}] + [\mathrm{IIa}] + [\mathrm{IIa}'] + [\mathrm{IIIa}] + [\mathrm{IIIa}']}$$

Two brGDGT-temperature calibrations specific to the East African lakes are presently available (Loomis et al., 2012; Tierney et al., 2010). Both are based on direct regressions of the fractional abundances of certain brGDGTs against LST. Since the calibrations are based on the fractional abundances of individual compounds within the total brGDGT pool, they can only be

applied to samples in which the full suite of brGDGT structures was analyzed for, as otherwise the fractional abundances are inaccurate. Both the Loomis et al. (2012) and Tierney et al. (2010) calibrations were generated prior to the widespread analysis of 5- and 6-methyl isomers, thus they have been revised to reflect the inclusion of both isomers that would have co-eluted under the old method. The Tierney et al. (2010) calibration, based on a set of 41 African lakes, is as follows:

$$\mathrm{MAAT} = 50.47 - 74.18 \times [\mathrm{IIIa} + \mathrm{IIIa}'] - 31.60 \times [\mathrm{IIa} + \mathrm{IIa}'] - 34.69 \times [\mathrm{Ia}]$$

$R^2 = 0.94$, RMSE = 2.2°C

The Loomis et al. (2012) study expanded the Tierney et al. (2010) dataset to 111 lakes. This enabled the authors to refine the East African lakes calibration, resulting in the following equation that now includes some of the minor brGDGTs in the equation:

$$\mathrm{MAAT} = 22.77 - 33.58 \times [\mathrm{IIIa} + \mathrm{IIIa}'] - 12.88 \times [\mathrm{IIa} + \mathrm{IIa}'] - 418.53 \times [\mathrm{IIc} + \mathrm{IIc}'] + 86.43 \times [\mathrm{Ib}]$$

$R^2 = 0.94$, RMSE = 2.1°C

A lacustrine-specific calibration has yet to be produced since the establishment of the separate quantification of 5- and 6-methyl brGDGT isomers. De Jonge et al. (2014a) did conduct a reanalysis of the dataset from Peterse et al. (2012) of 222 globally distributed soils, from which the following calibration was calculated:

$$\mathrm{MAT_{mr}} = 7.17 + 17.1 \times [\mathrm{Ia}] + 25.9 \times [\mathrm{Ib}] + 34.4 \times [\mathrm{Ic}] - 28.6 \times [\mathrm{IIa}]$$

$R^2 = 0.68$, RMSE = 4.6 °C

The isomerization ratio (IR) describes the relative proportion of the 6-methyl and 5-methyl isomers detected with the improved brGDGT chromatographic method (Hopmans et al., 2016) and was calculated according to De Jonge et al. (2014a):

$$\mathrm{IR_x} = \frac{\mathrm{x_{y'}}}{\mathrm{x_y} + \mathrm{x_{y'}}}$$ where X = I, II, or III, and y = a, b, or c

Similarly, HG-based indices describe the relative abundance of HG diols to HG keto-ols (Heterocyst Diol Index, HDI) and HG triols to HG keto-diols (Heterocyst Triol Index, HTI). These indices were calculated according to Bauersachs et al. (2015):

$$\mathrm{HDI}_{26} = \frac{\mathrm{HG}_{26}\mathrm{diol}}{\mathrm{HG}_{26}\mathrm{diol} + \mathrm{HG}_{26}\mathrm{keto} - \mathrm{ol}}$$

$$\mathrm{HDI}_{28} = \frac{\mathrm{HG}_{28}\mathrm{diol}}{\mathrm{HG}_{28}\mathrm{diol} + \mathrm{HG}_{28}\mathrm{keto} - \mathrm{ol}}$$

$$\mathrm{HTI}_{28} = \frac{\mathrm{HG}_{28}\mathrm{triol}}{\mathrm{HG}_{28}\mathrm{triol} + \mathrm{HG}_{28}\mathrm{keto} - \mathrm{diol}}$$

Temperatures reconstructed from these HG indices are also calculated according to Bauersachs et al. (2015):

$\mathrm{LST} = (\mathrm{HDI}_{26} - 0.4381)/0.0224$ R^2 = 0.93, RMSE = 0.97 °C

$\mathrm{LST} = (\mathrm{HDI}_{28} - 0.0401)/0.0405$ R^2 = 0.70, RMSE = 1.62 °C

$\mathrm{LST} = (\mathrm{HTI}_{28} - 0.2292)/0.0288$ R^2 = 0.78, RMSE = 1.69 °C

3. RESULTS

3.1 BULK GEOCHEMICAL DATA

3.1.1 Thermistor temperatures

The NB and SB exhibit clear seasonal changes in lake surface temperatures to depths of ~20m (Figure 3.1). In both basins, the 7 m and 20 m thermistors record the coolest temperatures in August and maximum temperatures in January – February. Temperatures at 20 m water depth generally track those at 7 m, though there are a few instances where the amplitude of temperature change is greater at the deeper site. Surface water temperatures in the NB are more stable than those in the SB; SB surface water trends are frequently punctuated by abrupt cooling events in the austral spring, summer, and autumn months (Figure 3.1).

The strong seasonal changes in temperature are not apparent below 20 m water depth. Rather, high frequency, high-amplitude fluctuations in temperature are recorded at the intermediate depths in both basins (Figure 3.1). In the NB, thermistors at 40 m and 60 m water depth recorded fluctuations of up to 4.3 °C and 3.8 °C in a single month, respectively. A similar pattern is observed at the 40 m thermistor in the SB, with recorded temperatures at this depth varying by up to 4.6 °C in a single month. These oscillations in temperature occur primarily during the stratified summer season, though it is difficult to confirm with the current dataset due to the incomplete logs from several thermistors. The dramatic temperature swings are likely the result of internal circulation dynamics rather than warming/cooling associated with seasonal radiative forcing which takes months to develop. One possible explanation is the presence of an internal seiche that continuously moves the thermocline across the fixed thermistors as the wave oscillates (Bootsma 1993).

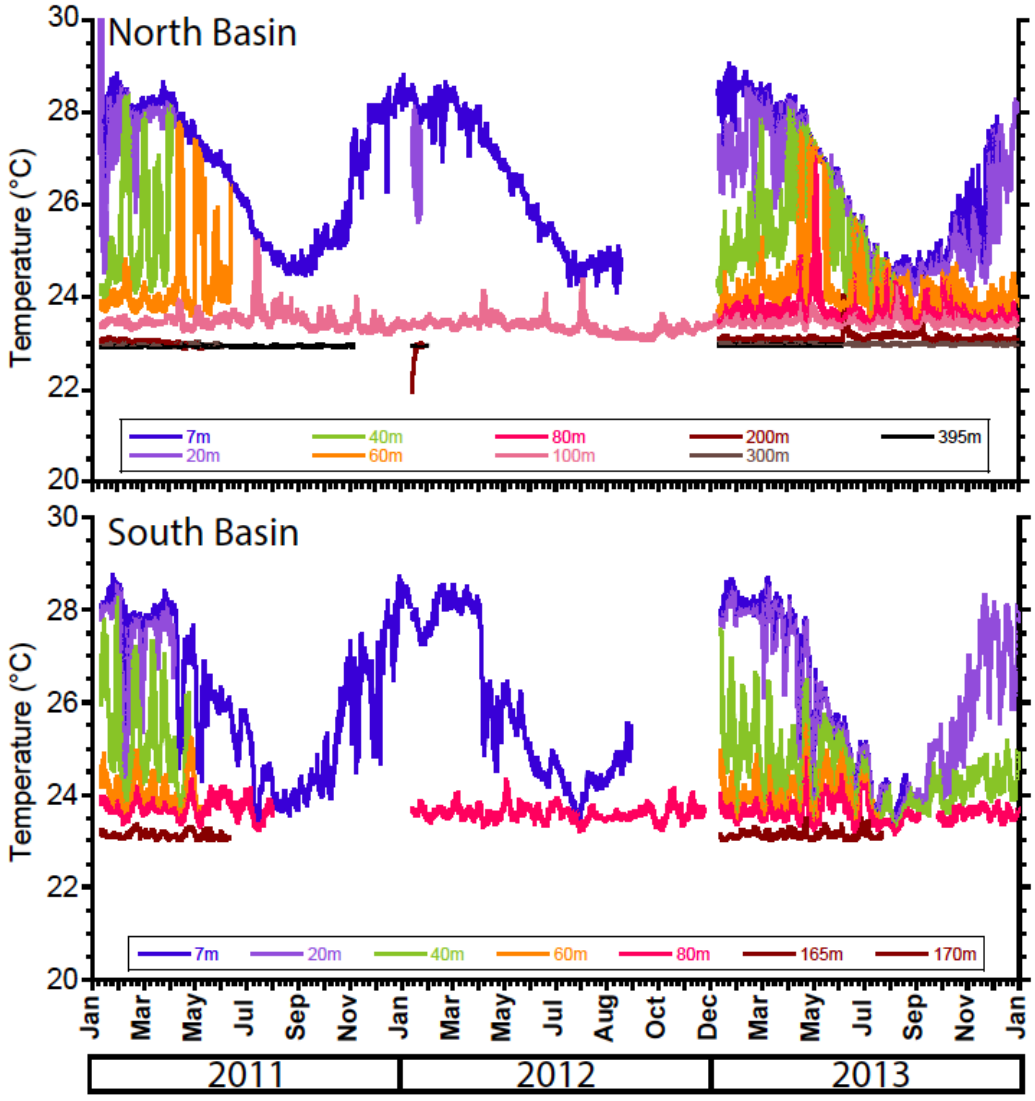

Figure 3.1: Temperature recorded by thermistors placed along NST and SST mooring lines. Periods of instrument malfunctions are represented by gaps in the record.

Temperature variability is significantly reduced at 80 m and 100 m in the NB and at 60 m and 80 m in the SB, though patterns at these depths appear linked to the intermediate waters in both basins (Figure 3.1). Temperatures stabilize at depths >100m, below which there is virtually no change in recorded temperatures for the periods where thermistor data is available.

Temperatures in the monimolimnion were only recorded at one depth, 300 m, in the NB. The average temperature at this depth across the three year study period was 22.98 °C +/- 0.02. This is the warmest recorded temperature at this depth in Lake Malawi, suggesting the ongoing deep water-warming trend in the lake is continuing (Vollmer et al., 2005).

Measured temperatures from 2011 – 2013 can be summarized into three modes of variability: 1) Surface waters, 0 m – 20 m, exhibit a distinct seasonal pattern driven by solar radiation; 2) Internal circulation dynamics drive temperature variability at depths <100 m – >20 m in the NB, and <80 m – >20 m in the SB; 3) Water temperatures remain consistent throughout the year at depths >100 m in the NB and >80 m in the SB. These observed patterns are in agreement with past reports of water column temperature in Lake Malawi (Vollmer et al., 2005).

Monthly average temperature profiles were generated using the thermistor measurements. Water column profiles are based on 2013 temperatures, as this was the most complete year of data (Figure 3.2). The thermocline is weakest in July – August, coinciding with the period of strong winds and mixing. The thermocline is most pronounced in March, following the warm temperatures and weak winds characteristic of austral summer in the region. The depth of the thermocline varies annually as well, consistent with previous studies (Guildford et al. 2007; Hamblin et al., 1999; 2003).

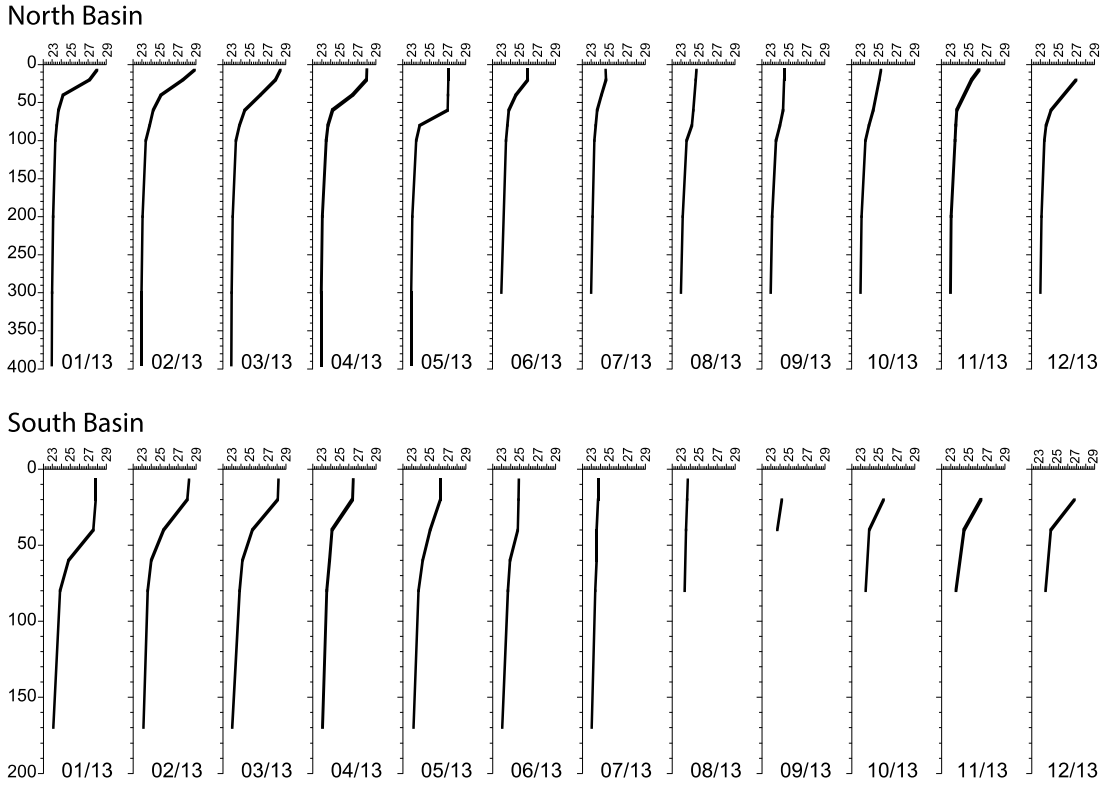

Figure 3.2: Annual variability in the strength and position of the thermocline in Lake Malawi's north and south basins. Profiles were created with the sediment trap thermistor data.

3.1.2 Bulk mass accumulation rates

Bulk sedimentation at the NST ranged from 0.07 - 3.35 g/m^2/day (Appendix G). The maximum flux occurred in November in both 2011 and 2012. Secondary peaks were additionally present in May – July each year (Figure 3.3**)**. SST-D malfunctioned at the end of 2011, resulting in no material collected from September 2011 – January 2012. Sedimentation was extremely low during this same period in 2012 and 2013, so it is likely that not much sediment was missed. Bulk sedimentation at SST-D ranged from 0.02 - 3.12 g/m^2/day. Sedimentation in the SB had two maxima each year, with one in late austral summer (~March-April) and the other in early austral winter (~June-July) (Figure 3.3a). Patterns of sedimentation were similar between SST-D and SST-S in 2013. SST-S mass accumulation rates ranged from 0.07 – 2.74 g/m^2/day. Though there were also two periods of elevated sedimentation rates at SST-S, one in mid-March and the other in late-July, the duration of the latter peak was half of the concurrent maxima at SST-D (Figure 3.3a**)**. The consistent presence of two peaks in sedimentation in the sediment traps from this study differs from the result of a previous sediment trap study conducted nearby in the SB. In the study by Bootsma and Hecky (1999), the authors noted only a single period of elevated mass accumulation rates occurring from December – May in their shallow traps (100 m and 140 m).

3.1.3 Organic Carbon and Nitrogen

SPM total organic carbon (TOC) content was higher overall in the southern traps compared to NST, and SST-S had the greatest percentage of TOC of all three traps. Average TOC content was 3.3% ± 1.0, 4.4% ± 0.8, and 6.1% ± 3.2 in the NST, SST-D, and SST-S, respectively (Figure 3.3e; Appendix B**)**. The high standard deviation in SST-S is due to six measurements that were outside the linearity of standards (SST13-S-1, S-10, S-18, S-19, S-20, and S-21). The flux of TOC in the NST was greatest from November – January. Flux of TOC in SST-S and SST-D was greatest in the beginning of the year, with peaks in March – April and July for both the deep and shallow traps, likely due to the low overall sedimentation during the dry, stratified season at this site.

Average total organic nitrogen (TON) was 0.4% ± 0.1, 0.6% ± 0.3, and 0.9 ± 0.6 in the NST, SST-D, and SST-S, respectively (Figure 3.3c; Appendix B**)**. Low levels of TON in SST13-D-3, D-21 and SST13-S-2, S-4, S-5, S-7 resulted in values that were outside the linearity of standards. The flux of TON generally co-varied with TOC throughout the time series, though with a couple of exceptions. At the NST, from October – December 2012, the flux of TOC is at a maximum while the flux of TON does not increase as significantly. This event is accompanied by a two-fold increase in C_{org}/N_{org} from average values (Figure 3.3d**)**. A similar event occurs in December 2013 at SST-D.

Overall, C_{org}:N_{org} values do not vary significantly, but any deviations that do occur are driven by changes in %TON. Average SPM C_{org}:N_{org} from this study are lower than published values for Lake Malawi surface sediments, SPM, and POM, though within the range of error (Table 3.1).

Table 3.1: Average C_{org}:N_{org} values of various types of smaterial collected in Lake Malawi.

Reference	Location/Year	Sample Type	Depth (m)	C_{org}:N_{org}
This study	NST (2011/2012)	SPM	170	8.5 ± 1.8
	SST-D (2011 – 2013)	SPM	115 – 125	8.0 ± 2.3
	SST-S (2013)	SPM	50	7.5 ± 1.1
Pilskaln, 2004	North Basin (1987 – 1990)	SPM	450	10.8 ± 1.5
	Central Basin (1991/1992)	SPM	390	9.8 ± 0.3
Bootsma & Hecky, 1999	Central Basin (1997/1998)	SPM	100	10.2 ± 1.3
	South Basin (1997/1998)	SPM	100	10.9 ± 1.2
Guildford et al., 2007	South Basin (1997 – 2000)	POM	0 – 40	9.3 ± 1.6
Castañeda et al., 2009	North Basin (1998)	sediment	403	12.0

3.1.4 Bulk C and N isotopes

The carbon isotopic composition of TOC is relatively stable throughout the time series, though this trend is punctuated by a few dramatic events (Figure 3.3g**)**. NST-$\delta^{13}C_{TOC}$ ranged from –26.5 ‰ to –18.2 ‰ (Appendix B). NST-$\delta^{13}C_{TOC}$ mirrors patterns in C_{org}/N_{org}. The most positive values occur during a period of low overall TOC concentrations but very high C_{org}/N_{org}. SST-D-$\delta^{13}C_{TOC}$ ranged from –26.0‰ to –1.5‰. The relationship between $\delta^{13}C_{TOC}$ and C_{org}/N_{org} in SST-D is the opposite of that in NST, with the most positive isotopic values occurring during periods of low C_{org}/N_{org}. The very positive values recorded at SST-D at the end of 2013 were

outside the range of the standards (SST13-D-14, D-15, D-16, D-17, D-18, D-19, D-20, D-21). Interestingly, this event is not recorded in the SST-S-$\delta^{13}C_{TOC}$ record, which shows little variability throughout 2013 ranging between –24.8‰ to –21.4‰. The discrepancy is due to the difficulty of making isotopic measurements on the small sample size of sediments from SST-D-13, and trends in SST-S are likely reflective of actual changes in the lake.

The isotopic composition of TON is similarly unique in the NB and SB of Lake Malawi (Figure 3.3h). NST-$\delta^{15}N_{TON}$ ranges from –5.2 ‰ to 5.1 ‰ (Appendix B). There appears to be an annual cycle in the NB from more positive values at the beginning of the year towards more negative values by the start of austral summer. SST-D-$\delta^{15}N_{TON}$ ranges from –6.7‰ to 12.9‰. At this trap, there is a long-term trend towards more positive values that persists throughout the time-series rather than a regular cycle (Figure 3.3h). SST-S-$\delta^{15}N_{TON}$ is relatively positive, ranging from 1.0‰ to 9.3‰. The $\delta^{15}N_{TON}$ for SST13-S-10 was outside the range of the standards. There is no clear trend in SST-S-$\delta^{15}N_{TON}$ in 2013, though values do seem to roughly co-vary with SST-D-$\delta^{15}N_{TON}$ (Figure 3.3h).

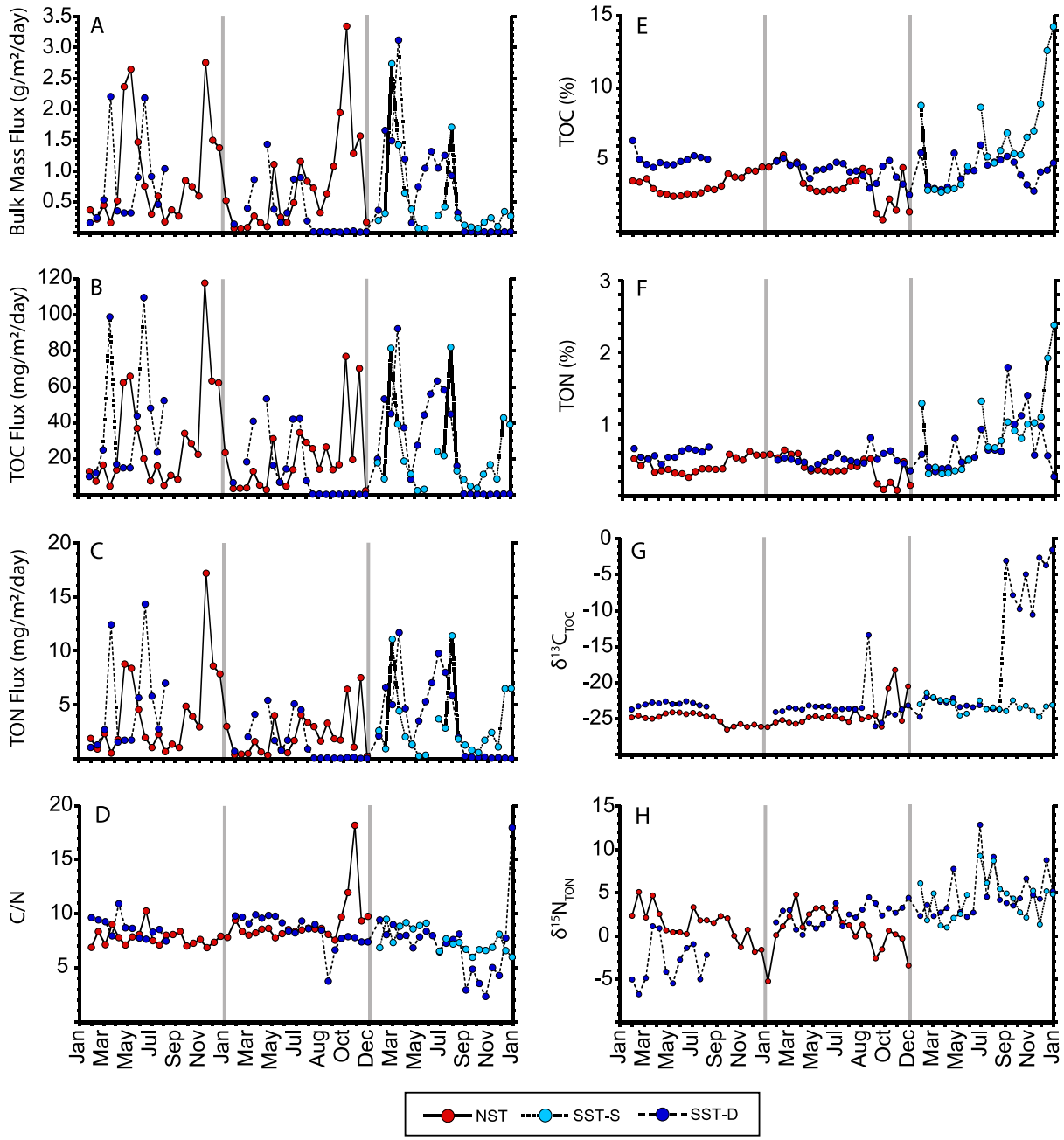

Figure 3.3: Accumulation rates of bulk sediment (a), total organic carbon (TOC) (b), and total organic nitrogen (TON) (c). Weight ratios of organic carbon and nitrogen (C/N) are shown in panel (d). Percent concentrations of bulk organic carbon (e) and bulk organic nitrogen (f), and the isotopic composition of TOC (g) and TON (h) are featured on the right of the figure.

3.2 GDGTS

3.2.1 Crenarchaeol IPLs

MH-, DH-, and HPH-crenarchaeol were detected in all SPM samples. Average total IPL fluxes were slightly higher in NST at 3.8e+6 area/m^2/day ± 2.4e+6, than in SST-D, 3.6e+6 area/m^2/day ± 1.4e+6 (Figure 3.4; Appendix G). However, the average flux of the most labile IPL, HPH-crenarchaeol, was actually higher in SST-D at 3.5e+5 area/m^2/day ± 4.3e+5 compared to the NST, in which it was 1.3e+5 area/m^2/day ± 1.7e+5. In SST-D, MH-crenarchaeol was the most abundant. MH-crenarchaeol also dominated the NST for the majority of the year, except during the period of maximum IPL flux in which DH-crenarchaeol fluxes were greatest. Maximum fluxes of total IPLs in both basins matched periods of maximum fluxes of CL isoGDGTs (Figure 3.4).

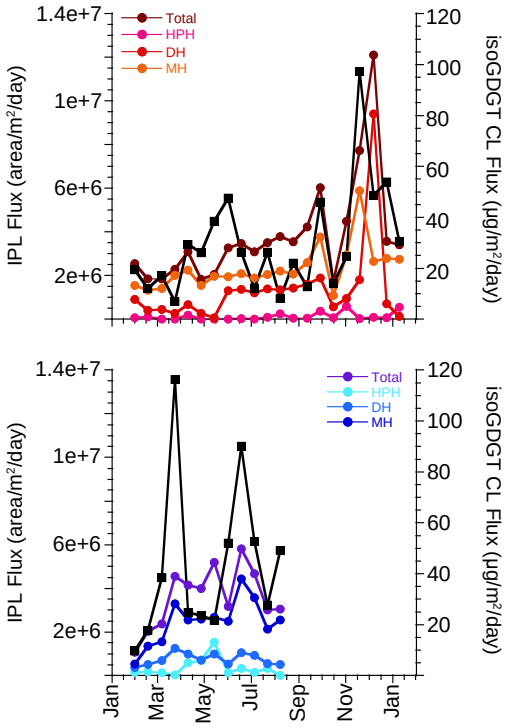

Figure 3.4: Fluxes of total crenarchaeol IPLs and of the individual MH-, DH-, HPH-crenarchaeol IPLs (colored lines) compared to the summed fluxes of CL isoGDGTs (black squares) in the NB and SB of Lake Malawi in 2011.

3.2.2 IsoGDGTs and TEX_{86}

The full suite of isoGDGTs scanned for were detected in every sample except for SST13-S-7. Fractional abundances are calculated as flux-weighted averages (Appendix C). Crenarchaeol was the dominant isoGDGT overall with fractional abundances ranging from 57% to 79%. The crenarchaeol regio-isomer was a much less significant portion of the total isoGDGT pool, with fractional abundances of 3—6% at NST, 2—3% at SST-D, and 0—2% at SST-S. The fractional abundances of the other minor isoGDGTs varied based on trap depth, with distinct patterns present in SST-S that differed from those in NST and SST-D. GDGT-2 was the second most abundant isoGDGT in NST and SST-D, making up 5—9% of total isoGDGTs from these sites. At SST-S, GDGT-0 was the second most abundant isoGDGT overall, with fractional abundances of 3—25%. Conversely, GDGT-0 was the third most abundant compound at NST and SST-D, contributing 3—24% of total isoGDGTs. Importantly, however, only 2 out of 76 samples (NST12-2 and SST13-D-6) actually had fractional abundances of GDGT-0 > 8%. GDGT-1 was the third most abundant isoGDGT in SST-S, with fractional abundances of 4—9%. GDGT-1 and GDGT-3 were the least abundant compounds in NST and SST-D, with fractional abundances of 4—8% and 5—7%, respectively. GDGT-2 and GDGT-3 were the least abundant compounds in SST-S, each making up only 5—6% of the total isoGDGT pool. At all sites, particularly low fractional abundances of crenarchaeol are attributed to increases in abundances of GDGT-0.

The average flux of total isoGDGTs for the three-year study period is higher in the NB than in the SB, though exceptionally high fluxes of isoGDGTs to SST-D do occur in 2011 (Figure 3.5; Appendix G). Total isoGDGT flux ranges from 0.05 to 97.27 $\mu g/m^2/day$ in the NST, with maximum fluxes at this site at the start of the rainy season in November in both 2011 and 2012. IsoGDGT fluxes in SST-D range from 0.07 to 116.44 $\mu g/m^2/day$, with the average flux value decreasing each year. There are two primary peaks in isoGDGT flux at SST-D: March and June/July. SST-D SPM collected in August – December, when available, was not analyzed for its GDGT content due to the low total mass of these samples. IsoGDGT fluxes generally co-vary with bulk sediment flux, so it is likely that fluxes were relatively insignificant at this time regardless. Fluxes of isoGDGTs were lowest at SST-S overall, ranging from 0.45 to 11.34 $\mu g/m^2/day$.

TEX_{86} showed little variability in the NST, ranging between 0.75 and 0.80 (Figure 3.6; Appendix D). There is a small increase in average NST-TEX_{86} values from 0.76 ± 0.008 in 2011 to 0.79 ± 0.007 in 2012. TEX_{86} values in SST-D range from 0.66 to 0.75. Despite the slightly higher variability compared to NST, average annual TEX_{86} is consistent at the site at 0.72 ± 0.012, 0.73 ± 0.015, and 0.72 ± 0.026 in 2011, 2012, and 2013, respectively (Figure 3.6; Appendix D). TEX_{86} showed the greatest variability at SST-S where values ranged from 0.60 to 0.76 (Figure 3.6; Appendix D).

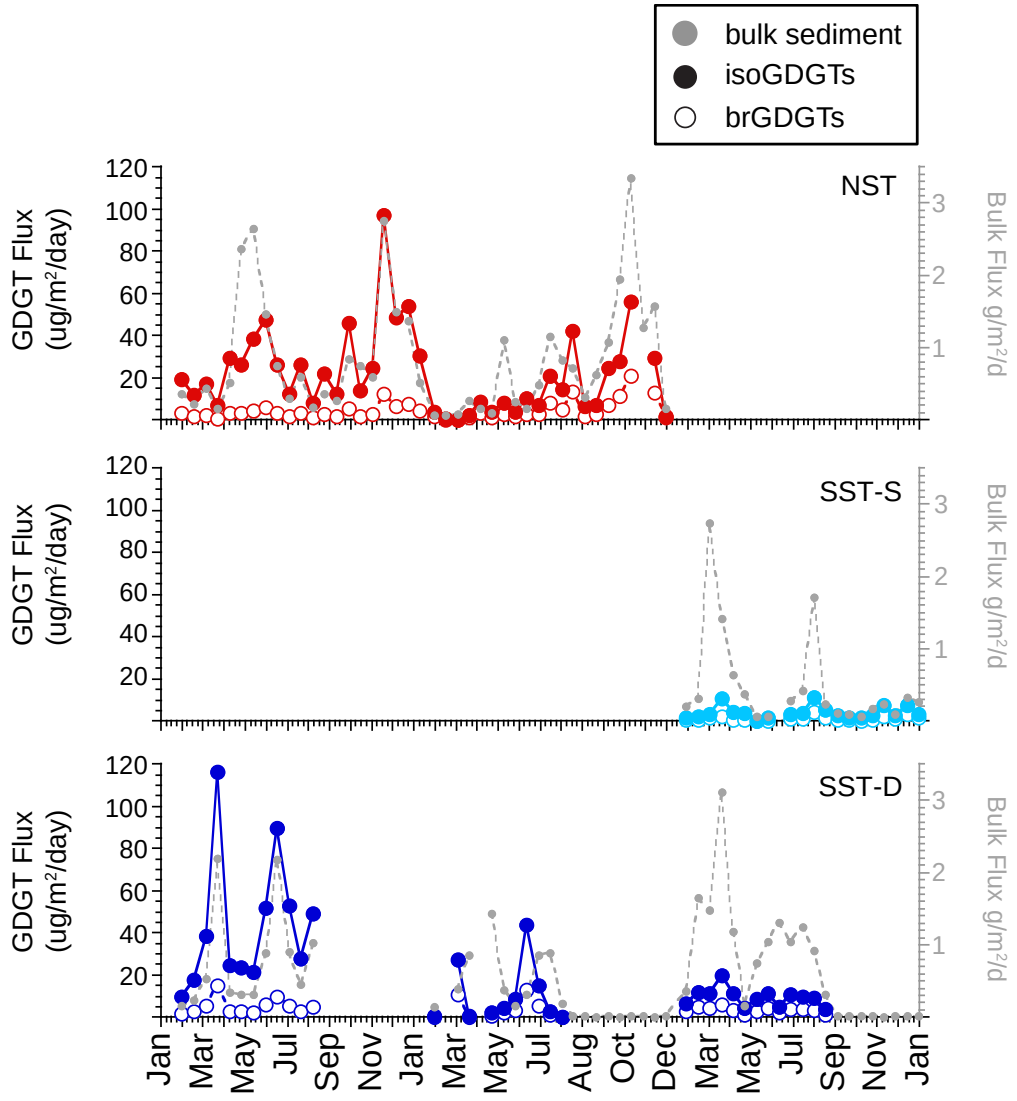

Figure 3.5: Fluxes of CL branched (colored open circles) and isoprenoid (colored closed circles) GDGTs in Lake Malawi SPM compared to bulk sediment fluxes (closed grey circles).

3.2.3 BIT

One of the primary consequences of using different instruments and methods for GDGT analyses (see section 4.3.1) is that BIT values are higher in those run with the Hopmans et al. (2016) method compared to those run with the Schouten et al. (2007a) method (Figure 3.6; Appendix D**)**. Hopmans et al. **(**2016) demonstrated that the use of 2 UHPLC silica columns in their method produces higher BIT values compared to those produced with the cyano column described in the Schouten et al. (2007a) method. Previous studies have found that MS instrumentation could strongly influence BIT values, though the direction of change associated with this factor can be positive or negative (Schouten et al., 2009; Schouten et al., 2013). Due to these factors, it is difficult to compare BIT values between methods. Nonetheless, BIT was similar between the northern and southern traps in each set, and was generally lowest during the austral winter and higher during the rainy season. As all BIT values are ≤ 0.4 (range 0.12 to 0.40), TEX_{86} is likely not significantly influenced by allochthonous isoGDGTs at any point in the record (Weijers, et al. 2006).

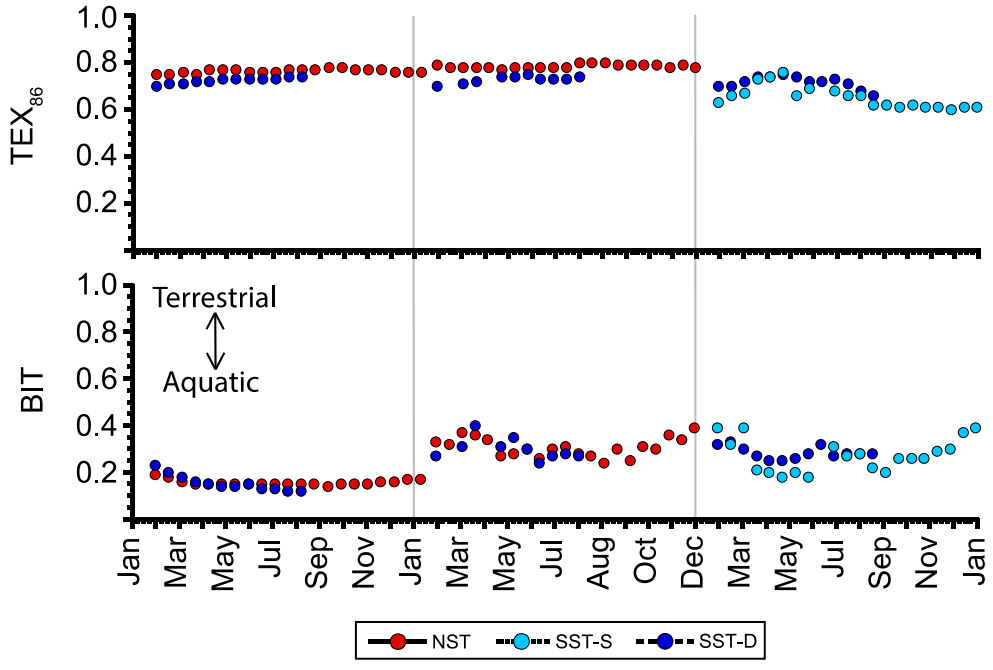

Figure 3.6: TEX_{86} and BIT indices calculated from GDGT distributions in Lake Malawi SPM.

3.2.4 BrGDGTs

Differences in GDGT analytical methods additionally led to discrepancies in brGDGT abundances and distributions between sets of samples. Concentrations of total brGDGTs are higher for samples run with the Hopmans et al. (2016) method. Cyclized brGDGTs composed 7.4—19.3% of the total brGDGT pool in NST12 samples and 9.9—24.7% of the brGDGT pool in SST12-D – SST13-D samples (Appendix E). Not accounting for these compounds in samples run with the Schouten et al. (2007a) method thus led to an underestimation of total brGDGT abundance. When only major brGDGTs were analyzed, IIa was the dominant compound (45—50%), followed by Ia (39—46%), and minor abundances of IIIa (8—12%) (Appendix E). When all 15 brGDGTs were analyzed, Ia and IIa (as combined 5-methyl and 6-methyl isomers) were in roughly equal abundance. Fractional abundances of cyclized brGDGTs were greater in the SST-D and SST-S than in the NST. BrGDGTs with two cyclopentane moieties were the least abundant overall.

6-methyl isomers comprised a substantial portion of the brGDGT pool (Figure 3.8). The C6 isomer was especially dominant for non-cyclized brGDGTs, representing over three-quarters of all IIa and IIIa structures in all but one sample, SST13-S-21, where IIIa and IIIa' were in equal abundance. Variability in the IR of cyclized brGDGTs is greater than that of the non-cyclized compounds. While there are no consistent trends in the IR of cyclized brGDGTs, annual variability in the isomerization of non-cyclized brGDGTs is both spatially and temporally consistent (Figure 3.9). The average IR of cyclized brGDGTs was also lower than that of the non-cyclized compounds.

Changes in the flux of brGDGTs in Lake Malawi SPM are in virtual lock step with isoGDGT fluxes, exhibiting significant positive correlations for both samples analyzed according to Schouten et al. (2007) (R^2=0.97; p<0.001) and samples analyzed using the methodology of Hopmans et al. (2016) (R^2=0.97; p<0.001) (Figure 3.7). Total brGDGT fluxes are highest in the NST overall, ranging from 0.02 to 20.95 μg/m^2/day. In the SB, brGDGT flux is greater in SST-D, ranging from 0.03 to 13.23 μg/m^2/day, while brGDGT fluxes in SST-S ranged from 0.08 to 4.62 μg/m^2/day (Appendix G).

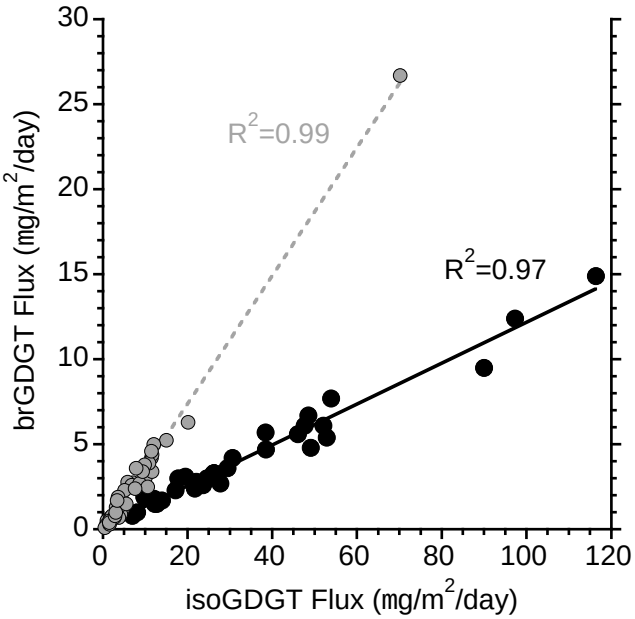

Figure 3.7: Correlations between isoGDGT and brGDGT fluxes from SPM samples collected from 2011-2013. Black circles represent samples run using the LC_{CN} method and grey circles represent circles run using the LC_{Si} method.

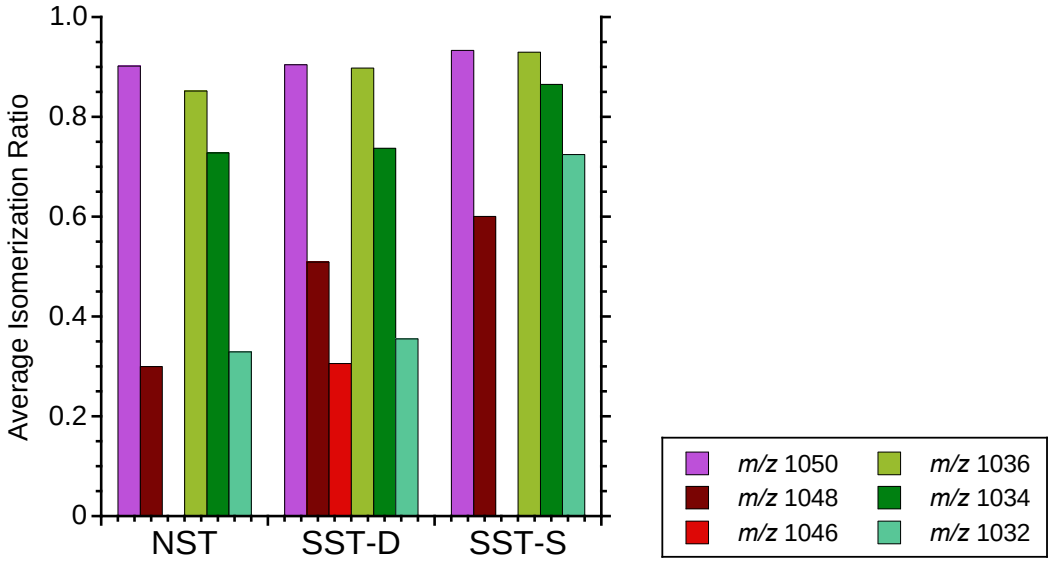

Figure 3.8: Average IR (De Jonge et al., 2014a**)** of all brGDGTs collected in each sediment trap from 2012 to 2013. IR could not be calculated from samples collected in 2011, as the appropriate method was not used for the complete separation of isomers. A higher ratio indicates a greater proportion of 6-methyls structures, while a value of 0.5 would mean 6-methyls and 5-methyls are in equal abundance.

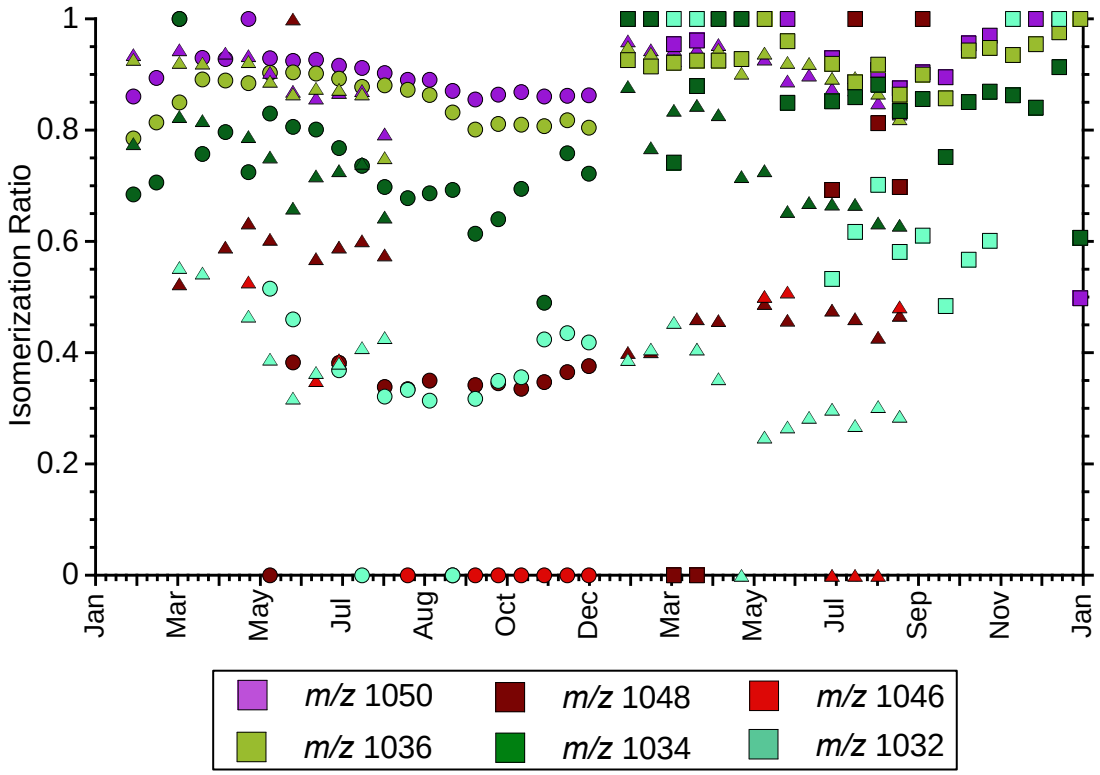

Figure 3.9: Annual trends in IR of brGDGTs collected between January 2012 – January 2014 in Lake Malawi. IR of samples from 2011 could not be calculated as they were analyzed with a method that does not separate the 5- and 6-methyl isomers.

3.3 HGS

3.3.1 HG distributions and abundances

Distributions of HGs in SPM are remarkably coherent across Lake Malawi where trends in the fractional abundances of the six HGs measured are highly similar in NST, SST-D, and SST-S. HG_{26} diols and HG_{28} diols are the most abundant (Figure 3.10) – together these two compounds comprise 70% to 99% of all HGs measured (Appendix H). There is only one sample where the sum of the two is < 79%, and the sample (NST11-10) had extremely low concentrations of HGs overall. The HG_{28} keto-ol is the next most abundant, contributing 1% to 30% of the HG pool. The HG_{28} triol, HG_{26} keto-ol, and HG_{28} keto-diol are minor components

throughout the time series, representing ≤ 2.6% each, though they were not present in every sample. Fractional abundances of HG_{28} diol are highest during austral summer and lowest during austral winter when the relative proportion of HG_{26} diols increase (Figure 3.10). The fractional abundance of HG_{28} keto-ols shows a distinct increase in December – January each year (Figure 3.10).

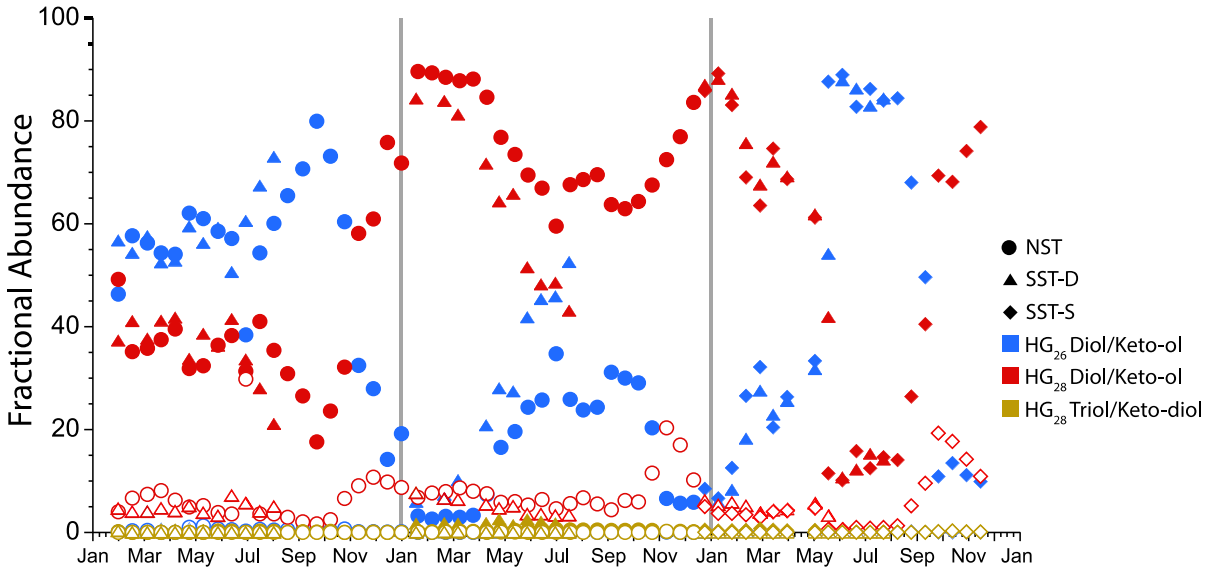

Figure 3.10: Fractional abundances of HGs in Lake Malawi SPM. Shapes correspond to sediment traps (circles = NST, triangles = SST-D, diamonds = SST-S), and colors correspond to pairs of HGs. Solid colors are diols or triols and open circles are the keto-ol or keto-diol counterpart. Grey lines separate between 2011/2012 and 2012/2013.

Similar to GDGTs, there is a difference in the HG data that is attributed to the length of time between analyses; peak areas of SPM samples run in 2012 are considerably lower compared to those run in 2017 (

Figure **3.11**). Select samples were re-run to determine if peak areas were influenced by unrelated variability in the sensitivity of the MS detector. HG peak areas from these duplicate samples were three orders of magnitude greater, which is on par with the other samples run in 2017 (

Response Factor

Sample	*m/z* 577	*m/z* 575	*m/z 605*	*m/z 603*	*m/z* 621
NST11-1	277.7	312.3	237.0	238.0	262.7
NST11-9	636.2	532.8	624.8	568.2	594.8
NST11-15	481.3	488.4	450.3	445.7	563.5
SST11-D-2	788.7	708.3	710.0	732.5	0.0
SST11-D-11	476.3	410.4	436.6	444.8	0.0
Average	532.0	490.4	491.7	485.8	284.2

Table 3.2). Relative increases in peak areas for individual HG structures within a single sample were consistent, however there was considerable variability between samples. Therefore, the emphasis for evaluating the results of these analyses is placed on the relative changes in peak areas between samples rather than their absolute magnitudes.

Table 3.2: Relative response of HGs of NST11 samples run in 2017 and 2012

	Response Factor				
Sample	*m/z* 577	*m/z* 575	*m/z 605*	*m/z 603*	*m/z* 621
NST11-1	277.7	312.3	237.0	238.0	262.7
NST11-9	636.2	532.8	624.8	568.2	594.8
NST11-15	481.3	488.4	450.3	445.7	563.5
SST11-D-2	788.7	708.3	710.0	732.5	0.0
SST11-D-11	476.3	410.4	436.6	444.8	0.0
Average	532.0	490.4	491.7	485.8	284.2

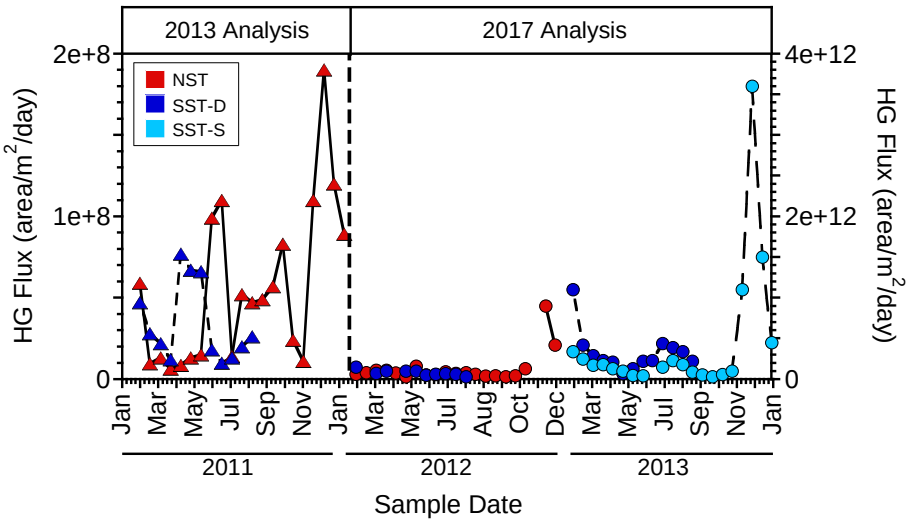

Figure 3.11: Fluxes of HGs in Lake Malawi SPM based on units of area $m^{2\text{-}1}$ d^{-1}. The differences in the magnitude of fluxes between samples run in 2013 (left of dashed black line) and those run in 2017 (right of dashed black line) is an artifact of variability in MS functionality.

The maximum flux of HGs in the NST occurs at the end of each year and is higher in 2012 than 2011 based on the relative increase in HG flux compared to the average for that year (Figure 3.11). HG flux in SST-S also shows a single peak at the end of the year (Figure 3.11). The magnitude of this peak is almost 8 times the average flux of HGs in SST-S. The SST-D trap failed to collect any complete year of samples so it is difficult to determine any certain annual trends. The available data show a minor peak in flux at the end of the stratified season/start of the windy season in 2011 and 2013, though this peak is absent in 2012. There is a maximum flux occurring at the transition between 2012 and 2013, but the lack of data from the end of 2012 makes it impossible to determine the duration of this peak.

3.3.2 HG-based indices

With the HDI_{26}, HDI_{28}, and HTI_{28}, a value of 1.0 indicates the lack of any ketonehydroxyls. The HDI_{26} index exhibits minimal variability in all three traps, with values ranging from 0.98 to 1.00, exemplifying the extremely low production of HG_{26} keto-ols compared to HG_{26} diols (Figure 3.12). The HDI_{28} exhibits semi-regular variability, remaining

stable at ~1 for most of the year ending with a distinct dip in values near the end of the year that spans ~September until the end of January of the following year. Aside from this regular pattern, HDI_{28} in the NST shows an irregular decrease in April 2011 and an anomalously low value of 0.51 in July 2011 (Figure 3.12). The latter value is observed in a sample that had very low HG concentrations so may be biased. The HDI_{28} values of all SPM samples other than this anomalous point range from 0.78 to 0.96. Due to the nature of the HTI_{28} calculation as a ratio, if the HG_{28} triol was not present it could not be calculated (Appendix H). For the available data, values range from 0.44 to 1.00. The majority of values are 1.00, indicating a complete dominance of the HG_{28} triol compared to the HG_{28} keto-diol, though there are a few significant declines in the NST and SST-S records that occur around the same time as declines in HDI_{28} in the same samples (Figure 3.12). In the future the samples could be run at higher concentrations in order to get more accurate measurements of the HG_{28} triol and HG_{28} keto-diol.

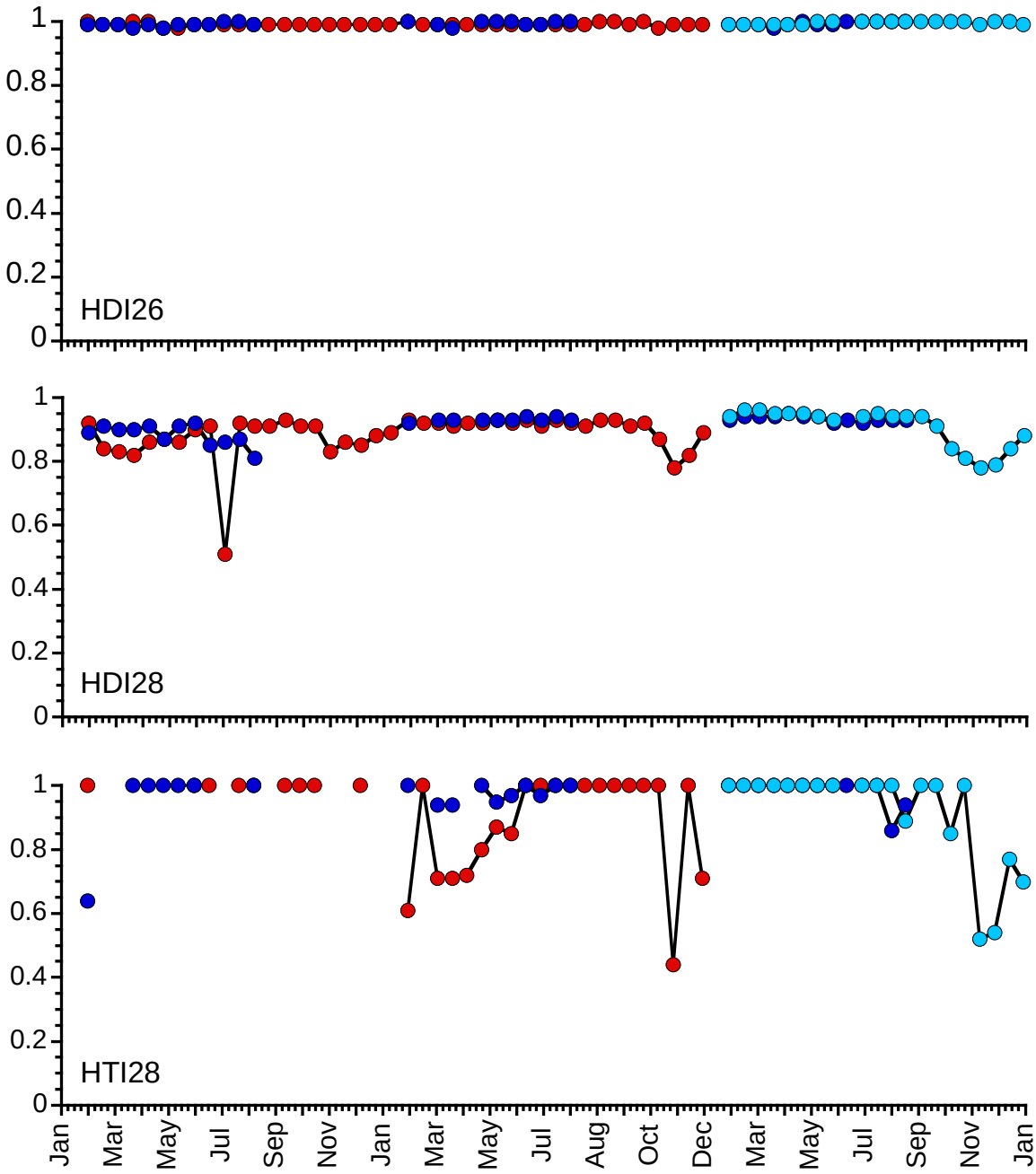

Figure 3.12: Variations in HDI_{26}, HDI_{28}, and HTI_{28} calculated from distributions of SPM HGs. Red circles = NST, dark blue circles = SST-D, and turquoise circles

4. DISCUSSION

4.1 MASS ACCUMULATION RATES AND SOURCES OF SPM IN THE METALIMNION

Surface cores previously collected from Lake Malawi exhibit seasonally deposited light-dark varves that represent the two primary modes of sedimentation at the lake floor (Owen & Crossley, 1989; Pilskaln & Johnson, 1991). The light laminae are completely dominated by diatom frustules, as they are deposited during austral winter when strong southerly winds drive the upwelling of nutrient-rich metalimnetic waters that sustain maximum diatom productivity (Johnson et al., 2001; Pilskaln & Johnson, 1991). The dark laminae reflect a mix of diatomaceous ooze, clay, fine organic matter, and terrestrial material, which includes plant fragments, mica flakes, and silt (Pilskaln & Johnson, 1991). Dark layers are deposited during austral summer when ephemeral rivers and streams carry terrestrial material into the lake and export of autochthonous material decreases due to reduced primary productivity under the stratified conditions that form when wind stress slackens during this season (Eccles, 1974; Pilskaln & Johnson, 1991; Pilskaln, 2004). Notably, surface cores in the SB only contain laminated sequences when the oxic-anoxic interface was above the basin's sediment surface during periods of high lake levels or low mixing strength (Pilskaln & Johnson, 1991; Brown et al., 2000).

This seasonal pattern of sedimentation in Lake Malawi was corroborated by an analysis of SPM collected in the hypolimnion from 1987 - 1992 by Pilskaln (2004). The study observed sedimentation in the NB and CB and found an annual peak in mass accumulation rates at both sites that was driven by fluxes of biogenic silica (BSi) generated during the dry/windy season. The exact timing of this peak within the dry/windy season (e.g. beginning of, end of), however,

did deviate between years, likely due to interannual variability in the environmental conditions of the epilimnion that stimulate diatom blooms (Pilskaln, 2004). Sedimentation during the remainder of the year was minimal, though what material was collected appeared terrestrial in origin (Pilskaln, 2004). A later sediment trap study detailed in Bootsma and Hecky (1999) and Bootsma et al. (2003) revealed the nuances of sedimentation in Lake Malawi. This later trap study describes seasonal (3-4 month) trends in SPM export in the upper mixed layer of the lake, rather than the hypolimnion, from 1997 – 1999. While the authors did also observe a primary peak in mass accumulation rates that occurred in the dry/windy season – between May – September in the NB and between September – December/January in the CB and SB – the SPM collected in the Bootsma and Hecky (1999) study differs from that of the Pilskaln (2004) study in both the composition and amount of sediment collected. The shallower Bootsma and Hecky (1999) study consistently recorded higher mass accumulation rates than those of the Pilskaln study, particularly in the traps positioned in the metalimnion at 140 m and 180 m depth (Bootsma and Hecky, 1999; Pilskaln, 2004). In addition, SPM collected in the Bootsma and Hecky (1999) study had greater overall percentages of lithogenic material, though the dry/windy season peaks in total mass flux still contained large percentages of BSi (Bootsma and Hecky, 1999; Bootsma et al., 2003), compared to that of the Pilskaln (2004) study. Interestingly, at the 100 m water depth SB site of Bootsma et al. (2003), secondary fluxes of BSi were recorded during May – September that, in some years, reached similar magnitudes as the primary BSi flux in September – January.

Trends in bulk sedimentation in Lake Malawi over the last two decades can be inferred by comparing the results presented here to the previous two sediment trap studies in the lake, described above. In contrast to the single seasonal peak in sedimentation observed in the previous studies, SST-D, SST-S and NST record two peaks in total mass flux each year. At NST, elevated sedimentation rates occur at the beginning of the cool/dry season and at the start of the warm/wet season, though the former is more pronounced in 2011 than in 2012. As only two years of data are available from this trap, it is unclear if the pattern in sedimentation in 2011 is anomalous or characteristic in the modern-day basin. In SST-D and SST-S, the timing of the two peaks in total mass flux is closer, with one at the end of the warm/wet season and the second at the beginning of the dry/windy season. The presence of two annual peaks in sedimentation in the SB appears to be a consistent pattern based on the three years of data collected here. The possible

origins of the secondary peaks in total mass flux will be discussed below after first exploring changes in the magnitude of mass flux in Lake Malawi.

The maximum peak in seasonally averaged (time frames for seasons were based on the definitions in Bootsma and Hecky, 1999) total mass flux at SST-D (115 – 125 m) was 1097 mg m^{-2} d^{-1}, which is greater than the maximum fluxes recorded at both 100 m and 140 m in the SB in 1997/1998 (Bootsma and Hecky, 1999**)**. Seasonal averages of bulk sedimentation reach up to 1432 mg m^{-2} d^{-1} at NST (170 m). This is more than twice as large as the maximum peak measured at 180 m water depth in the CB in 1997/1998, which was 601 mg m^{-2} d^{-1} (Bootsma and Hecky, 1999**)**. The highest mass accumulation rate at 350 m water depth in the NB in the Pilskaln (2004) study was only 484 mg m^{-2} d^{-1}, substantially lower than the average NST values from this study.

Bootsma and Hecky (1999) found that increases in sedimentation rates observed in both the water column and sediments of the SB were primarily due to higher accumulations of BSi, though a quarter of the increase was attributed to an additional rise in minerogenic material. The authors hypothesized that these changes are due to population growth concentrated in the SB that is fueling rapid land use change around this end of the lake. Deforestation and agricultural development in the basin has caused reduced vegetation cover in southern Malawi; resultant increases in erosion of watershed soils has contributed high sediment loads to the SB catchment rivers that are, in turn, delivering more lithogenic material to the lake than in previous decades (Bootsma, 1993; Cohen et al., 1997; Hudak and Wessman, 2000). Concomitant increases in bioavailable phosphorous concentrations in the Bootsma and Hecky (1999) samples are likely derived from riverine inputs of the phosphorous-laden fertilizers used in the catchment (Hecky et al., 2003). Increased loadings of such nutrients would promote and sustain elevated levels of diatom productivity that substantiates the observed increase in BSi fluxes (Bootsma and Hecky, 1999; Guildford et al., 2007). Low minerogenic fluxes accumulating in nearshore deposits in the NB led Bootsma and Hecky **(**1999**)** to claim that sedimentation in the basin decreased during the twentieth century. As cultivation of the northern end of the catchment is not as extensive as in the southern end, changes in the fluxes of terrestrial material to the NB are dictated by the intensity of precipitation during the wet season rather than anthropogenic effects (Milliman and Syvitski, 1992; Bootsma and Hecky, 1999). Low precipitation in the region from 1970 – 1994, relative to the 1896 – 1994 average (Calder et al., 1995), corroborates the findings of Bootsma and Hecky

(1999). In this study, however, total mass fluxes to NST are greater than those to SST-D in both 2011 and 2012, contradicting the notion that sedimentation is higher in the SB of Lake Malawi, and could indicate a change in sediment delivery and cycling in the lake since the turn of the century.

Detailed compositional analyses of SPM from this study are available for the samples collected in 2011. Average BSi fluxes to SST-D in 2011 are comparable to those of Bootsma and Hecky (1999) (Zakaria and Hecky, *unpublished data)*, suggesting that rates of diatom productivity in the basin have not increased substantially between 1997 and 2011. Furthermore, only the June – August peak in total mass flux in SST-D is associated with a peak in BSi flux (Zakaria and Hecky, *unpublished data*). The increases in total mass fluxes in the basin can instead be attributed to a 57% increase in the average lithogenic flux at this location (Zakaria and Hecky, *unpublished data).* If the increase in the flux of lithogenic material in the SB represents a continuation of the trend in increased contributions of topsoil erosion via terrestrial runoff, there should be a chemical signal of terrestrial material in the SPM. The low C_{org}:N_{org} values of SPM collected in SST-D (Appendix B) implies that the organic matter (OM) has a primarily aquatic source. The consistency of the C_{org}:N_{org} signal throughout the time series further suggests that terrestrial OM inputs are not significant at any point during the year, including the rainy season (Figure 3.3d). Both periods of high total mass fluxes in NST in 2011 were dominated by lithogenic material, but, as in SST-D, only the second peak in total mass flux contained elevated fluxes of BSi (Zakaria and Hecky, *unpublished data*). The peak in total mass flux that occurs earlier in the year, at the end of the warm/wet season, is almost entirely composed of lithogenic material (Zakaria and Hecky, *unpublished data)*, with increases in POC and PON flux at this time that are only half the size of those that are associated with the peak in sedimentation that takes place at the end of the dry, windy season (Figure 3.3b,c).

Examination of the timing of the peaks in bulk sedimentation in the NB and SB provides insights into the source of the lithogenic material that is driving high modern sedimentation rates. Bootsma et al. (2003) noted that at sites from their 1997 – 1999 sediment trap study where two traps were positioned along the same mooring, the deeper traps received higher relative fluxes of lithogenic material. The source of the additional lithogenic material at depth was believed to be resuspended slope material that laterally advected from non-depositional shallow environments to deeper waters. While complete compositional analyses are not available for SST-S or SST-D

samples collected in 2013, the only year from this study where a comparison of fluxes with depth can be made, the total mass fluxes during this period are higher in SST-D, suggesting a similar pattern of lateral transport in the basin. Furthermore, it is possible that this resuspended material was transported to the NB in 2011 during a period of strong internal circulation in the lake. This would provide a satisfactory explanation for the peak in lithogenic flux in May 2011 at the site that is not matched by elevated organic fluxes or changes in OM isotopic composition that would be expected with increases in primary productivity or terrestrial runoff. Oscillating temperatures in the warm/wet season recorded by the intermediate-depth thermistors are likely artifacts of internal seiche waves that rock the thermocline across the NST and SST moorings (Figure 3.1). Seiche activity has been demonstrated to intensify under stratified conditions in lakes as turbulence associated with high wind stress can reduce the degree of horizontal propagation of internal waves (Bootsma, 1993; Simpson et al., 2015). Amplification of internal waves varies interannually, therefore it is possible that favorable conditions for their formation were lacking in 2012 and thus there is no significant lithogenic flux in the NB that year, though it is difficult to say for certain due to the lack of complete thermistor data. Upwelling is typically stronger in the SB year round, and can even take place during the stratified season (Hamblin et al., 2003). This could explain the regular peak in mass flux in the SB at the end of the warm/wet season though unfavorable conditions for diatom productivity may be why there is no matched increase in BSi flux.

4.2 SOURCES OF GDGTS IN SPM

4.2.1 Seasonality of GDGT production

Fluxes of brGDGT and isoGDGT CLs in SPM generally follow trends in bulk sedimentation rates (Figure 3.5). Fluxes of TOC in SPM exhibit a significant positive correlation to bulk sedimentation in NST, SST-D, and SST-S (Figure 4.1). Coincident fluxes of CL GDGTs and C_{org} have been observed in other large (e.g. Woltering et al. 2012) and small lakes (e.g. Sinninghe Damsté et al. 2009), as well as in the marine water column (e.g. Wuchter et al. 2006;

Yamamoto et al. 2012). In these studies, the covariance of CL GDGT and TOC fluxes was interpreted as meaning that the export of GDGTs in the water column was due to particle entrainment, packaging of lipids into fecal pellets, and/or adsorption of lipids to clay grains/larger organic molecules. Consequently, elevated fluxes of CLs in Lake Malawi SPM do not necessarily reflect periods of active Thaumarchaeotal growth but are more likely related to large-scale sedimentation processes occurring in the lake.

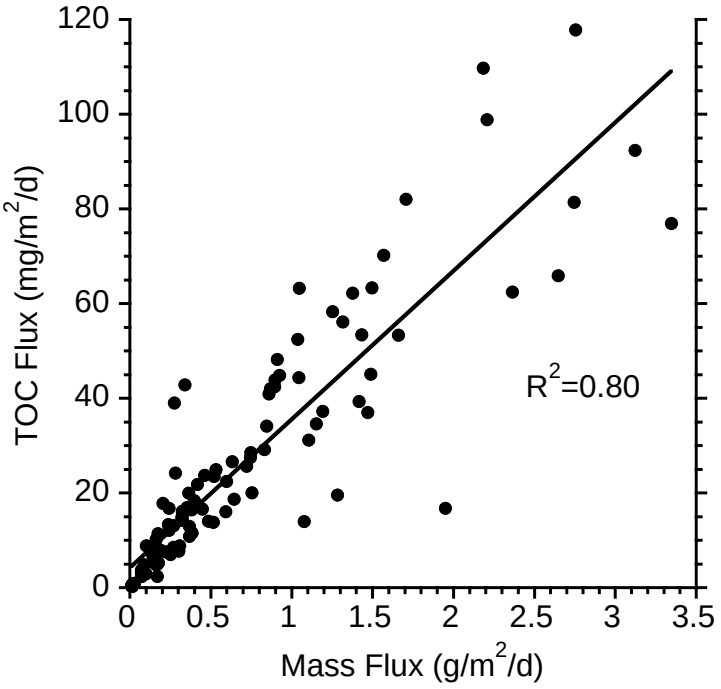

Figure 4.1: Correlation of total mass flux and TOC flux of all SPM samples, $p<0.001$

The strength of the correlation between CL and TOC fluxes does vary between the NB and SB, however, suggesting that additional factors drive the export of GDGTs in the water column of Lake Malawi (Figure 4.2). The correlation between isoGDGT flux and TOC flux is strongest in the NST with an R^2 of 0.71 and $p<0.001$ (Figure 4.2c,f). The much weaker correlation, $R^2=0.28$, between isoGDGT flux and TOC flux in SST-D is likely due to the diminished fluxes of isoGDGTs to the trap in 2013 despite relatively high bulk sedimentation, though the relationship is still significant, $p<0.001$ (Figure 3.5). This could possibly be due to low production of isoGDGTs in the South Basin in 2013 such that the size of the CL pool was smaller, resulting in less export of the lipids when sedimentation occurred. Similarly, the

correlation between isoGDGT flux and TOC flux in SST-S is stronger than that of SST-D with an R^2 of 0.4, but the relationship is not significant $p>0.001$. This might be due to lower abundances of isoGDGTs in the shallow trap overall as isoGDGTs are predominantly produced in deeper waters (Woltering, 2011), which will be discussed in further detail in the section below, or due to conflicting inputs of isoGDGTs from various planktonic archaea (Turich et al., 2007; Buckles et al., 2014; Villanueva et al., 2014).

The correlations between brGDGT flux and TOC flux decrease in both NST and SST-D when the full suite of brGDGTs was analyzed compared to samples for which only the non-cyclized structures were monitored, and the correlation for SST-D becomes insignificant, $p>0.05$ (Figure 4.2). The relative abundance of cyclized brGDGTs, particularly those with two cyclopentane moieties, correlate with depth of the water column in other African Lakes (Buckles et al., 2014; Loomis et al., 2014). The chemical structure of GDGTs is well preserved during export through the water column (Kim et al., 2009), even in the case of ingestion and packaging of the lipids into fecal pellets by zooplankton (Wuchter et al., 2006), so it is unlikely that changes in the distributions of GDGTs with depth are the result of diagenetic processes. The correlation between cyclized brGDGTs and water depth more likely indicates that deeper-dwelling brGDGT-producing bacteria preferentially synthesize brGDGTs with cyclopentane moieties. Thus, it is possible that the inclusion of these compounds in analyses reduces the correlation between brGDGT flux and TOC flux if their abundance in SPM is driven by different environmental controls. The decrease in correlation is most dramatic in SST-D due to an unusually high flux of brGDGTs at this site in April 2012. In a three-year analysis of CL and IPL brGDGTs in the water column of a smaller African lake, Lake Challa, Buckles et al. (2014) also observed an irregular pattern of brGDGT fluxes that contained only a single prominent peak during the time series. Given that the SB of Lake Malawi is shallower than the NB, conditions affecting bacteria in the SB may be more comparable to those in Lake Challa. As such, the dominant brGDGT producing community in the SB may be outcompeted by other microbial groups for much of the duration of the time series and only flourish when certain conditions are met. In Lake Challa, the primary flux in brGDGTs occurred during a year of especially low precipitation. Precipitation around Lake Malawi in 2012 was near average values for 1991 – 2015, so it remains unclear what could have prompted the rise in brGDGT flux at this time.

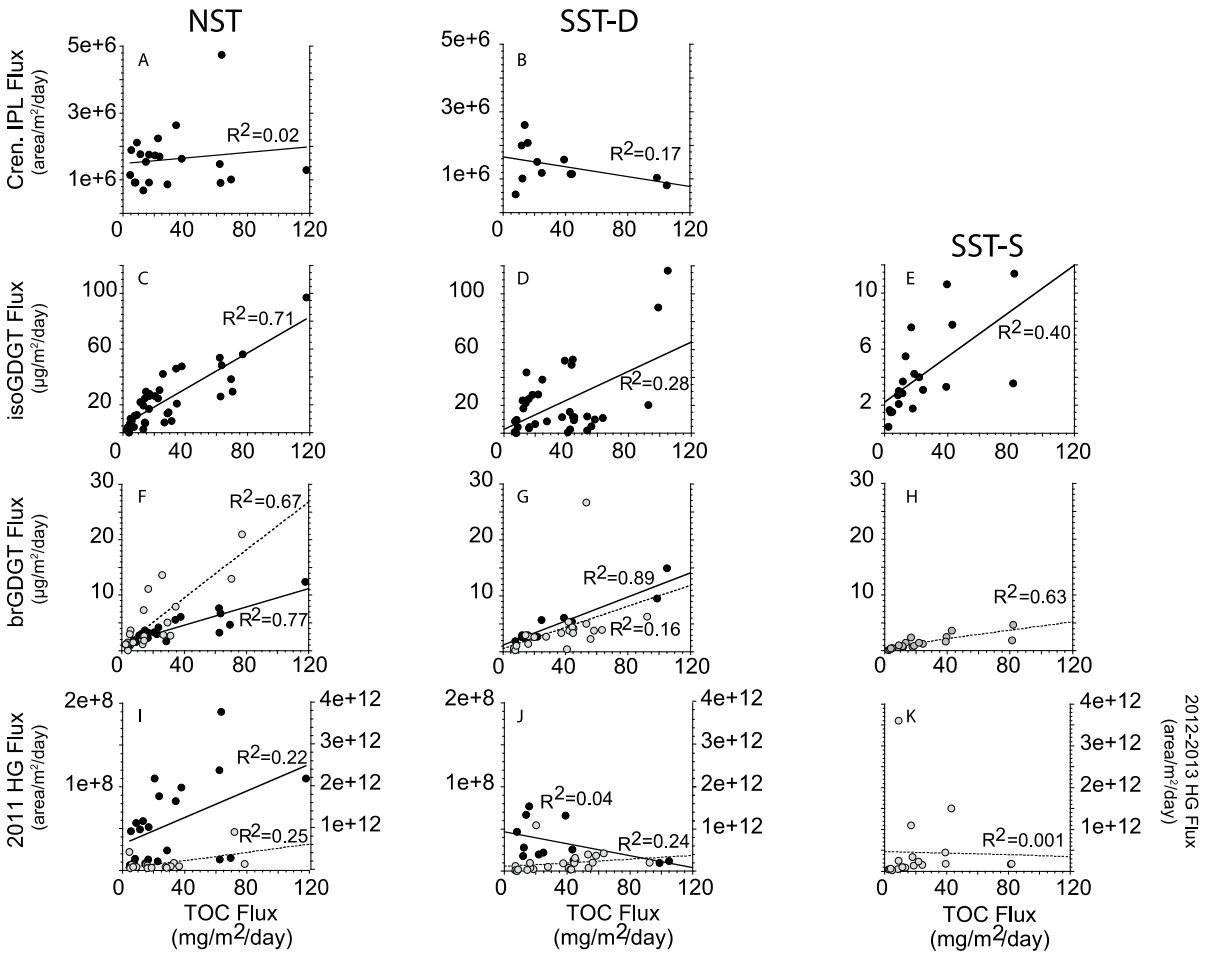

Figure 4.2: Correlations among TOC fluxes and fluxes of crenarchaeol IPLs (a, b), CL GDGTs (c – h), and HGs (i – k) in NST, SST-D, and SST-S. Grey circles in panels f – k represent samples that were run using different methods that samples with black dots, which may have altered the distributions of the lipid class.

The relative lability of IPLs to CLs makes them more reliable tracers of active GDGT production; the presence of intact polar head groups in SPM is an indicator of active or recently living cells because generally the phospholipid head groups are degraded quickly after cell death (White et al. 1979; Harvey et al., 1986; Pitcher et al., 2009b). The fluxes of HPH-, DH-, and MH-crenarchaeol in both the NST and SST-D show very weak correlations with TOC flux, R^2 of 0.02 and 0.17 for NST and SST-D respectively, that are highly insignificant $p>0.1$ (Figure 4.2a,b), illustrating that trends in IPL export are largely independent of bulk sedimentation processes. Examining the abundances of crenarchaeol IPLs collected should therefore provide a better picture of when Thaumarchaeota are living in Lake Malawi.

In other lacustrine systems, the period of maximum Thaumarchaeotal activity follows the primary phytoplankton bloom (e.g. Sinninghe Damsté et al. 2009**)** due to the abundance of NH_4^+ released from the mineralization of planktonic biomass that stimulates growth of nitrifying Thaumarchaeotal communities living near the oxic-anoxic interface. BSi and TOC fluxes are closely related to the period of the primary phytoplankton bloom, and both reach maximums in the NB in 2011 in November. This timing is consistent with previous studies of biomass and photosynthetic rates in Lake Malawi, which also determined that peak phytoplankton activity, dominated by diatoms, takes place during/at the end of the dry/windy season (Bootsma & Hecky, 1999; Guilford et al. 2007). Maximum fluxes of HPH-, DH-, and MH-crenarchaeol in NST also occur in November (Figure 3.4), thus it appears the Thaumarchaeotal community of Lake Malawi responds to the same ecological conditions as in other systems. A study by Guildford and Taylor (1999) demonstrated that lake-wide NH_4^+ concentrations are highest at this time as well, which lends further support to the source of isoGDGTs in Lake Malawi are nitrifying archaea. The flux of isoGDGT CLs in NST at this time is twice as large as the peak that occurs earlier in the year, so it is possible that GDGTs in SPM reflect a mix of fresh and old material. The residence time of GDGTs in the water column of Lake Malawi has not been previously determined, though it likely depends on a combination of factors, including the composition of bulk sediment in the epilimnion, the strength of the seasonal diatom bloom, and the strength of mixing of the epilimnion and metalimnion. Interannual variability in these factors would determine the relative amounts of material exported to deeper waters and, consequently, the amount of the CL pool that remains in suspension. Only half of the annual trend in crenarchaeol IPL fluxes is resolved at SST-D, thus the timing of primary crenarchaeol production remains uncertain. Nonetheless, at this location BSi, TOC, and crenarchaeol IPL fluxes peak in June, so if the relationship observed between these fluxes in the NB holds for the SB, then this may represent the actual period of Thaumarchaeota activity in the basin.

As brGDGT IPLs were not analyzed in this study, it difficult to determine with certainty when brGDGTs are produced in the lake with the current dataset. It is still possible to speculate based on what is known about the ecology of aquatic brGDGT producers, though information on this subject is extremely limited. Weber et al. (2015) suggested that aquatic-brGDGT producers living in the alpine Lake Hinterburg in Switzerland are methanotrophs due to the extremely depleted $\delta^{13}C$ composition of brGDGT alkyl chains (-43‰ to -46‰). However, a recent study by

Colcord et al. (2017) found that the brGDGTs in Greenland lake sediments have $\delta^{13}C$ compositions of ~ -27‰ to -32‰, which are not nearly as depleted as the lipids from Lake Hinterburg. Colcord et al. (2017) suggest that the source organisms of these brGDGTs use distinct pools of carbon under varying seasonal conditions due to the difference in carbon isotopic composition of IIIa and IIa, the latter of which would be preferentially produced in the winter. To date, there are no compound specific isotope measurements of GDGTs from tropical lakes so it is unclear how aquatic brGDGTs living in these environments behave relative to those living in the polar and alpine regions examined in the aforementioned studies. A study of brGDGT IPLs in a different east African lake, Lake Challa, has demonstrated that *in situ* production of brGDGTs in that water column was highest in the anoxic portion of the water column (Buckles et al., 2014). In Lake Malawi, CL brGDGTs are in higher abundance in the anoxic water column (Figure 3.5; Woltering, 2011), so it is possible that brGDGT producers in Lake Malawi also live below the chemocline. As such, the aquatic brGDGT-producing community is likely more active during the warm, wet stratified season rather than the dry, cool season when convective mixing expands the oxygenated portion of the water column.

Slight increases in the BIT index during the warm/wet season in all basins lend support to this idea (Figure 3.6). It is also possible that the increase in BIT during the warm/set season is due to influxes of terrestrial brGDGTs to the lake. As there is no available data on brGDGT distributions of Lake Malawi catchment soils, it is difficult to say with certainty if the increase in BIT during the rainy season is due to enhanced input of soil-derived brGDGTs or enhanced production of *in situ* brGDGTs. But if the rise in BIT index were related to surface runoff, brGDGT distributions in SPM should contain terrestrial signals such as an increase in the relative proportion of brGDGT I and decreases in the isomerization ratio, as these distributions are typical of terrestrial brGDGTs in mesoclimatic regions (De Jonge, Hopmans, et al., 2014; Günther et al., 2014; Peterse et al., 2012; Tierney et al., 2012; Xiao et al., 2015). Neither trend occurs in Lake Malawi SPM. Furthermore, all of the major rivers flowing into Lake Malawi are situated along the western shore. As the sediment traps were moored at center-east locations within the NB and SB, they should be at distances great enough such that the influence of river-borne sediment is minimal (Halfman & Scholz, 1993; McCullough et al., 2007; Ellis et al., 2015). The Ruhuhu River is an exception as it flows into the lake from the northeastern shore, but it is still further south than the location of the NST, and too far from the SB to have any

significant influence on the southern traps SST-D and SST-S. Based on these lines of evidence, it can be concluded that brGDGTs in Lake Malawi are most likely produced during the warm, wet season.

4.2.2 Sources of isoGDGTs in settling particulate matter

Many groups of archaea produce isoGDGTs, however the TEX_{86} proxy is exclusively based on those produced by Thaumarchaeota. In order to appropriately apply the proxy, it must first be demonstrated that contributions of GDGTs to the total CL pool from other sources are minimal. We have several lines of evidence to suggest that non-Thaumarchaeotal lipids do not significantly impact the Lake Malawi SPM samples.

First, the presence of Thaumarchaeota in Lake Malawi is indirectly apparent due to the presence of the Thaumarchaeota biomarker, crenarchaeol (Sinninghe Damsté et al., 2002**),** in SPM in both the CL and IPL form. The only organisms observed to produce crenarchaeol in culture studies thus far belong to Thaumarchaeota or Group I.1a Crenarchaeota, the latter of which is mostly of importance in contributing crenarchaeol in soil environments (Pitcher et al., 2010; Schouten et al., 2008; Sinninghe Damsté et al., 2002; Wuchter et al., 2004, 2006). As discussed above, the timing of peaks in crenarchaeol IPL abundance coincides with periods of elevated NH_4^+ in the lake. This lends support to the idea that the producers of crenarchaeol in the lake are nitrifying organisms, which, thus far, Thaumarchaeota are the only archaea identified with this capacity (de La Torre et al., 2008; Könneke et al., 2005; Pester et al., 2011; Stahl & de la Torre, 2012). Crenarchaeol is overwhelmingly the most abundant isoGDGT in all SPM samples (Appendix C), further suggesting a dominance of Thaumarchaeota throughout the time series. This is not absolutely conclusive, however, as CL isoGDGTs may have a long residence time in the water column such that distributions are not necessarily reflective of the active populations (Ingalls et al., 2006; Turich et al., 2007; Lengger et al., 2014).

Analyzing the distributions of the other isoGDGTs will additionally help to disentangle the source of these lipids, as there are consistent trends in distributions associated with different groups of archaea. Methanogenic Euryarchaeota are associated with a dominance of GDGT-0 (Turich et al., 2007), thus the ratio of GDGT-0/crenarchaeol is indicative of the relative

abundance of methanogens to Thaumarchaeota (Zhang et al., 2016). Values < 2 indicate that samples are likely not significantly impacted by methanogen-derived GDGTs, a standard that has been broadly adopted when interpreting TEX_{86}-based paleotemperature records, including in Lake Malawi (Johnson et al., 2016). Though there are a few samples where the GDGT-0/crenarchaeol ratio increases slightly, all SPM samples fall well under the benchmark value, and the ratio remains mostly unchanging throughout the three-year period (Figure 4.3)

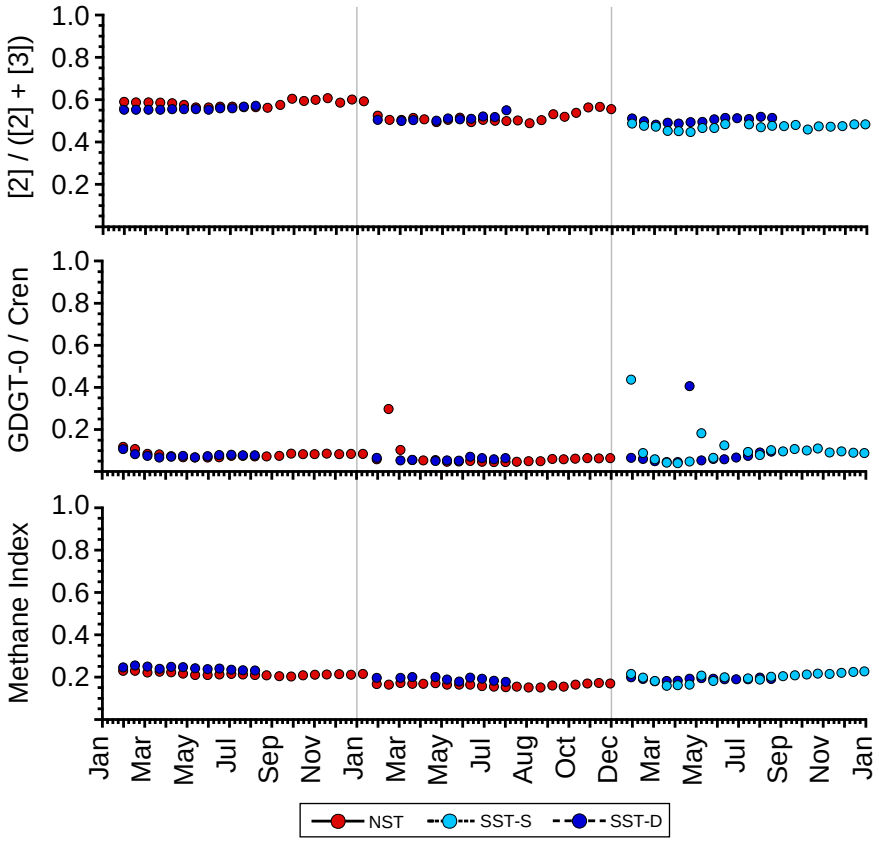

Figure 4.3: Variability in the Methane Index, GDGT-0/Crenarchaeol, and GDGT-2/GDGT-2 + GDGT-3 isoGDGT-based indices in Lake Malawi that are used to determine archaeal sources of isoGDGTs in environmental samples.

Methanotrophic Euryarchaeota can produce GDGT-1, GDGT-2, and GDGT-3, but not crenarchaeol (Blumenberg et al. 2004; Pancost et al., 2001). Zhang et al. (2011) thus proposed the Methane Index (MI) to examine the relative proportions of GDGTs with 1 – 3 rings to crenarchaeol and its regio-isomer to detect past changes in abundances of methane oxidizing archaea in marine environments. MI values of < 0.3 reflect "normal marine" environments, while

values above this indicate greater contribution of GDGTs from methanotrophic Euryarchaeota, and which is possibly related to the presence of methane-hydrates at the sediment floor. All Lake Malawi SPM values from this study fall well within the normal marine range, with the highest value reaching 0.26 (Figure 4.3). As Thaumarchaeota still do produce GDGT 1 – 3, and tend to produce the more cyclized structures in warmer environments, it is expected that the MI values of GDGTs in tropical environments would be on the upper end of this range (Zhang et al., 2011). Moreover, the extremely strong correlation between GDGT-0 + crenarchaeol and crenarchaeol fluxes throughout the time-series (Figure 4.4) indicates a single source for crenarchaeol and the other isoGDGTs to the sediment traps (Woltering et al., 2012).

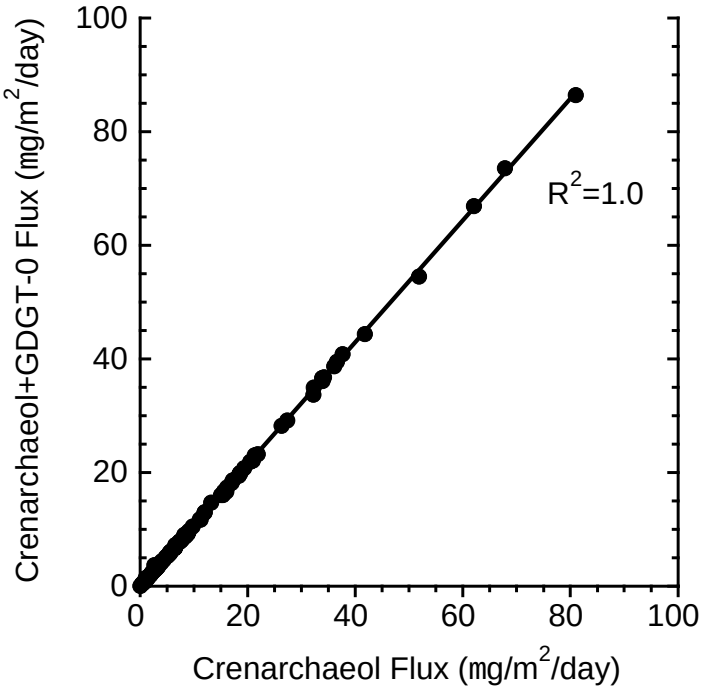

Figure 4.4: Correlation between crenarchaeol and crenarchaeol+GDGT-0 fluxes. Fluxes are in μg/m^2/day and normalized to TOC, p<0.001

Lastly, a study by Villanueva et al. (2014) examined parallel changes in GDGT distributions and archaeal populations with depth in the Arabian Sea. The authors found that Thaumarchaeota living in shallow and deep waters belong to distinct phylogenetic groups based on differences in the gene that encodes for GDGT precursor molecules. The deeper-dwelling group was observed to produce higher proportions of GDGT-2 relative to GDGT-3, with ratios of GDGT-2/GDGT-3 reaching ~6 for CLs and ~12 for IPLs at the depth of their maximum

abundance (Villanueva et al., 2014). GDGT-2/GDGT-3 of CLs in globally distributed surface sediments (Kim et al., 2010b) can reach up to ~7, indicating that this deep-dwelling Thaumarchaeotal community can impact sedimentary distributions of isoGDGTs (Villanueva et al., 2014). The lower values for CLs are likely because the CL pools at depth in the water column and in sediments reflect mixtures of *in* situ-derived isoGDGTs and GDGTs exported from the oxic waters above. The link between isoGDGTs and Thaumarchaeota phylogeny by Villanueva et al. (2014) confirms the hypotheses of earlier studies of isoGDGTs in the marine column (Hernández-Sánchez et al., 2014; Villanueva et al., 2014; Wuchter et al., 2005) and lacustrine water column (Sinninghe Damsté et al., 2009**)** that attributed similar changes in the GDGT-2/GDGT-3 ratio with depth as reflective of changing archaeal communities. The ratio of GDGT-2/GDGT-3 in Lake Malawi SPM has a much narrower range that what is observed in these marine environments, with values measured between 0.8 – 1.6. The stability of the ratio in throughout the time-series further suggests that inputs of isoGDGT lipids to the traps from any deeper dwelling community to the traps are minimal.

A recent analysis of archaeal populations inhabiting the water column of Lake Malawi conducted by Woltering (2011) confirms much of what is hypothesized above. As the sediment traps of this study were moored in both the metalimnion and epilimnion, it is important to turn to the Woltering (2011) study in order to comprehensively evaluate isoGDGT production throughout the upper layers of the water column. Woltering (2011) analyzed archaeal genetic material and GDGT distributions in particulate organic matter (POM) along vertical profiles that extended to 300 m in the NB and CB, and to 150 m in the SB, during Malawi's warm/wet season. The study noted maximum abundances of HPH-crenarchaeol, the most labile form of intact polar crenarchaeol (Lengger et al., 2014b), at ~50 m water depth in the NB and CB, and ~30 m water depth in the SB, which are coincident with peaks in 16s rRNA counts of archaeal genetic material detected with a general archaeal primer (Woltering, 2011) and amoA gene abundances (Muñoz Ucros, 2014). Taken together, this information strongly supports the presence of a Thaumarchaeotal community living at the oxic-suboxic boundary, consistent with numerous other studies of Thaumarchaeota in stratified systems (e.g. Sinninghe Damsté et al., 2009; Zhang et al., 2011; Schouten et al., 2012; Schouten et al., 2013). In the NB, a primer intended to detect 16s rRNA material specific to Marine Crenarchaeota Group 1 (MCG1), identified a second archaeal community at 200 m. However, concentrations of HPH-crenarchaeol

at this depth are an order of magnitude lower than the peak at 50 m in the basin and there is 0.2 increase in the GDGT-2/GDGT-2 + GDGT-3 ratio between the two locations, implying that this deeper archaeal community may not actually belong to Thaumarchaeota. Indeed, since the time of the Woltering (2011) study, the MCG1 primer has been revealed as ineffective at appropriately specifically capturing Thaumarchaeotal populations (Buckles et al., 2013) but may instead be a more general archaeal primer.

Though the POM data from Woltering (2011) is only a snapshot of annual isoGDGT production in the water column, the greater magnitude of the HPH-crenarchaeol peak at 50 m relative to the one at 200 m implies that this deeper dwelling archaeal group does not contribute a significant portion of crenarchaeol to the CL pool. Abundances of all CL isoGDGTs are also greater at 50 m compared to 200 m water depth, with concentrations that are twice as great (Woltering, 2011). The GDGT-2/GDGT-2+GDGT-3 ratio of CL isoGDGTs collected in the sediment traps of this study exhibit average values of 0.55 in the NST and 0.52 in SST-D (Appendix D). These values are more similar to the measurements by Woltering (2011) of POM samples collected near the depth of maximum Thaumarchaeota abundance, where at 50 m in the NB the index was 0.54 ± 0.04, and at 30 m in the SB the index was 0.55 ± 0.03. The deep-dwelling archaeal population was only detected in the NB where the GDGT-2/GDGT-2+GDGT-3 index had a value of 0.74 at 200 m water depth (Woltering, 2011). The low standard deviation of the index in NST SPM provides additional evidence that contributions of isoGDGTs from the deeper-dwelling archaeal population in Lake Malawi are insignificant.

4.2.3 Sources of brGDGTs in settling particulate matter

BrGDGTs in Lake Malawi SPM may be derived from soil runoff, an *in situ* source, or some combination of both. As discussed above, soil-derived GDGTs are likely minimal in the SPM samples from this study due to the location of the traps within the lake and the lack of evidence for significant terrestrial OM inputs. If brGDGTs in Lake Malawi SPM are primarily derived from soil runoff, their fluxes are expected to be highest during the rainy season, as observed in Lake Challa (Buckles et al., 2014; Sinninghe Damsté et al., 2009). However, similar to isoGDGTs, brGDGT fluxes correlate more strongly to TOC fluxes, which are driven by

internal processes in Lake Malawi (Figure 3.3f,g,h). Many studies of brGDGTs in lacustrine environments have documented *in situ* production of the lipids in the water column, potentially contributed by multiple distinct bacterial communities living in both oxic and anoxic waters (Blaga et al., 2011; Buckles et al., 2014; Colcord et al., 2015; Liu et al., 2014; Tierney et al., 2012; Weber et al., 2015). In Lake Malawi, CL brGDGT concentrations in POM increase significantly below the thermocline, showing maximum abundances at 100 m in both the NB and CB and at 50 m in the SB (Woltering, 2011), depths at which suboxic conditions are present in the lake. Fluxes of brGDGTs to the traps on the same mooring in the SB in 2013 were greater in the deeper trap at 115 m than in the shallow trap at 50 m, however this could be due to higher export of brGDGTs that are produced around the depth of the 50 m trap to the deeper site. Moreover, concentrations of brGDGTs at 150 m in the SB were still significant (75% as great as concentrations at 50 m), so there may be an additional source of brGDGTs in the deeper waters of the basin. The location of maximum brGDGT production in suboxic waters may point to source organisms that are microaerophilic or a facultive anaerobes/aerobes.

The distributions of brGDGTs in Lake Malawi SPM are similar to those from other aquatic environments (e.g. Huguet et al., 2015; Loomis et al. 2014b; Naeher et al., 2014; Tierney et al., 2012). Moreover, the high abundance of 6-methyl isomers relative to 5-methyl isomers (Figure 3.8) appears to be diagnostic of aquatically-produced brGDGTs (De Jonge et al., 2014; Ding et al., 2016; Sinninghe Damsté, 2016; Weber et al., 2015). In the study by Weber et al. (2015) that examined brGDGT distributions in the seasonally stratified alpine Lake Hinterburg, the authors found additional isomers of brGDGT IIIa with a methyl group at each the C5 (C5') and C6 (C6') positions rather than all previously identified brGDGTs that have additional methyl branches at either exclusively the C5/C5' or C6/C6'. This 5/6-methly isomer was not present in the surrounding soils, and was thus deemed a biomarker for aquatically produced brGDGTs (Weber et al., 2015). Notably we do not find any of these 5/6-methyl isomers in Lake Malawi SPM, though it may have been present below the detection limit as overall concentrations of brGDGTs were quite low.

Weber et al. (2015) additionally found the compound specific $\delta^{13}C$ of brGDGTs from Lake Hinterburg had extremely ^{13}C-depleted values, suggesting the producers of brGDGTs in that system were methanotrophs. As isoGDGT distributions indicate low abundances of methanotrophic archaea, it is likely that methanotrophic bacteria are in similarly low abundances

in Lake Malawi, which would explain why the 5/6-methyl isomer is not detected in our samples. Colcord et al. (2015) did not find this structure in their Greenland lake sediments and suggested it may be because methanotrophy is not a dominant process in the Greenland lakes studied. The only other study to detect 5/6-methyl isomers was Ding et al. (2016), who analyzed surface sediments from a set of 37 alkaline lakes. The authors did not detail dominant microbial nutrient cycling processes in the lake so it is unclear how the abundance of the compounds in their samples relates to the ecology of organisms in the studied lakes. Therefore determining the lack of information regarding the bacterial communities living at depth in Lake Malawi makes it difficult to draw any conclusions about a (lack of a) methanotrophic source of brGDGTs based on the absence of 5/6 methyl compounds. Still, a significant presence of denitrifying bacteria living near the chemocline in Lake Malawi has been identified (Hecky et al., 1996) based on estimates of nitrogen fluxes. The abundance of brGDGTs in the suboxic waters of the lake where bacterially-mediated denitrification is occurring could possibly lend support to the Mueller-Niggemann et al. (2016) hypothesis that brGDGT-producers are denitrifiers.

4.3 APPRAISAL OF GDGT-BASED TEMPERATURE PROXIES

4.3.1 Effect of analytical methodology on GDGT abundances and distributions

Different analytical instrumentation and methodology were used for the measurement of GDGTs from SPM collected in 2011 versus SPM samples collected from 2012 – 2013, thus it is necessary to consider the extent to which these differences may have impacted the results presented here. A round-robin study of GDGT measurements in 35 labs found that the intralaboratory repeatability of TEX_{86} measurements made using the HPLC method described by Schouten et al. (2007) (LC_{CN}) fall within <1°C, while interlaboratory reproducibility ranges from 1°C to 3°C, proving that the robustness of the TEX_{86} proxy is comparable to other geochemical paleothermometers, such as Mg/Ca of foraminifera shells or $U_k^{37'}$ (Schouten et al., 2013). Some of the variability in the round-robin study was derived from differences in mass spectrometry employed, however there was no significant difference in measurements made using quadrupole

MS ($p > 0.5$) (Schouten et al., 2013). As both sets of Lake Malawi SPM samples were analyzed with a single quadrupole MS, variability due to instrumentation likely did not influence the dataset. The round-robin study additionally analyzed the repeatability and reproducibility of BIT measurements in the same samples, and found a higher degree of interlaboratory variability within samples of intermediate BIT composition ($0.2 < x < 0.8$) (Schouten et al., 2013). The scatter in BIT measurements between labs was attributed to differences in the response of MS systems to the lower molecular weight brGDGTs relative to isoGDGTs, which was previously described by Escala et al. (2009) and Schouten et al. (2009). In brief, the relative mass difference between brGDGT structures is much greater than that between isoGDGT structures, thus detection of the former is more sensitive to MS settings (e.g. mass calibration, tuning). As a standard mixture of crenarchaeol to the C_{46} internal standard was measured alongside both sets of samples here, changes in MS response for isoGDGTs were easily accounted for. Schouten et al. (2013) proposed the use of a standard mixture of isoGDGTs/brGDGTs based on molar ratios to correct for such MS biases (this had substantially improved reproducibility of BIT measurements). However, as the use of such a standard was not employed in this study it is impossible to ascertain differences in brGDGT detection between the two methods used.

Furthermore, it is possible that the analysis of samples using a cyano column/HPLC method (LC_{CN}) versus a two silica column/UHPLC method (LC_{Si}) may have also biased the detection of certain groups of GDGTs in one set over the other. Hopmans et al. (2016) found that the elution of GDGTs using the LC_{Si} method resulted in lower TEX_{86} values due to the separation of previously co-eluting isoGDGT isomers leading to decreased peak heights overall. Interestingly, we see no change in average TEX_{86} measurements in SST-D samples and actually a slight increase in average TEX_{86} from NST (Figure 3.6**)**, suggesting that, at least, the relative distributions of isoGDGTs are not affected by the stationary phase used for separation**.** BIT values of Lake Malawi SPM analyzed using the LC_{CN} method are similar to published values from surface sediments that were analyzed with the same method (Powers et al., 2011), however both are lower than values for SPM analyzed using LC_{Si}. The LC_{Si} method has been reported by Hopmans et al. (2016) to produce higher BIT values compared to samples run with LC_{CN}, however the authors did not provide an explanation for this beyond that the variability in BIT measurements between chromatographic methods fell within the range of interlaboratory reproducibility (Schouten et al., 2013).

The bias of BIT towards greater values in our SPM samples could be due to several factors. First, only a limited set of brGDGTs was monitored in SPM samples from 2011. Cyclized brGDGTs make up 5—30% of the total brGDGT pool in SPM samples from 2012—2013, therefore their exclusion would result in lower total brGDGT abundances. The BIT index is only based on the major brGDGT structures however, so inclusion or exclusion of cyclized brGDGTs would not affect this index. Interestingly, though average flux of brGDGTs in the NST is higher in 2012 samples as expected, the flux of brGDGTs in SST-D is similar between the three years despite the exclusion of cyclized compounds from detection in the 2011 samples. Higher BIT values could also result from lower detected abundances of isoGDGTs/crenarchaeol with the LC_{Si} method. Concentrations of crenarchaeol were tied to an internal standard and differences in MS detection of the internal standard and crenarchaeol were accounted for, so it is unlikely that isoGDGT abundances would be significantly skewed in this way. As changes in the relative detection efficiency of C_{46} and brGDGTs was not accounted for, applying the same correction factor for Crenarchaeol/C_{46} to brGDGT peaks could have led to an overestimation of brGDGTs in the 2012—2013 samples. This could explain why declines in fluxes of isoGDGTs in both the NB and SB in 2012 and 2013 are not matched by declines in brGDGT (Figure 3.5). While these constraints prohibit drawing comparisons of BIT values between 2011 and 2012-2013 samples, observing trends within sets analyzed under the same method is reasonable.

4.3.2 Temperatures reconstructed with TEX_{86}

TEX_{86} is remarkably consistent throughout the time-series in the NB (Figure 3.6), resulting in inferred temperatures that fail to capture seasonal variability in LST (Figure 4.5). The flux-weighted average TEX_{86} at this location is 0.77, which corresponds to a temperature of 28.9°C using the Powers et al. (2010) calibration. This value most closely matches the warmest temperature recorded at 7 m water depth in the basin, which was recorded during the austral summer. IsoGDGT distributions in Lake Malawi SPM that reflect summer temperatures are consistent with peaks in IPL crenarchaeol production early in the warm/wet season. If this is the singular period of isoGDGT production in the NB, then it makes sense that the CL pool consistently reflects summer temperatures regardless of the timing of export of CLs out of the

epilimnetic pool. That these TEX_{86}-inferred temperatures also match surface water measurements despite evidence that the dominant Thaumarchaeota live at ~50 m depth in the basin, agrees with some studies of isoGDGTs in SPM (Sinninghe Damsté et al., 2009; Wuchter et al., 2005, 2006). The RMSE of the Powers et al. (2010) TEX_{86} calibration is 5.6°C, so it is possible that the calibration simply produces a warm bias as the <3°C temperature difference between waters at 7 m and 50 m is well within the range of error for the calibration. Though this is true, it seems especially contradictory in Lake Malawi where TEX_{86}-inferred temperatures calculated from GDGTs in POM collected during the warm, wet season in January 2010 match the measured temperatures at the depth where Thaumarchaeota are proposed to live in the water column (50 m depth) (Woltering, 2011).

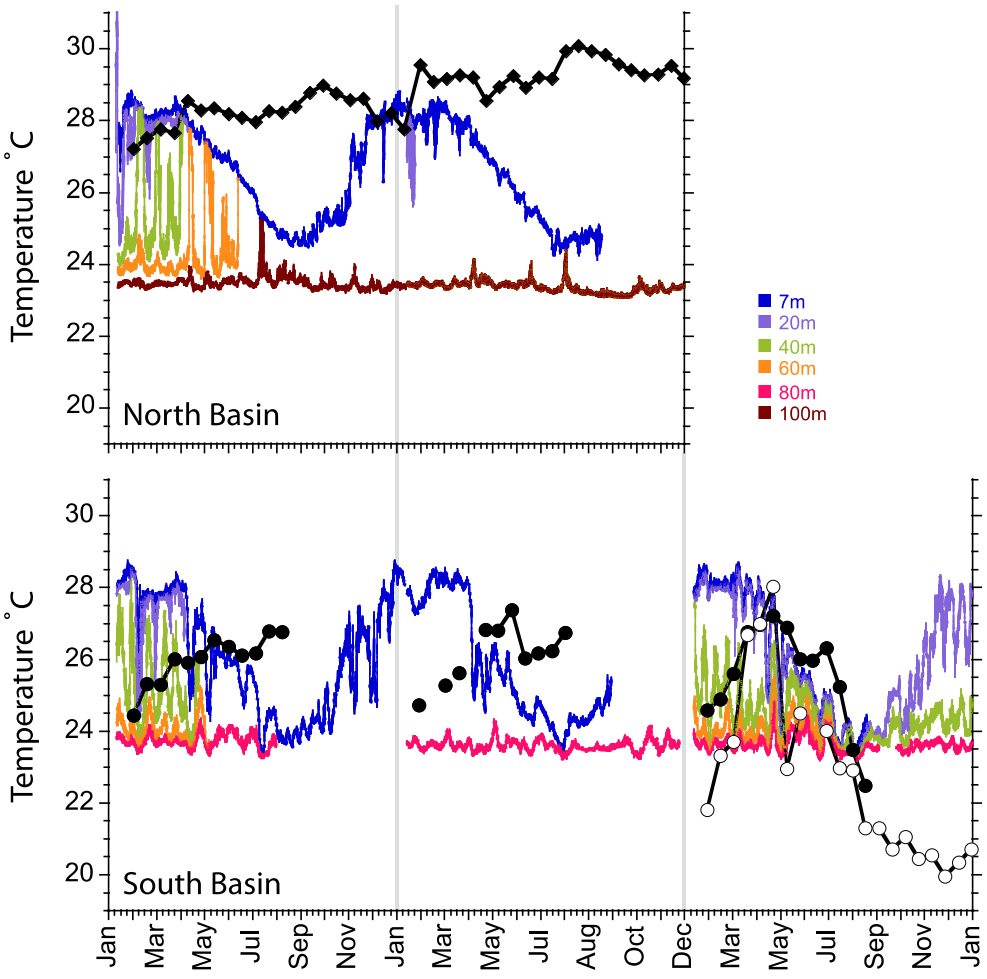

Figure 4.5: TEX_{86} reconstructed temperatures from CL GDGTs in Lake Malawi SPM (black lines) compared to thermistor temperatures.

In contrast to the pattern observed in the NB, TEX_{86}-reconstructed temperatures in POM from the SB are lower than *in situ* temperatures at the depth of maximum Thaumarchaeotal activity (Woltering, 2011), but in agreement with SPM-based temperatures from SST-D. Though TEX_{86}-reconstructed temperatures in SST-D and SST-S are more variable, they still do not capture measured trends in LST. Instead, TEX_{86}-based temperatures in the basin record intermediate values at the beginning of the warm/wet season that increase to warmer values at the transition to the cool/dry season. As there is no complete year of trap records from the deeper site from this location, changes in isoGDGT distributions at depth during the transition out of the cool/dry season into the warm/wet season is uncertain. TEX_{86} in SST-S at this time returns to the cooler values recorded at the beginning of the year. Maximum temperatures recorded by CL distributions are coincident with the period of elevated IPL crenarchaeol fluxes and the two peaks in total isoGDGT CL flux, all taking place during the dry/windy season. Apparent maxima in temperatures at this time are due to increases in the relative abundance in crenarchaeol at the expense of GDGT-1 (Figure 4.6); abundances of GDGT-1/crenarchaeol are significantly correlated in samples that are likely not influenced by contributions from Euryarchaeota (Figure 4.6b). In the marine water column, isoGDGT distributions are sometimes correlated with nutrient concentrations, in particular nitrate (Wuchter et al., 2005; Turich et al., 2007), such that residual temperatures between lipid-based values and measurements are significantly higher during periods of nutrient upwelling. Turich et al. (2007) proposed that the upwelling of nitrate stimulates growth of mesopelagic Thaumarchaeota populations, and that distributions of isoGDGTs produced during this time may actually reflect a biophysical response rather than a temperature signal. The increases in fractional abundance of crenarchaeol and the higher temperatures recorded by isoGDGTs in Lake Malawi SPM during the dry/windy season may then be an artifact of Thaumarchaeota ecology. Thaumarchaeota in the NB of Lake Malawi might not exhibit this behavior due to weaker upwelling in the basin. In other lakes where upwelling is not a significant process, TEX_{86} based temperatures also show little annual variability (Sinninghe Damsté et al., 2009; Blaga et al., 2011). In a study of isoGDGTs in the dimictic Lake Superior, Woltering et al. (2012) specifically collected SPM at a location in the lake where upwelling is not significant, and again found that TEX_{86}-temperatures do not record any seasonal variability. Therefore, it appears that even if upwelling can be a significant overall process in large lakes, local limnological processes ultimately drive Thaumarchaoteal ecology.

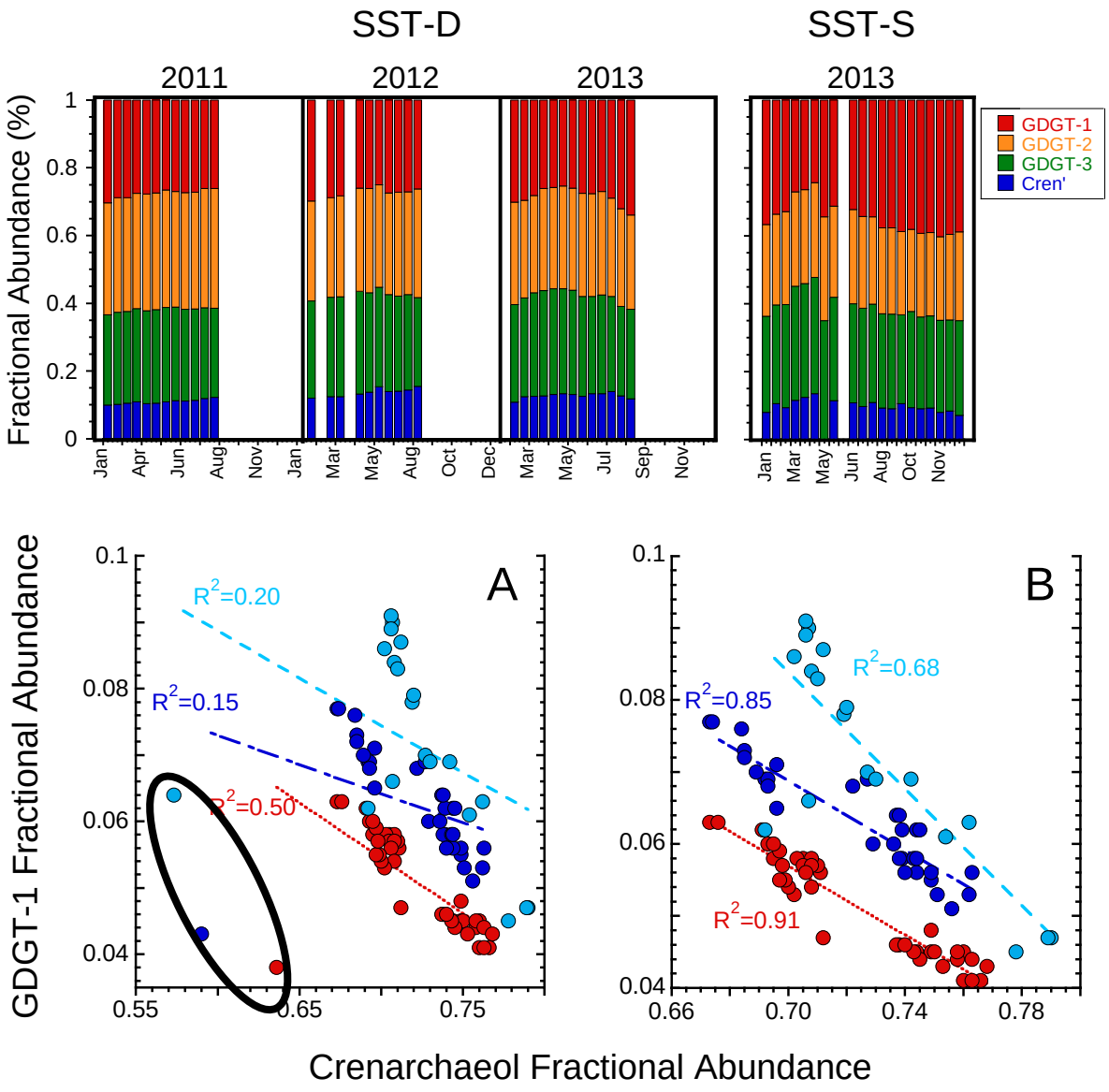

Figure 4.6: Fractional abundances of isoGDGTs used for the calculation of TEX_{86} in SST-D and SST-S (above). Correlations between fractional abundances of crenarchaeol and GDGT-1 are shown for NST (red circles), SST-D (dark blue circles), and SST-S (turquoise circles) are shown in panels A and B. Correlations in panel A include three outliers, circled, where high concentrations of GDGT-0 bias fractional abundances of the other isoGDGTs. Correlations with these points excluded are in panel B. Correlations between crenarchaeol and GDGT-1 fractional abundance are not significant for SST-D and SST-S with the outliers included (p>0.1), but are significant for NST with and without the outlier (p<0.001) and for SST-D and SST- when the outlier is excluded (p<0.001).

SPM TEX_{86} temperatures are warmer than those calculated from GDGTs in sediments. In their 1.3 million year record of TEX_{86}-temperatures from the CB of Lake Malawi calculated with the Powers et al. (2010) calibration, Johnson et al. (2016) measured TEX_{86} temperatures of 18°C to 28°C, with a surface sediment (1 cm) temperature of ~25°C. The surface sediment collected from Lake Malawi in the Powers et al. (2010) study was from the NB and had a TEX_{86} value of 0.73, equating to temperature of ~27°C. Warmer temperatures in the NB compared to the CB, and in the NST compared to the SST, could be due to the more equatorial location of the NB where average surface water temperatures are higher than those in the SB.

4.3.3 Are brGDGT distributions driven by temperature?

Beyond the BIT index, discussion of brGDGTs in Lake Malawi SPM will be focused on the 2012 – 2013 SPM samples as these were analyzed for the full suite of brGDGTs. By resolving both the 5-methyl and 6-methyl isomers, unique patterns arise in brGDGT abundances that elucidate trends in brGDGT production and sources that are not apparent from the major brGDGT distributions alone. However, at present there are no calibrations relating brGDGT distributions and temperature that have been produced from lacustrine-specific samples (i.e. with no input from soils). BrGDGT producers inhabiting soils and those in lakes have already been shown to have unique manners of adapting membrane lipid compositions in response to changing environmental conditions, thus the isomerization of brGDGTs by aquatic brGDGT producers needs to be explored further. Therefore, it is not surprising that neither brGDGT calibration produced prior to the separation of 5- and 6-methyl isomers nor the soil-based calibration developed after the analytical improvement fail to reasonably relate brGDGTs in Lake Malawi SPM to water temperatures at any depth.

De Jonge et al. (2014) re-analyzed the global dataset of soils utilized for the development of the MBT/CBT and MBT'/CBT calibrations for their brGDGT composition to reflect abundances of both 5- and 6-methyl brGDGT isomers. The authors found only the abundances of 5-methyl structures to be significantly correlated with temperature, and thus defined the MAT_{mr} calibration based on the relative abundance of the 5-methyl tetramethylated brGDGTs and the 5-methyl non-cyclized pentamethylated brGDGT. Applying this calibration to

brGDGTs in Lake Malawi SPM results in a drastic underestimation of LST by ~10°C, consistent with previous studies that attempted to apply soil-based brGDGT calibrations to lacustrine brGDGTs (e.g. Tierney et al., 2010) (Figure 4.7).

Two brGDGT calibrations, by Loomis et al. (2012) and Tierney et al. (2010), have been developed specifically for East African lakes. To determine if these calibrations produce realistic temperatures, values were calculated first as originally calibrated, with the abundances of 5- and 6-methyl isomers combined, and then calculated again with the exclusion of the 6-methyl isomers. When brGDGT-based temperatures are calculated using the 5- and 6-methyl isomers together, both calibrations produce apparent temperatures that are significantly lower than measured values (Figure 4.7). The Tierney et al. (2010) calibration uses only the fractional abundances of non-cyclized brGDGTs, thus increases in IIc, IIc', and Ib at the expense of IIa' during the cool/dry season results in an increase in temperatures that is not apparent when reconstructing temperatures with the Loomis et al. (2012) calibration, which includes IIc and Ib in the calculation (Figure 4.8). Excluding the 6-methyl isomers from these calibrations changes the trends and magnitudes of reconstructed temperatures (Figure 4.7). The Tierney et al. (2010) calibration now drastically overestimates LST, while the Loomis et al. (2012) calibration with 6-methyl brGDGTs only results in the most accurate temperatures of any lacustrine or soil-based calibration applied here. As the Loomis et al. (2012) calibration includes only the penta- and hexa-methylated structures, and utilizes IIc, all of which have been demonstrated to be of significance in aquatic systems, this could explain why it performs the best of any brGDGT calibration. Still, the Loomis et al. (2012) calibration also does not resolve annual trends in LST. Moreover, it performs especially poorly in the SST-S, which may be a result of the low overall brGDGT concentrations and thus an unreliability of measurements of minor components such as IIc utilized in the calibration.

An interesting feature of brGDGT distributions is that the relative abundance of cyclized structures in SST-D and SST-S increases during the cool, dry upwelling season (Figure 4.7). It is possible that there is a deeper-dwelling brGDGT community that become apparent in the traps during the dry season due to resuspension of their lipids (Loomis et al., 2014) and may have been missed by Woltering (2011) who did not analyze cyclized brGDGTs. Distributions in lakes can also be affected by nutrient concentrations, so upwelling during the dry season in the SB may be driving a single bacterial community to alter their lipids (Loomis et al., 2014).

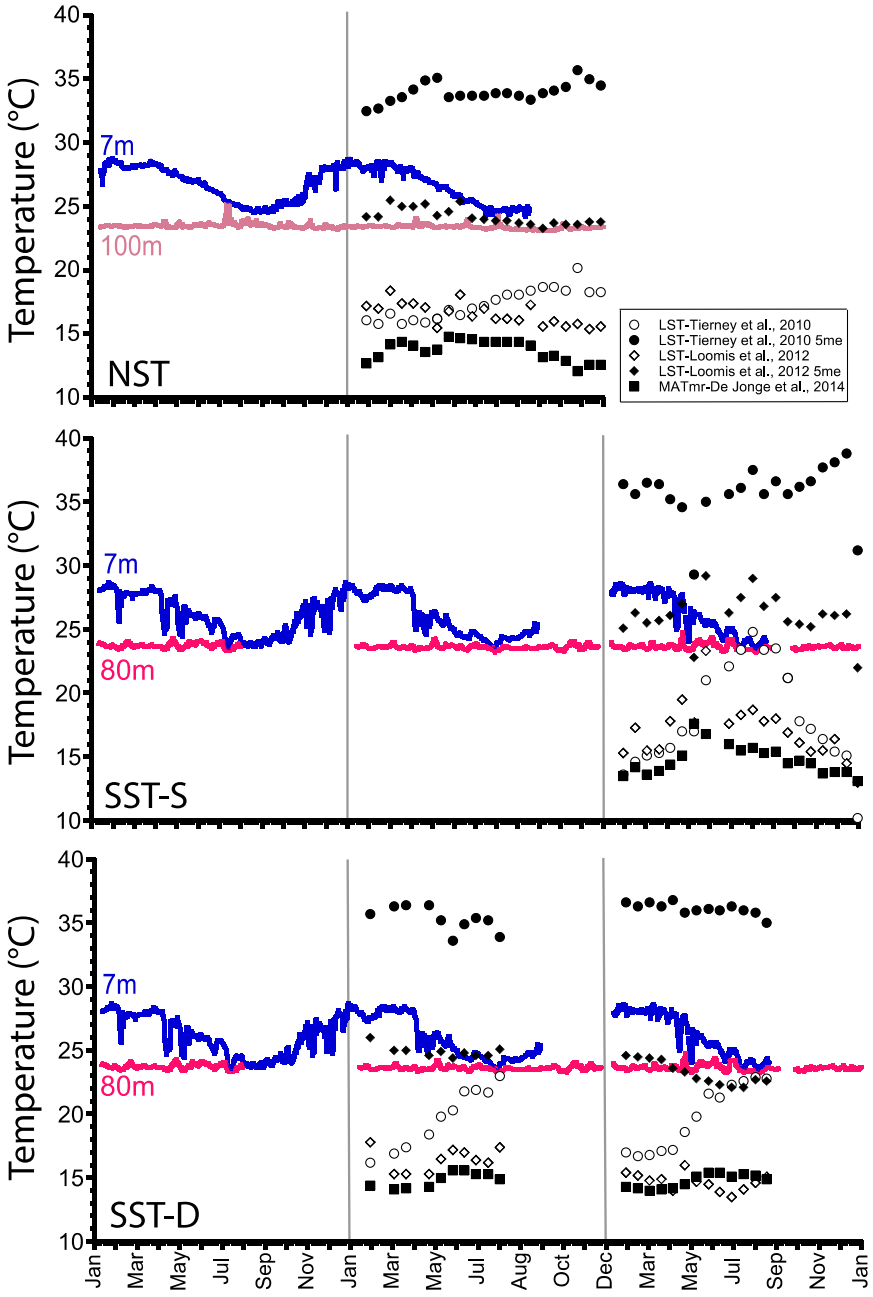

Figure 4.7: Temperatures reconstructed from brGDGTs using the lacustrine based calibrations from Loomis et al. (2012) and Tierney et al. (2010) and the soil-based calibration from De Jonge et al. (2014). Open symbols reflect temperatures calculated with the inclusion of both 5- and 6-methyl isomers while closed symbols are temperatures calculated exclusively from 5-methyl structures. Reconstructed temperatures are compared to thermistor measurements from 7 m (blue line) and 100 m in the NB (pink line) and 7 m and 80 m the SB (magenta line). Temperatures are only calculated for 2012 and 2013 when the full suite of brGDGTs were analyzed.

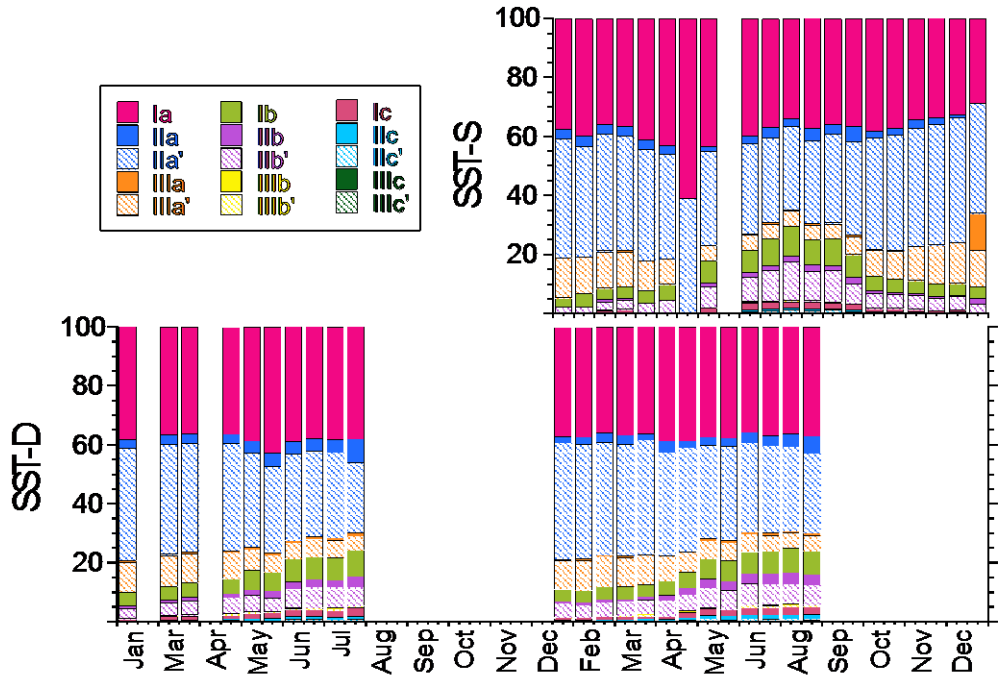

Figure 4.8: Fractional abundances of brGDGTs in SPM collected between January 2012 to December 2013 in the SB of Lake Malawi. All samples were run using the LC_{CN} method.

4.4 HGS AS ENVIRONMENTAL INDICATORS IN LAKE MALAWI

4.4.1 Temporal and spatial variability in HG production

Fluxes of HGs in NST and SST-S exhibit regular maxima in December of each year from 2011–2013 (Figure 3.11). Unlike diatom blooms that are generally spatially heterogeneous, the timing of cyanobacterial blooms across Lake Malawi has been shown to be coherent (Bootsma, 1993). Therefore, though HG fluxes are not resolved in SST-D in the latter half of each year due to the lack of sediment collection, it is likely that the maximum HG flux at this site also occurs around December. Elevated fluxes of HGs in SST-D at the beginning of 2013 may be a continuation of a maximum from the end of 2012, as indicated by the peak in HG flux at this time in NST, providing support for this interpretation (Figure 3.11). The low correlation between

HG flux and TOC flux (Figure 4.2) indicates that export of HGs is largely independent of bulk sedimentary processes. The chlorphyll-A maximum in the SB sits around 35 m (Woltering, 2011**)**, therefore the position of SST-S at 50 m is makes it the sediment trap best suited to collect freshly produced phytoplankton material, and is unlikely to be influenced by lipids in resuspended sediments due to its distance from the sediment-water interface compared to SST-D. As expected, fluxes of HGs in SST-S do exhibit the lowest correlation with TOC flux (Figure 4.2). The correlations between HG fluxes and TOC fluxes in SST-D and NST are slightly higher than in SST-S, but are still weak ($R^2 \leq 0.25$). Regardless, all correlations between TOC flux and HG flux are insignificant ($p>0.01$). Magnitudes and trends of HG fluxes in SST-D and SST-S in 2013 are very similar ($R^2=0.69$, $p<0.001$; Figure 4.9), indicating that export of HGs out of the epilimnion is rapid. As such, trends in HG distributions in the traps positioned at depth can be fairly interpreted as representative of actively living cyanobacterial populations.

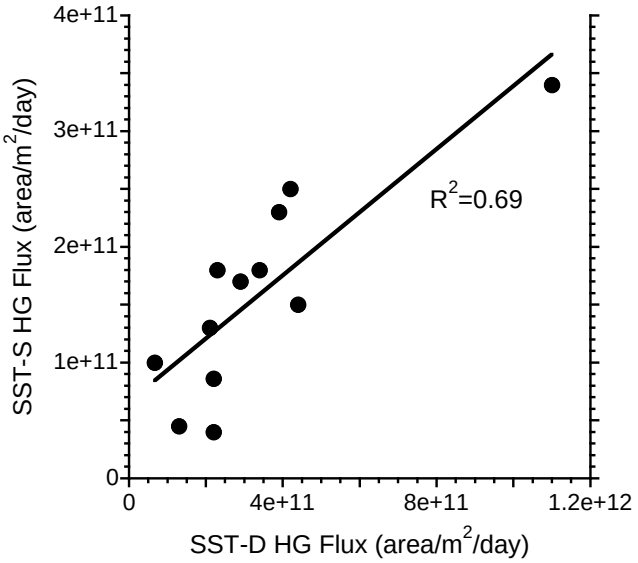

Figure 4.9: Correlation between fluxes of HGs to SST-S and SST-D in 2013.

HGs were detected in all samples, consistent with the presence of active cyanobacteria populations in Lake Malawi throughout the year, as determined by floristic analyses of phytoplankton that utilized cell-counting techniques (Bootsma, 1993). The timing of principal HG fluxes in December is also consistent with these floristic analyses, in which maximum cyanobacterial biomass was identified in November – December (Bootsma, 1993; Hecky et al., 1999; Patterson and Kachinjika, 1995). Conditions in the lake at this time are most favorable for cyanobacterial blooms for two reasons. First, the depletion of nutrients in the epilimnion by

diatoms during the dry/windy season create low-nutrient, specifically low-nitrogen conditions, in which nitrogen-fixing cyanobacteria thrive (Hecky and Kling, 1987). Secondly, the slackening of winds and reduced upwelling during this season leads to diminished turbidity in the epilimnion that supplies cyanobacteria with the high irradiance these organisms prefer (Staal et al., 2003; Stal, 1995). Bootsma (1993) suggested that the timing of cyanobacterial blooms in Lake Malawi is most strongly driven by the reduction in wind stress. As variations in windspeed across the lake are relatively instantaneous, this would explain the synchronicity of cyanobacteria blooms in the NB and SB as recorded by HG fluxes. This is in contrast to the spatial heterogeneity of the cooling of surface waters that drives entrainment and upwelling that ultimately dictates the timing of diatom blooms (Bootsma, 1993**).**

4.4.2 Distributions of HGs and temperature

Culture studies have demonstrated that cyanobacteria produce higher proportions of HG diols relative to the keto-ol homologues under warmer growth conditions (Bauersachs et al. 2009b, 2014). For cyanobacteria grown at 27°C, HDI_{26} values have ranged between 0.93 – 0.95 (Bauersachs et al. 2009b, 2014). In a study of HG distributions in natural freshwater environments, HDI_{26} ranged between 0.96 – 0.99 at locations with surface water temperatures ≥25°C, though the correlation between HDI_{26} and MAT at these sites diverged from the trend observed in temperate environments (Wörmer et al., 2012). Importantly, the linear relationship between HDI_{26} and MAT was only robust for the temperate environments where MAT was ≤ 25°C and ≥ 15°C (Wörmer et al., 2012). Summer surface water temperatures in Lake Malawi are generally ~28 – 29°C (Figure 4.11), so heterocystous cyanobacteria in the lake may possess a nonlinear adaption of the production of HG_{26}-diols and HG_{26}-keto-ols relative to temperate organisms, which could explain why HDI_{26} in SPM frequently reaches its maximum value of 1.0.

Likewise, the HDI_{26} of Lake Malawi SPM shows virtually no variability over the three-year study period due to a complete dominance of HG_{26}-diols relative to HG_{26}-keto-ols (Figure 4.11; Appendix H). It is curious that HDI_{26} does not vary with seasonal temperatures despite the observation that fluxes of HGs generally correspond to actively growing heterocystous

cyanobacteria. This further suggests that heterocystous cyanobacteria in Lake Malawi do not alter the structure of their HG_{26} lipids in response to seasonal variations in temperature in the same manner as temperate organisms, as this finding is in contrast to a study of HGs in POM from the temperate Lake Schreventeich where HDI_{26} was the most highly correlated HG-based index to seasonal variability in LST (Bauersachs et al., 2015).

Variability in HDI_{28} also does not follow seasonal patterns in LST, despite exhibiting a fairly strong relationship with LST in temperate lacustrine POM (Bauersachs et al., 2015) and in culture studies (Bauersachs et al., 2014). The most prominent feature of the HDI_{28} record in Lake Malawi is the semi-regular decrease in values that occurs around the periods of elevated HG flux (Figure 3.12). The cause for this pattern will be discussed in further detail in section 4.4.3 below.

Whether the pattern in HTI_{28} is more similar to HDI_{26} or HDI_{28} is difficult to resolve due to the low abundances of HG_{28}-triols and HG_{28}-keto-ols overall. Abundances of the HG_{28}-keto-ol may have been additionally underestimated as the structural isomers of this compound which were not integrated may have represented a significant portion of its abundance (Bauersachs et al., 2014).

Patterns in HG distributions, as recorded by the HDI_{26}, HDI_{28}, and HTI_{28}, in SST-D and SST-S are well correlated (R^2 of 0.58, 0.53, and 0.82, respectively; Figure 4.10) and significant (p<0.001). This pattern provides additional evidence that HGs at depth in the water column are exclusively sourced from cyanobacteria inhabiting the surface waters, and that export of the HGs through the water column is rapid.

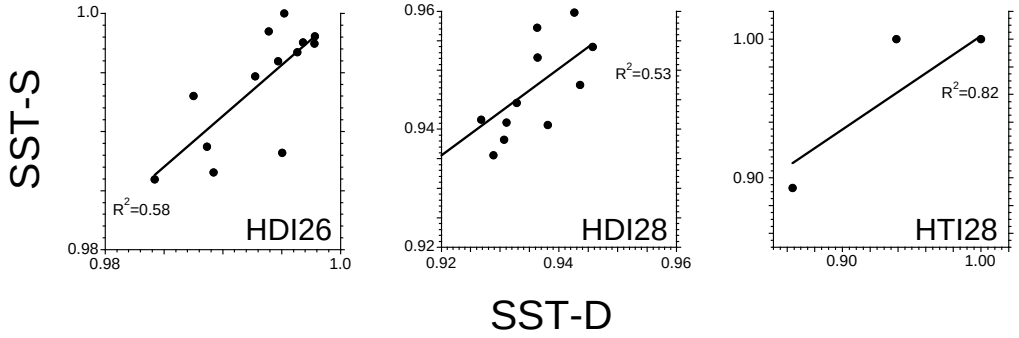

Figure 4.10: Correlations between HDI_{26}, HDI_{28}, and HTI_{28} measured in SST-D and SST-S SPM. Many points are overlapping in the panel for HTI_{28} due to low abundances of the HG_{28} keto-diol that lead to a frequent value of 1.0 in SPM from both traps.

As the variability in HDI_{26}, HDI_{28}, and HTI_{28} do not follow seasonal trends in surface

water temperatures, it is no surprise that reconstructed temperatures based on these indices do not match measured temperatures in Lake Malawi (Figure 4.11). Furthermore, the only LST calibrations presently available for these indices are based on HG distributions in the temperate Lake Schreventeich (Bauersachs et al., 2015), and thus consistently underestimate LST in the tropical Lake Malawi. Conducting a surface sediment calibration of the indices in a suite of African lakes, similar to those produced by Loomis et al. (2014) and Tierney et al. (2010) for brGDGTs, could provide an equation that results in more reasonable temperature estimates. Still, even with such a calibration, the indices would still fail to resolve patterns in LST over time as they appear to be driven by physiological and ecological factors rather than growth temperature. Therefore it is not recommended that these indices be used for temperature reconstructions in East African lakes.

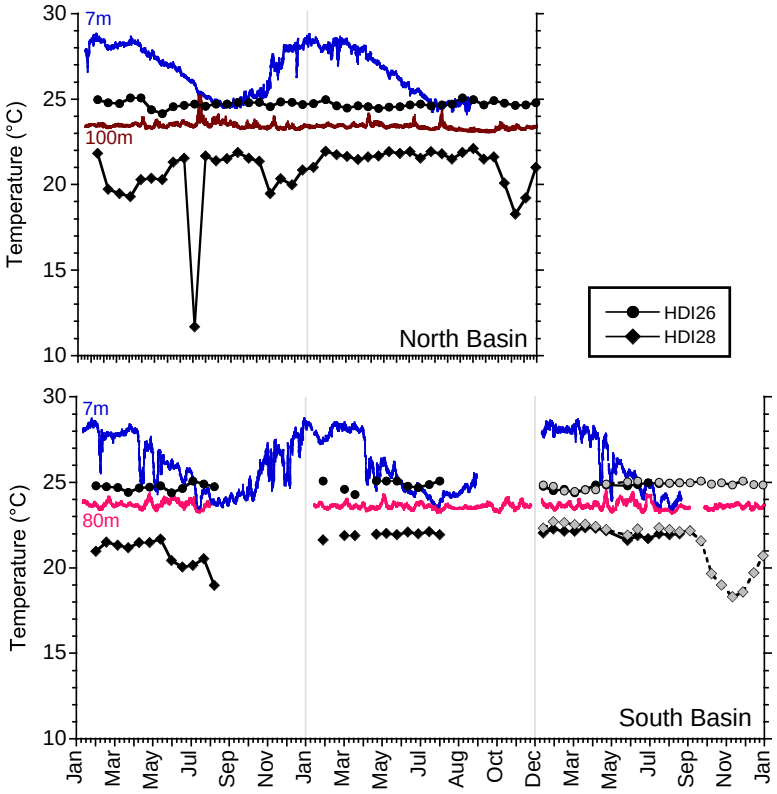

Figure 4.11: Reconstructed temperatures using the HDI_{26} and HDI_{28} compared to thermistor temperatures measured at 7 m and 100 m in the NB and 7 m and 80 m in the SB. Grey symbols are temperatures reconstructed from HGs in SST-S.

The strains of freshwater heterocystous cyanobacteria used for the culture experiments by Bauersachs et al. (2014) and from which the temperature-index relationship was partially

developed were all temperate organisms; *Anabaena* CCY9613 had been isolated from a microbial mat in the German Wadden Sea, while *Nostoc* CCY9926 (Gomont, 1892) is commonly found in Northern Europe. Detailed information on the type locations of strains used in the Bauersachs et al. (2009b) study could not be found. Bauersachs et al. (2013) conducted culture studies of the heterocystous cyanobacteria *M. laminosus,* isolated from an Icelandic hot spring, to determine if thermophilic heterocystous cyanobacteria exhibit the same temperature relationship as temperate organisms. The authors found that *M. laminosus* did not, in fact, produce more HG keto-ols when grown under cooler temperatures in a controlled environment (Bauersachs et al., 2013). It is possible that heterocystous cyanobacteria inhabiting warm environments, such as hot springs or tropical lakes, generally do not alter the composition of their heterocyst glycolipid layer in response to the same environmental parameters as temperate organisms (Wörmer et al., 2012; Bauersachs et al., 2013).

The elongation of membrane lipids in response to growth temperature is a demonstrated physiological mechanism of microorganisms. Longer chain lengths stabilize the membrane, thus are observed in warmer growth conditions (Archer & Mer, 1955; Sandercock & Russell, 1980). Bauersachs et al. (2009b, 2013) noted an increase in longer HGs in their initial study of *Anabaena* and *Nostoc* species (2009b) and in their growth chamber experiments of the thermophilic *M. laminosus* (2013). In Lake Malawi, the relative abundance of HG_{28}-diols in SPM is indeed greatest during periods of the warmest surface water temperatures, while HG_{26}-diol abundances are at their lowest (Figure 4.12). This relationship persists for the majority of the time-series, with the exception of the end of the 2011 warm/wet season when HG_{26}-diols and HG_{28}-diols are in roughly equal abundance from January until July. It is possible that the aforementioned strong internal seiche wave activity present at this time could be disturbing normal behavior of the cyanobacterial community. Internal waves that propagate along the thermocline promote mixing at the boundary of the epilimnion and metalimnion in addition to driving resuspension of slope material when the waves break. These processes would increase the turbidity and nutrient concentrations of the surface waters that could be driving the heterocystous cyanobacteria to behave as if they were living in winter conditions and thus produce more HG_{26} diols than is typical at this time.

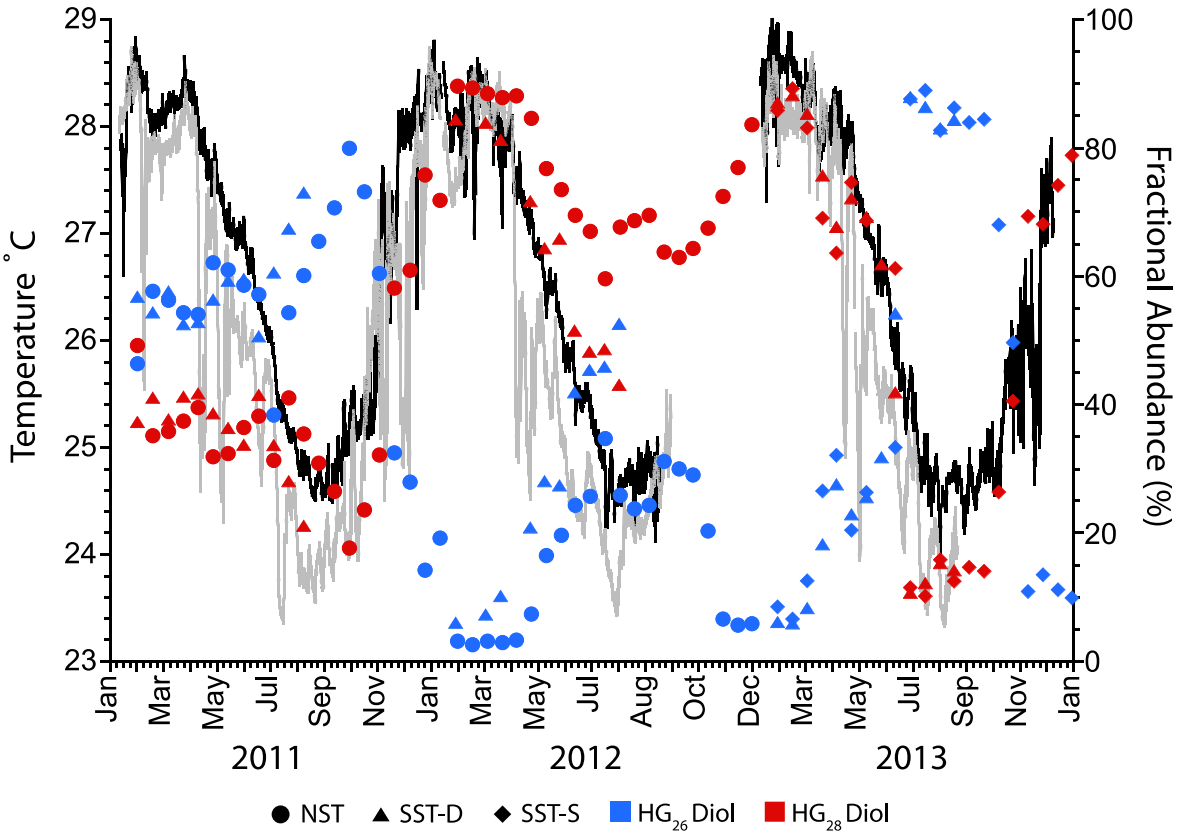

Figure 4.12: Fractional abundances of HG_{26} and HG_{28} diols compared to measured lake water temperatures are 7 m depth in the NB (black line) and SB (grey line).

4.4.3 HG production and heterocystous cyanobacteria physiology

Differentiation of vegetative cells into heterocysts is triggered by combined nitrogen limitation, as this limitation makes the expenditure of energy for heterocyst formation and subsequent nitrogen fixation metabolically favorable for the organism (Kulasooriya et al., 1972; Fleming and Haselkorn, 1973; Adams and Duggan, 1999; Flores and Herrero, 2010). Therefore, fluxes of HGs are likely driven by both the size of heterocystous cyanobacteria populations and the frequency of heterocyst cells along individual heterocystous cyanobacterial filaments, though in Lake Malawi these two parameters are highly correlated (R^2=0.99; Gondwe et al., 2008). One of the primary functions of the heterocyst is to provide a microoxic environment to protect the

nitrogenase enzyme from deactivation by free O_2 (Fay and Cox, 1967; Gallon, 1981; Gallon et al., 1993; Kangatharalingam et al., 1992; Walsby, 1985). Differences in the glycolipid composition of protoheterocysts and mature heterocysts have been observed in some culture studies (Abreu-Grobois et al., 1977; Krepski and Walton, 1983), though these were conducted prior to the development of extraction and analytical techniques that allow for the rapid analysis of HGs and are consequently only based on results from a few organisms. Krepski and Walton (1983) specifically found that C_{28} and C_{26} HGs produced during the most active phase of HG biosynthesis contained more hydroxyl and hydroxyl-fatty acid groups on the alkane side chains. The addition of these functional groups along the HG chain would decrease the permeability of the glycolipid layer (Bauersachs et al., 2014), which may be needed in order to rapidly deplete O_2 concentrations inside the heterocyst as it develops.

The association of HDI_{28} variability with HG fluxes in Lake Malawi gives the appearance that the index is related to heterocystous cyanobacteria proliferation (Figure 4.13). Declines in HDI_{28} in SPM consistently occur ~1 month prior to the primary HG flux in the basins (Figure 4.13). The relationship is exceptionally clear for the major peak in HG flux at SST-S, in addition to the major and minor peaks in HG flux recorded in NST. While there is a slight depression in HDI_{28} in SST-D that occurs before the minor peaks in HG flux in May 2011 and July 2013 at this site, these declines are very small compared to those associated with the period of maximum HG fluxes in the other traps. There is a larger decline in HG_{28} in SST-D during the 2011 dry/windy season that is of similar magnitude to depressions in the index in NST and SST-S, but it is unclear if this is related to a period of HG production due to the absence of sediment collected over the remainder of the year. Lower HDI_{28} values indicate an increase in the relative abundance of HG_{28}-keto-ols to HG_{28}-diols, thus it is possible that cyanobacteria in Lake Malawi produce more of these compounds during heterocyst differentiation. More information is needed on the effect of ketone functional groups on the permeability of the glycolipid to confirm if their purpose is to produce a more limiting gas diffusion barrier. Additionally, it is unclear why heterocystous cyanobacteria in Lake Malawi appear to contain this physiological response for C_{28} HGs but not C_{26} HGs.

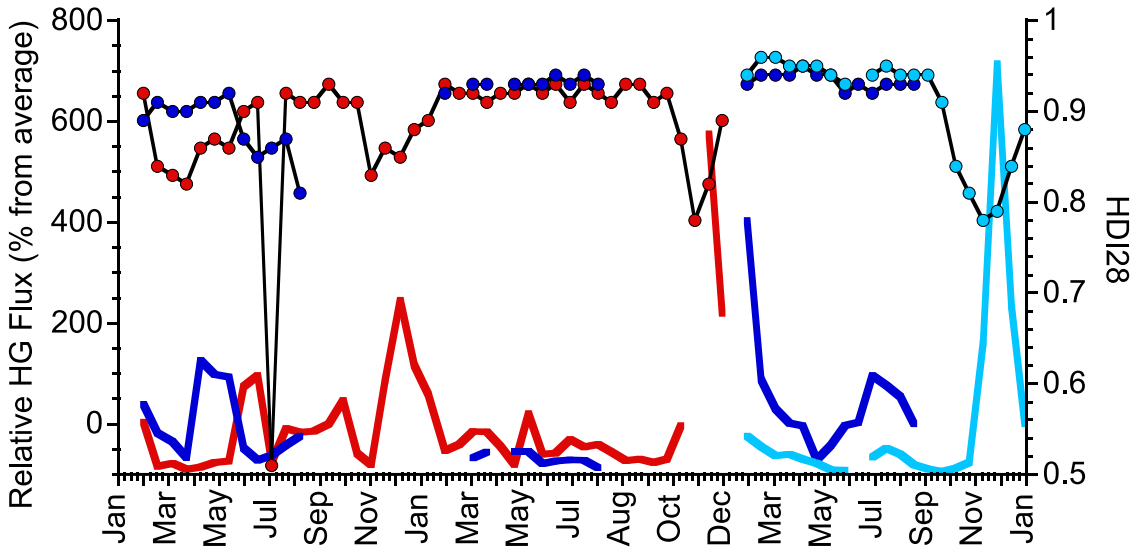

Figure 4.13: HDI_{28} (solid lines) compared to relative HG flux (circles). For both parameters red=NST, dark blue=SST-D, and light blue=SST-S. Relative HG flux was calculated separately for samples run in 2013 and those run in 2017 to account for differences in MS sensitivity.

5. CONCLUSIONS

This study reveals several complications that need to be considered when interpreting sedimentary isoGDGT, brGDGT, or HG distributions in Lake Malawi sediments. The sources of all three classes of lipids in SPM are predominantly autochthonous, but vary in regards to the timing and depth of production within the water column. The export of isoprenoid and branched GDGTs is primarily associated with bulk sedimentation processes. Thus the relative retention time of the CL GDGT pool is possibly subjected to changes in zooplankton activity and/or turbidity in the water column. The export of HGs is largely independent of bulk sedimentation processes and the distributions of HGs in deeper traps closely match those in the surface water. Thus the fluxes of HGs in SPM reflect real-time changes in heterocystous cyanobacteria populations.

IsoGDGTs are produced below the thermocline; Thaumarchaeotal sources of these lipids live near the anoxic-oxic boundary while Euryarchaeotal sources reside in the hypolimnion. Concentrations of crenarchaeol IPLs are highest at the depths at which Thaumarchaeota live, confirming that they are the dominant producers of this biomarker in Lake Malawi. IPLs of isoGDGTs 0—3 were not analyzed, therefore the relative production of the minor lipids by the deeper-dwelling Euryarchaeota compared to that by Thaumarchaeota is unknown. Seasonal upwelling of nutrients at the beginning of the dry/windy season appears to impact Thaumarchaeota in the SB, driving shifts in the relative abundances of crenarchaeol and GDGT-1 that bias TEX_{86} temperatures towards warmer values. TEX_{86} remains fairly constant in the NB throughout the annual cycle, resulting in reconstructed temperatures that reflect LST at the time of maximum Thaumarchaeotal activity.

Results of the brGDGT analyses corroborate the findings of the growing body of literature that has examined the distributions of 5-methyl and 6-methyl isomers in aquatic environments. The 6-methyl isomers of brGDGTs with no or one cyclopentane moiety are

especially abundant in SPM. BrGDGTs with two cyclopentane moieties were in low abundance overall, but, when present, had a slightly greater proportion of 5-methyl isomers. The fractional abundances of brGDGTs in SPM may also record an upwelling signal in the SB. The relative abundances of the cyclized brGDGTs Ib, IIb, IIb', IIIb, Ic, and IIc increase during the dry, windy season at the expense of IIa' and IIIa'. This distribution pattern may be indicative of a yet-unknown brGDGT-producing bacterial community that lives deep below the thermocline in the lacustrine water column. The primary period of brGDGT production in surface waters appears to be during the warm/wet season when stratification is strong. Variability in brGDGT distribution reflects changes in lake water circulation. As such, neither temperatures reconstructed from brGDGT distributions using the East African lake-based calibrations nor the novel soil-based MAT_{mr} resolve seasonal variability in water temperature at any depth. This finding underscores the need for a better understanding of the ecology of brGDGT producers inhabiting lacustrine environments and the relationship of their membrane lipids with temperature, or other environmental parameters. There is evidence that the bacterial sources of brGDGTs in Lake Malawi's water column are anaerobic organisms, though this is only speculative and more robust analyses need to be conducted to confirm this hypothesis.

HGs are present in all SPM samples, but maximum fluxes occur during the primary cyanobacterial bloom. This confirms the use of these lipids as reliable tracers of heterocystous cyanobacteria activity in lakes. The relative abundance of HG_{28}-keto-ols increases just before the onset of heterocystous cyanobacteria blooms and may be a physiological response of cyanobacteria to provide extra protection of the heterocyst cell during differentiation. Though HDI_{26}, HDI_{28}, and HTI_{28} have been demonstrated to correlate with temperature in temperate lakes, they do not reflect seasonal changes in LST in Lake Malawi. This is mostly due to the dominance of HG diols and triols over HG keto-ols and keto-diols throughout the year. Instead, the relative abundance of HG_{26}-diols/HG_{28}-diols tracks LST at 7m remarkably well and may be a more robust temperature index in tropical lakes.

6. BIBLIOGRAPHY

Abreu-Grobois, F. A., Billyard, T. C., & Walton, T. J. (1977). Biosynthesis of heterocyst glycolipids of Anabaena cylindrica. *Phytochemistry*, *16*(3), 351–354. doi:10.1016/0031-9422(77)80063-0

Adams, D. G., & Duggan, P. S. (1999). Heterocyst and akinete differentiation in cyanobacteria. *New Phytologist*, *144*(1), 3–33. doi:10.1046/j.1469-8137.1999.00505.x

Ajioka, T., Yamamoto, M., Takemura, K., Hayashida, A., & Kitagawa, H. (2014). Water pH and temperature in Lake Biwa from MBT'/CBT indices during the last 280 000 years. *Climate of the Past*, *10*(5), 1843–1855. doi:10.5194/cp-10-1843-2014

Archer, R. J., & Mer, V. K. La. (1955). The Rate of Evaporation of Water through Fatty Acid Monolayers. *The Journal of Physical Chemistry*, *59*(3), 200–208. doi:10.1021/j150525a002

Balch, W. E., Fox, G. E., Magrum, L. J., Woese, C. R., & Wolfe, R. S. (1979). Methanogens: reevaluation of a unique biological group. *Microbiol Rev*, *43*(2), 260–296. doi:10.1016/j.watres.2010.10.010

Bale, N. J., Hopmans, E. C., Zell, C., Sobrinho, R. L., Kim, J.-H., Sinninghe Damsté, J. S., … Schouten, S. (2015). Long chain glycolipids with pentose head groups as biomarkers for marine endosymbiotic heterocystous cyanobacteria. *Organic Geochemistry*, *81*, 1–7. doi:10.1016/j.orggeochem.2015.01.004

Barns, S. M., Cain, E. C., Sommerville, L., & Kuske, C. R. (2007). Acidobacteria phylum sequences in uranium-contaminated subsurface sediments greatly expand the known diversity within the phylum. *Applied and Environmental Microbiology*, *73*(9), 3113–3116. doi:10.1128/AEM.02012-06

Bauersachs, T., Hopmans, E. C., Compaoré, J., Stal, L. J., Schouten, S., Sinninghe Damsté, J. S. (2009a). Rapid analysis of long-chain glycolipids in heterocystous cyanobacteria using high-performance liquid chromatography coupled to electrospray ionization tandem mass spectrometry. *Rapid Communications in Mass Spectrometry*, *23*, 1387–1394.

Bauersachs, T., Compaoré, J., Hopmans, E. C., Stal, L. J., Schouten, S., & Sinninghe Damsté, J. S. (2009b). Distribution of heterocyst glycolipids in cyanobacteria. *Phytochemistry*, *70*(17–18), 2034–2039. doi:10.1016/j.phytochem.2009.08.014

Bauersachs, T., Compaoré, J., Severin, I., Hopmans, E. C., Schouten, S., Stal, L. J., & Sinninghe Damsté, J. S. (2011). Diazotrophic microbial community of coastal microbial mats of the southern North Sea. *Geobiology*, *9*(4), 349–359. doi:10.1111/j.1472-4669.2011.00280.x

Bauersachs, T., Miller, S. R., van der Meer, M. T. J., Hopmans, E. C., Schouten, S., & Sinninghe Damsté, J. S. (2013). Distribution of long chain heterocyst glycolipids in cultures of the thermophilic cyanobacterium Mastigocladus laminosus and a hot spring microbial mat. *Organic Geochemistry*, *56*, 19–24. doi:10.1016/j.orggeochem.2012.11.013

Bauersachs, T., Rochelmeier, J., & Schwark, L. (2015). Seasonal lake surface water temperature trends reflected by heterocyst glycolipid-based molecular thermometers. *Biogeosciences*, *12*(12), 3741–3751. doi:10.5194/bg-12-3741-2015

Bauersachs, T., Speelman, E. N., Hopmans, E. C., Reichart, G. J., Schouten, S., & Sinninghe Damsté, J. S. (2010). Fossilized glycolipids reveal past oceanic N2 fixation by heterocystous cyanobacteria. *Proceedings of the National Academy of Sciences U.S.A.*, *107*(45), 19190–19194. doi:10.1073/pnas.1007526107

Bauersachs, T., Stal, L. J., Grego, M., & Schwark, L. (2014). Temperature induced changes in the heterocyst glycolipid composition of N2 fixing heterocystous cyanobacteria. *Organic Geochemistry*, *69*, 98–105. doi:10.1016/j.orggeochem.2014.02.006

Bendle, J. A., Weijers, J. W. H., Maslin, M. A., Sinninghe Damsté, J. S., Schouten, S., Hopmans, E. C., … Pancost, R. D. (2010). Major changes in glacial and Holocene terrestrial temperatures and sources of organic carbon recorded in the Amazon fan by tetraether lipids. *Geochemistry, Geophysics, Geosystems*, *11*(12), 1–13. doi:10.1029/2010GC003308

Berke, M. A., Johnson, T. C., Werne, J. P., Grice, K., Schouten, S., & Sinninghe Damsté, J. S. (2012). Molecular records of climate variability and vegetation response since the Late Pleistocene in the Lake Victoria basin, East Africa. *Quaternary Science Reviews*, *55*, 59–74. doi:10.1016/j.quascirev.2012.08.014

Berke, M. A., Johnson, T. C., Werne, J. P., Livingstone, D. A., Grice, K., Schouten, S., & Sinninghe Damsté, J. S. (2014). Characterization of the last deglacial transition in tropical East Africa: Insights from Lake Albert. *Palaeogeography, Palaeoclimatology, Palaeoecology*, *409*, 1–8. doi:10.1016/j.palaeo.2014.04.014

Blaga, C. I., Reichart, G. J., Heiri, O., & Sinninghe Damsté, J. S. (2009). Tetraether membrane lipid distributions in water-column particulate matter and sediments: A study of 47 European lakes along a north-south transect. *Journal of Paleolimnology*, *41*(3), 523–540. doi:10.1007/s10933-008-9242-2

Blaga, C. I., Reichart, G. J., Schouten, S., Lotter, A. F., Werne, J. P., Kosten, S., Mazzeo, N., Lacerot, G., Sinninghe Damsté, J. S. (2010). Branched glycerol dialkyl glycerol tetraethers in lake sediments: Can they be used as temperature and pH proxies? *Organic Geochemistry*, *41*(11), 1225–1234. doi:10.1016/j.orggeochem.2010.07.002

Blaga, C. I., Reichart, G. J., Vissers, E. W., Lotter, A. F., Anselmetti, F. S., & Sinninghe Damsté, J. S. (2011). Seasonal changes in glycerol dialkyl glycerol tetraether concentrations and fluxes in a perialpine lake: Implications for the use of the TEX86 and BIT proxies. *Geochimica et Cosmochimica Acta, 75*(21), 6416–6428. doi:10.1016/j.gca.2011.08.016

Blöschl, G. (2006). Hydrologic synthesis: Across processes, places, and scales. *Water Resources Research*, *42*(3), 2–4. doi:10.1029/2005WR004319

Blöschl, G., Ardoin-Bardin, S., Bonell, M., Dorninger, M., Goodrich, D., Gutknecht, D., Matamoros, D., Merz, B., Shand, P., Szolgay, J. (2007). At what scales do climate variability and land cover change impact on flooding and low flows? *Hydrological Processes*, *21*, 1241–1247. doi:10.1002/hyp

Blumenberg, M., Seifert, R., Reitner, J., Pape, T., & Michaelis, W. (2004). Membrane lipid patterns typify distinct anaerobic methanotrophic consortia. *Proceedings of the National Academy of Sciences*, *101*(30), 11111–11116. doi:10.1073/pnas.0401188101

Bootsma, H. A. (1993). Algal Dynamics in an African Great Lake, and Their Relation to Hydrographic and Meteorlogical Conditions. Ph.D. Thesis, University of Manitoba.

Bootsma, H. A., & Hecky, R. E. (2003). A Comparative Introduction to the Biology and Limnology of the African Great Lakes. *Journal of Great Lakes Research*, *29*(Supplement 2), 3–18. doi:10.1016/S0380-1330(03)70535-8

Bootsma, H. A., Hecky, R. E., Johnson, T. C., Kling, H. J., & Mwita, J. (2003). Inputs, outputs, and internal cycling of silica in a large, tropical lake. *Journal of Great Lakes Research*, *29*(Supplement 2), 121–138. doi:10.1016/S0380-1330(03)70543-7

Brassell, S. C. (1992). Biomarkers in sediments, sedimentary rocks and petroleums: biological origins, geological fate and applications. *Geochemistry of Organic Matter in Sediments and Sedimentary Rocks*, pp. 29–72. doi:10.2110/scn.92.27.0029

Brochier-Armanet, C., Boussau, B., Gribaldo, S., & Forterre, P. (2008). Mesophilic crenarchaeota: proposal for a third archaeal phylum, the Thaumarchaeota. *Nature Reviews Microbiology*, *6*(3), 245–252. doi:10.1038/nrmicro1852

Brown, E. T., & German, C. R. (2000). Geochemical cycling of redox-sensitive metals in sediments from Lake Malawi, *64*(20), 3515–3523. doi:10.1016/S0016-7037(00)00460-9

Buckles, L. K., Villanueva, L., Weijers, J. W. H., Verschuren, D., & Sinninghe Damsté, J. S. (2013). Linking isoprenoidal GDGT membrane lipid distributions with gene abundances of ammonia-oxidizing Thaumarchaeota and uncultured crenarchaeotal groups in the water column of a tropical lake (Lake Challa, East Africa). *Environmental Microbiology*, *15*(9), 2445–2462. doi:10.1111/1462-2920.12118

Buckles, L. K., Weijers, J. W. H., Verschuren, D., & Sinninghe Damsté, J. S. (2014). Sources of core and intact branched tetraether membrane lipids in the lacustrine environment: Anatomy of Lake Challa and its catchment, equatorial East Africa. *Geochimica et Cosmochimica Acta*, *140*, 106–126. doi:10.1016/j.gca.2014.04.042

Calder, I., Hall, R., Bastable, H., Gunston, H., Shela, O., Chirwa, a, & Kafundu, R. (1995). The impact of land use change on water resources in sub-Saharan Africa: a modelling study of Lake Malawi. *Journal of Hydrology*, *170*, 123–135. doi:10.1016/0022-1694(94)02679-6

Carballeira, N. M., Reyes, M., Sostre, a, Huang, H.-P., Verhagen, M. F., & Adams, M. W. (1997). Unusual fatty acid compositions of the hyperthermophilic archaeon Pyrococcus furiosus and the bacterium Thermotoga maritima. *Journal of Bacteriology*, *179*(8), 2766–2768.

Clarke, L., Edmonds, J., Jacoby, H., Pitcher, H., Reilly, J., & Richels, R. (2007). Scenarios of greenhouse gas emissions and atmospheric concentrations. *US Department of Energy Publications*, (July), 1–164.

Cohen, A. S., Lezzar, K. E., Tiercelin A, J. J., & Soreghan, M. (1997). New palaeogeographic and lake-level reconstructions of Lake Tanganyika: Implications for tectonic, climatic and biological evolution in a rift lake. *Basin Research*, *9*(2), 107–132. doi:10.1046/j.1365-2117.1997.00038.x

Colcord, D. E., Cadieux, S. B., Brassell, S. C., Castañeda, I. S., Pratt, L. M., & White, J. R. (2015). Assessment of branched GDGTs as temperature proxies in sedimentary records from several small lakes in southwestern Greenland. *Organic Geochemistry*, *82*, 33–41. doi:10.1016/j.orggeochem.2015.02.005

Colcord, D. E., Pearson, A., & Brassell, S. C. (2017). Carbon isotopic composition of intact branched GDGT core lipids in Greenland lake sediments and soils. *Organic Geochemistry*, *110*, 25–32. doi:10.1016/j.orggeochem.2017.04.008

Contreras, S., Werne, J. P., Brown, E. T., Anderson, R. S., & Fawcett, P. J. (2016). A molecular isotope record of climate variability and vegetation response in southwestern North America during mid-Pleistocene glacial/interglacial cycles. *Palaeogeography, Palaeoclimatology, Palaeoecology*, *459*, 338–347. doi:10.1016/j.palaeo.2016.07.019

D'Andrea, W. J., & Huang, Y. (2005). Long chain alkenones in Greenland lake sediments: Low $\delta^{13}C$ values and exceptional abundance. *Organic Geochemistry*, *36*(9), 1234–1241. doi:10.1016/j.orggeochem.2005.05.001

Dai, A. (2012). Increasing drought under global warming in observations and models. *Nature Climate Change*, *3*(1), 52–58. doi:10.1038/nclimate1633

Dang, X., Yang, H., Naafs, B. D. A., Pancost, R. D., & Xie, S. (2016). Evidence of moisture control on the methylation of branched glycerol dialkyl glycerol tetraethers in semi-arid and arid soils. *Geochimica et Cosmochimica Acta*, *189*, 24–36. doi:10.1016/j.gca.2016.06.004

De Jonge, C., Hopmans, E. C., Stadnitskaia, A., Rijpstra, W. I. C., Hofland, R., Tegelaar, E., & Sinninghe Damsté, J. S. (2013). Identification of novel penta- and hexamethylated branched glycerol dialkyl glycerol tetraethers in peat using HPLC-MS2, GC-MS and GC-SMB-MS. *Organic Geochemistry*, *54*, 78–82. doi:10.1016/j.orggeochem.2012.10.004

De Jonge, C., Stadnitskaia, A., Hopmans, E. C., Cherkashov, G., Fedotov, A., & Sinninghe Damsté, J. S. (2014a). In situ produced branched glycerol dialkyl glycerol tetraethers in suspended particulate matter from the Yenisei River, Eastern Siberia. *Geochimica et Cosmochimica Acta*, *125*, 476–491. doi:10.1016/j.gca.2013.10.031

De Jonge, C., Hopmans, E. C., Zell, C. I., Kim, J.-H., Schouten, S., & Sinninghe Damsté, J. S. (2014b). Occurrence and abundance of 6-methyl branched glycerol dialkyl glycerol tetraethers in soils: Implications for palaeoclimate reconstruction. *Geochimica et Cosmochimica Acta*, *141*, 97–112. doi:10.1016/j.gca.2016.03.038

De Jonge, C., Stadnitskaia, A., Fedotov, A., & Sinninghe Damsté, J. S. (2015a). Impact of riverine suspended particulate matter on the branched glycerol dialkyl glycerol tetraether composition of lakes: The outflow of the Selenga River in Lake Baikal (Russia). *Organic Geochemistry*, *83–84*, 241–252. doi:10.1016/j.orggeochem.2015.04.004

De Jonge, C., Stadnitskaia, A., Hopmans, E. C., Cherkashov, G., Fedotov, A., Streletskaya, I. D., Vasiliev, A. A., Sinninghe Damsté, J. S. (2015b). Drastic changes in the distribution of branched tetraether lipids in suspended matter and sediments from the Yenisei River and Kara Sea (Siberia): Implications for the use of brGDGT-based proxies in coastal marine sediments. *Geochimica et Cosmochimica Acta*, *165*, 200–225. doi:10.1016/j.gca.2015.05.044

De La Torre, J. R., Walker, C. B., Ingalls, A. E., Könneke, M., & Stahl, D. A. (2008). Cultivation of a thermophilic ammonia oxidizing archaeon synthesizing crenarchaeol. *Environmental Microbiology*, *10*(3), 810–818. doi:10.1111/j.1462-2920.2007.01506.x

De Rosa, M., Gambacorta, A., & Nicolaus, B. (1980). Regularity of isoprenoid biosynthesis in the ether lipids of Archaebacteria, *19*, 791–793.

De Rosa, M., Gambacorta, A., & Gliozzi, A. (1986). Structure, biosynthesis, and physicochemical properties of archaebacterial lipids. *Microbiological Reviews*, *50*(1), 70–80.

DeLong, E. F. (1992). Archaea in coastal marine environments. *Proc Natl Acad Sci U.S.A.*, *89*, 5685–5689. doi:10.1073/pnas.89.12.5685

Ding, S., Schwab, V. F., Ueberschaar, N., Roth, V. N., Lange, M., Xu, Y., Glexiner, G., Pohnert, G. (2016). Identification of novel 7-methyl and cyclopentanyl branched glycerol dialkyl glycerol tetraethers in lake sediments. *Organic Geochemistry*, *102*, 52–58. doi:10.1016/j.orggeochem.2016.09.009

Eccles, D. H. (1974). An outline of the physical limnology of Lake Malawi (Lake Nyasa). *Limnology and Oceanography*, *19*(5), 730–742. doi:10.4319/lo.1974.19.5.0730

Ellis, G. S., Katz, B. J., Scholz, C. A., & Swart, P. K. (2015). Organic sedimentation in modern lacustrine systems: A case study from Lake Malawi, East Africa, *2515*(2), 19–47. doi:10.1130/2015.2515(02)

Fawcett, P. J., Werne, J. P., Anderson, R. S., Heikoop, J. M., Brown, E. T., Berke, M. A., Smith, S. J., Goff, F., Donohoo-Hurley, L., Cisneros-Dozal, L. M., Schouten, S., Sinninghe Damsté, J. S., Huang, Y., Toney, J., Fessenden, J., WoldeGabriel, G., Atudorei, V., Geissman, J. W., Allen, C. D. (2011). Extended megadroughts in the southwestern United States during Pleistocene interglacials. *Nature*, *470*(7335), 518–521. doi:10.1038/nature09839

Fay, P., & Cox, R. M. (1967). Oxygen inhibition of nitrogen fixation in cell-free preparations of blue-green algae. *Biochimica et Biophysica Acta (BBA) - Bioenergetics*, *143*(3), 562–569.

Fleming, H., & Haselkorn, R. (1973). Differentiation in Nostoc muscorum: Nitrogenase is Synthesized in Heterocysts. *Proceedings of the National Academy of Sciences U.S.A.*, *70*(10), 2727–2731.

Flores, E., & Herrero, A. (2010). Compartmentalized function through cell differentiation in filamentous cyanobacteria. *Nature Reviews Microbiology*, *8*(1), 39–50. doi:10.1038/nrmicro2242

Foster, L. C., Pearson, E. J., Juggins, S., Hodgson, D. A., Saunders, K. M., Verleyen, E., & Roberts, S. J. (2016). Development of a regional glycerol dialkyl glycerol tetraether (GDGT)-temperature calibration for Antarctic and sub-Antarctic lakes. *Earth and Planetary Science Letters*, *433*, 370–379. doi:10.1016/j.epsl.2015.11.018

Fox, G. E., Pechman, K. R., & Woese, C. R. (1977). Comparative Cataloging of 16S Ribosomal Ribonucleic Acid: Molecular Approach to Procaryotic Systematics. *International Journal of Systematic Bacteriology*, *27*(1), 44–57. doi:10.1099/00207713-27-1-44

Fox, G. E., Stackebrandt, E., Hespell, R. B., Gibson, J., Maniloff, J., Dyer, T. A., Wolfe, R. S., Balch, W. E., Tanner, R. S., Magrum, L. J., Zablen, L. B., Blakemore, R., Gupta, R., Bonen, L., Lewis, B. J., Stahl, D. A., Luehrsen, K. R., Chen, K. N., Woese, C. R. (1980). The phylogeny of prokaryotes. *Science*, *209*, 457–463. doi:10.1126/science.6771870

Gallon, J. R. (1981). The oxygen sensitivity of nitrogenase: a problem for biochemists and micro-organisms. *Trends in Biochemical Sciences*, *6*(C), 19–23. doi:10.1016/0968-0004(81)90008-6

Gallon, J. R., Pederson, D. M., Smith, G. D. (1993). The Effect of Temperature on the Sensitivity of Nitrogenase to Oxygen in the Cyanobacteria Anabaena cylindrica (Lemmermann) and Gleothece (Nägeli), *124*(2), 251–257.

Gambacorta, A., Pagnotta, E., Romano, I., Sodano, G., & Trincone, A. (1998). Heterocyst glycolipids from nitrogen-fixing cyanobacteria other than nostocaceae. *Phytochemistry*, *48*(5), 801–805. doi:10.1016/S0031-9422(97)00954-0

Gibson, R. A., van der Meer, M. T. J., Hopmans, E. C., Reysenbach, A.-L., Schouten, S., & Sinninghe Damsté, J. S. (2013). Comparison of intact polar lipid with microbial community composition of vent deposits of the Rainbow and Lucky Strike hydrothermal fields. *Geobiology*, *11*(1), 72–85. doi:10.1111/gbi.12017

Gomont, M. M. (1892). Monographie des Oscillariees (Nostocacees Homocystees). *Annales Des Sciences Naturelles, Botanique, Série*, *7*(16), 91–264.

Gondwe, M. J., Guildford, S. J., & Hecky, R. E. (2008). Planktonic nitrogen fixation in Lake Malawi/Nyasa. *Hydrobiologia*, *596*(1), 251–267. doi:10.1007/s10750-007-9101-6

Guildford, S. J., Bootsma, H. A., Taylor, W. D., & Hecky, R. E. (2007). High Variability of Phytoplankton Photosynthesis in Response to Environmental Forcing in Oligotrophic Lake Malawi/Nyasa. *Journal of Great Lakes Research*, *33*(1), 170–185. oi:10.3394/0380-1330(2007)33

Guildford, S. J., & Taylor, W. D. (1999). Factors controlling pelagic algal abundance and composition in Lake Malawi/Nyasa. *Water Quality Report, Lake Malawi/Nyasa Biodiversity Conservation Project*, pp. 143–190.

Günther, F., Thiele, A., Gleixner, G., Xu, B., Yao, T., & Schouten, S. (2014). Distribution of bacterial and archaeal ether lipids in soils and surface sediments of Tibetan lakes: Implications for GDGT-based proxies in saline high mountain lakes. *Organic Geochemistry*, *67*, 19–30. doi:10.1016/j.orggeochem.2013.11.014

Halfman, J. D., & Scholz, C. A. (1993). Suspended Sediments in Lake Malawi, Africa: A Reconnaissance Study. *Journal of Great Lakes Research*, *19*(3), 499–511. doi:http://dx.doi:10.1016/S0380-1330(93)71236-8

Hamblin, P. F., Bootsma, H. a., & Hecky, R. E. (1999). Modeling Nutrient Upwelling in Lake Malawi/Nyasa. *Journal of Great Lakes Research*, *29*(Supplement 2), 34–47. doi:10.1016/S0380-1330(03)70537-1

Hamblin, P. F., Bootsma, H. A., & Hecky, R. E. (2003). Surface Meteorological Observations over Lake Malawi/Nyasa. *Journal of Great Lakes Research*, *29*(Supplement 2), 19–33. doi:10.1016/S0380-1330(03)70536-X

Harvey, H. R., Fallon, R. D., & Patton, J. S. (1986). The effect of organic matter and oxygen on the degradation of bacterial membrane lipids in marine sediments. *Geochimica et Cosmochimica Acta*, *50*(5), 795–804.

Hayes, J. M. (1994). Global methanotrophy at the Archean-Proterozoic transition. In S. Bengston (Ed.), *Early Life on Earth. Nobel Symposium* (Vol. 84). Columbia University Press, New York.

Hecky, R. E., Bootsma, H. A., & Kingdon, M. L. (2003). Impact of Land Use on Sediment and Nutrient Yields to Lake Malawi/Nyasa (Africa). *Journal of Great Lakes Research*, *29*(Supplement 2), 139–158. doi:10.1016/S0380-1330(03)70544-9

Hecky, R. E., & Kling, H. J. (1987). Phytoplankton Ecology of the Great Lakes in the Rift Valleys of Central Africa. *Arch. Hydrobiol. Beih. Ergebn. Limnol.*, *25*, 197–228.

Hecky, R. E., Kling, H. J., Johnson, T. C., Bootsma, H. A., & Wilkinson, P. (1999). Algal and sedimentary evidence for recent changes in the water quality and limnology of Lake Malawi/Nyasa. *Water Quality Report, Lake Malawi/Nyasa Biodiversity Conservation Project*, pp. 191–214.

Hernández-Sánchez, M. T., Woodward, E. M. S., Taylor, K. W. R., Henderson, G. M., & Pancost, R. D. (2014). Variations in GDGT distributions through the water column in the South East Atlantic Ocean. *Geochimica et Cosmochimica Acta*, *132*, 337–348. doi:10.1016/j.gca.2014.02.009

Hershberger, K. L., Barns, S. M., Reysenbach, A.-L., Dawson, S. C., & Pace, N. R. (1996). Wide diversity of Crenarchaeota. *Nature*. doi:10.1038/384420a0

Hopmans, E. C., Schouten, S., Pancost, R. D., van der Meer, M. T. J., & Sinninghe Damsté, J. S. (2000). Analysis of intact tetraether lipids in archaeal cell material and sediments by high performance liquid chromatography/atmospheric pressure chemical ionization mass spectrometry. *Rapid Communications in Mass Spectrometry*, *14*(7), 585–589. doi:10.1002/(SICI)1097-0231(20000415)14:7<585::AID-RCM913>3.0.CO;2-N

Hopmans, E. C., Weijers, J. W. H., Schefuß, E., Herfort, L., Sinninghe Damsté, J. S., & Schouten, S. (2004). A novel proxy for terrestrial organic matter in sediments based on branched and isoprenoid tetraether lipids. *Earth and Planetary Science Letters*, *224*(1–2), 107–116. doi:10.1016/j.epsl.2004.05.012

Hopmans, E. C., Schouten, S., & Sinninghe Damsté, J. S. (2016). The effect of improved chromatography on GDGT-based palaeoproxies. *Organic Geochemistry*, *93*, 1–6. doi:10.1016/j.orggeochem.2015.12.006

Huber, R., Rossnagel, P., Woese, C. R., Rachel, R., Langworthy, T. A., & Stetter, K. O. (1996). Formation of Ammonium from Nitrate During Chemolithoautotrophic Growth of the Extremely Thermophilic Bacterium Ammonifex degensii gen. nov. sp. nov. *Systematic and Applied Microbiology*, *19*(1), 40–49. doi:10.1016/S0723-2020(96)80007-5

Huber, R., Wilharm, T., Huber, D., Trincone, A., Burggraf, S., König, H., … Stetter, K. O. (1992). Aquifex pyrophilus gen. nov. sp. nov., Represents a Novel Group of Marine Hyperthermophilic Hydrogen-Oxidizing Bacteria. *Systematic and Applied Microbiology*, *15*(3), 340–351. doi:10.1016/S0723-2020(11)80206-7

Hudak, A. T., & Wessman, C. A. (2000). Deforestation in Mwanza District, Malawi, from 1981 to 1992, as determined from Landsat MSS imagery. *Applied Geography*, *20*(2), 155–175. doi:10.1016/S0143-6228(00)00002-3

Huguet, A., Grossi, V., Belmahdi, I., Fosse, C., & Derenne, S. (2015). Archaeal and bacterial tetraether lipids in tropical ponds with contrasting salinity (Guadeloupe, French West Indies): Implications for tetraether-based environmental proxies. *Organic Geochemistry*, *83–84*, 158–169. doi:10.1016/j.orggeochem.2015.02.010

Huguet, C., de Lange, G. J., Gustafsson, Ö., Middelburg, J. J., Sinninghe Damsté, J. S., & Schouten, S. (2008). Selective preservation of soil organic matter in oxidized marine sediments (Madeira Abyssal Plain). *Geochimica et Cosmochimica Acta*, *72*(24), 6061–6068. doi:10.1016/j.gca.2008.09.021

Huguet, C., Hopmans, E. C., Febo-Ayala, W., Thompson, D. H., Sinninghe Damsté, J. S., & Schouten, S. (2006). An improved method to determine the absolute abundance of glycerol dibiphytanyl glycerol tetraether lipids. *Organic Geochemistry*, *37*(9), 1036–1041. doi:10.1016/j.orggeochem.2006.05.008

Ingalls, A. E., Shah, S. R., Hansman, R. L., Aluwihare, L. I., Santos, G. M., Druffel, E. R. M., & Pearson, A. (2006). Quantifying archaeal community autotrophy in the mesopelagic ocean using natural radiocarbon. *Proceedings of the National Academy of Sciences*, *103*(17), 6442–6447. doi:10.1073/pnas.0510157103

Janssen, P. H. (2006). Identifying the Dominant Soil Bacterial Taxa in Libraries of 16S rRNA and 16S rRNA Genes MINIREVIEWS Identifying the Dominant Soil Bacterial Taxa in Libraries of 16S rRNA and 16S rRNA Genes. *Applied and Environmental Microbiology*, *72*(3), 1719–1728. doi:10.1128/AEM.72.3.1719

Johnson, T. C., Barry, S. L., Chan, Y., & Wilkinson, P. (2001). Decadal record of climate variability spanning the past 700 yr in the Southern Tropics of East Africa. *Geology*, *29*(1), 83–86. doi:10.1130/0091-7613

Johnson, T. C., Werne, J. P., Brown, E. T., Abbott, A., Berke, M. A., Steinman, B. A., Halbur, J., Contreras, S., Grosshuesch, S., Deino, A., Lyons, R. P., Scholz, C. A., Schouten, S., Sinninghe Damsté, J. S. (2016). A progressively wetter climate in southern East Africa over the past 1.3 million years. *Nature*, *537*(7619), 220–224. doi:10.1038/nature19065

Jones, R. T., Robeson, M. S., Lauber, C. L., Hamady, M., Knight, R., & Fierer, N. (2009). A comprehensive survey of soil acidobacterial diversity using pyrosequencing and clone library analyses. *The ISME Journal*, *3*(4), 442–453. doi:10.1038/ismej.2008.127

Kangatharalingam, N., Priscu, J. C., & Hans, W. P. (1992). Heterocyst envelope thickness, heterocyst frequency and nitrogenase activity in *Anabaena flos-aquae*: influence of exogenous oxygen tension. *Journal of General Microbiology*, *138*(1992), 2673–2678.

Karner, M. B., DeLong, E. F., & Karl, D. M. (2001). Archaeal dominance in the mesopelagic zone of the Pacific Ocean. *Nature*, *409*(6819), 507–510. doi:10.1038/35054051

Kates, M. (1977). The phytanyl ether-linked polar lipids and isoprenoid neutral lipids of extremely halophilic bacteria. *Progress in the Chemistry of Fats and Other Lipids*, *15*(4), 301–342. doi:10.1016/0079-6832(77)90011-8

Keough, B. P., Schmidt, T. M., & Hicks, R. (2003). Archaeal nucleic acids in picoplankton from Great Lakes on three continents. *Microbial Ecology*, *46*(2), 238–248. doi:10.1007/s00248-003-1003-1

Kielak, A. M., Barreto, C. C., Kowalchuk, G. A., van Veen, J. A., & Kuramae, E. E. (2016). The ecology of Acidobacteria: Moving beyond genes and genomes. *Frontiers in Microbiology*, *7*(MAY), 1–16. doi:10.3389/fmicb.2016.00744

Kim, J. H., Huguet, C., Zonneveld, K. A. F., Versteegh, G. J. M., Roeder, W., Sinninghe Damsté, J. S., & Schouten, S. (2009). An experimental field study to test the stability of lipids used for the TEX_{86} and $U^{K'}_{37}$ palaeothermometers. *Geochimica et Cosmochimica Acta*, *73*(10), 2888–2898. doi:10.1016/j.gca.2009.02.030

Kim, J.-H., van der Meer, J., Schouten, S., Helmke, P., Willmott, V., Sangiorgi, F., Nalân, K., Hopmans, E.C., Sinninghe Damsté, J. S. (2010a). New indices and calibrations derived from the distribution of crenarchaeal isoprenoid tetraether lipids: Implications for past sea surface temperature reconstructions. *Geochimica et Cosmochimica Acta*, *74*(16), 4639–4654. doi:10.1016/j.gca.2010.05.027

Kim, J.-H., Zarzycka, B., Buscail, R., Peterse, F., Bonnin, J., Ludwig, W., Schouten, S. Sinninghe Damsté, J. S. (2010b). Contribution of river-borne soil organic carbon to the Gulf of Lions (NW Mediterranean). *Limnology and Oceanography*, *55*(2), 507–518. doi:10.4319/lo.2010.55.2.0507

Kim, J.-H., Ludwig, W., Buscail, R., Dorhout, D., & Sinninghe Damsté, J. S. (2015). Tracing tetraether lipids from source to sink in the Rhône River system (NW Mediterranean). *Frontiers in Earth Science*, *3*(22). doi:10.3389/feart.2015.00022

Kingdon, M. J., Bootsma, H. A., Mwita, J., Mwichande, B., & Hecky, R. E. (1999). River discharge and water quality. *Water Quality Report, Lake Malawi/Nyasa Biodiversity Conservation Project*, pp. 30-69.

Könneke, M., Bernhard, A. E., de la Torre, J. R., Walker, C. B., Waterbury, J. B., & Stahl, D. A. (2005). Isolation of an autotrophic ammonia-oxidizing marine archaeon. *Nature*, *437*(7058), 543–546. doi:10.1038/nature03911

Krepski, W. J., & Walton, T. J. (1983). Biosynthesis of the envelope glycolipids during heterocyst development in Anabaena cylindrica. *Journal of General Microbiology*, *129*(1983), 105–110.

Kulasooriya, S. A., Lang, N., J., Fay, P. (1972). The Heterocysts of Blue-Green Algae . III . Differentiation and Nitrogenase Activity. *Proceedings of the Royal Society of London*, *181*(1063), 199–209.

Langworthy, T. A., Mayberry, W. R., & Smith, P. F. (1974). Long chain glycerol diether and polyol dialkyl glycerol triether lipids of Sulfolobus acidocaldarius. *Journal of Bacteriology*, *119*(1), 106–116.

Langworthy, T. A., Holzer, G., Zeikus, J. G., & Tornabene, T. G. (1983). Iso- and Anteiso-Branched Glycerol Diethers of the Thermophilic Anaerobe Thermodesulfotobacterium commune. *Systematic and Applied Microbiology*, *4*(1), 1–17. doi:10.1016/S0723-2020(83)80029-0

Lauber, C. L., Hamady, M., Knight, R., & Fierer, N. (2009). Pyrosequencing-based assessment of soil pH as a predictor of soil bacterial community structure at the continental scale. *Applied and Environmental Microbiology*, *75*(15), 5111–5120. doi:10.1128/AEM.00335-09

Lengger, S. K., Hopmans, E. C., Sinninghe Damsté, J. S., & Schouten, S. (2014a). Fossilization and degradation of archaeal intact polar tetraether lipids in deeply buried marine sediments (Peru Margin). *Geobiology*, *12*(3), 212–220. doi:10.1111/gbi.12081

Lengger, S. K., Hopmans, E. C., Sinninghe Damsté, J. S., & Schouten, S. (2014b). Impact of sedimentary degradation and deep water column production on GDGT abundance and distribution in surface sediments in the Arabian Sea: Implications for the TEX_{86} paleothermometer. *Geochimica et Cosmochimica Acta*, *142*, 386–399. doi:10.1016/j.gca.2014.07.013

Lincoln, S. A., Bradley, A. S., Newman, S. A., & Summons, R. E. (2013). Archaeal and bacterial glycerol dialkyl glycerol tetraether lipids in chimneys of the Lost City Hydrothermal Field. *Organic Geochemistry*, *60*, 45–53. doi:10.1016/j.orggeochem.2013.04.010

Liu, X. L., Summons, R. E., & Hinrichs, K.-U. (2012). Extending the known range of glycerol ether lipids in the environment: Structural assignments based on tandem mass spectral fragmentation patterns. *Rapid Communications in Mass Spectrometry*, *26*(19), 2295–2302. doi:10.1002/rcm.6355

Liu, X. L., Zhu, C., Wakeham, S. G., & Hinrichs, K.-U. (2014). In situ production of branched glycerol dialkyl glycerol tetraethers in anoxic marine water columns. *Marine Chemistry*, *166*, 1–8. doi:10.1016/j.marchem.2014.08.008

Llirós, M., Gich, F., Plasencia, A., Auguet, J. C., Darchambeau, F., Casamayor, E. O., Borrego, C. (2010). Vertical distribution of ammonia-oxidizing crenarchaeota and methanogens in the epipelagic waters of lake kivu (rwanda-democratic republi of the congo). *Applied and Environmental Microbiology*, *76*(20), 6853–6863. doi:10.1128/AEM.02864-09

Loomis, S. E., Russell, J. M., Ladd, B., Street-Perrott, F. A., & Sinninghe Damsté, J. S. (2012). Calibration and application of the branched GDGT temperature proxy on East African lake sediments. *Earth and Planetary Science Letters*, *357–358*, 277–288. doi:10.1016/j.epsl.2012.09.031

Loomis, S. E., Russell, J. M., Eggermont, H., Verschuren, D., & Sinninghe Damsté, J. S. (2014a). Effects of temperature, pH and nutrient concentration on branched GDGT distributions in East African lakes: Implications for paleoenvironmental reconstruction. *Organic Geochemistry*, *66*, 25–37. doi:10.1016/j.orggeochem.2013.10.012

Loomis, S. E., Russell, J. M., Heureux, A. M., D'Andrea, W. J., & Sinninghe Damsté, J. S. (2014b). Seasonal variability of branched glycerol dialkyl glycerol tetraethers (brGDGTs) in a temperate lake system. *Geochimica et Cosmochimica Acta*, *144*, 173–187. doi:10.1016/j.gca.2014.08.027

López-García, P., Brochier, C., Moreira, D., & Rodríguez-Valera, F. (2004). Comparative analysis of a genome fragment of an uncultivated mesopelagic crenarchaeote reveals multiple horizontal gene transfers. *Environmental Microbiology*, *6*(1), 19–34. doi:10.1046/j.1462-2920.2003.00533.x

Magrum, L. J., Luehrsen, K. R., & Woese, C. R. (1978). Are extreme halophiles actually "bacteria"? *Journal of Molecular Evolution*, *11*(1), 1–8. doi:10.1007/BF01768019

Männistö, M. K., Rawat, S., Starovoytov, V., & Häggblom, M. M. (2012). Granulicella arctica sp. nov., granulicella mallensis sp. nov., granulicella tundricola sp. nov. and granulicella sapmiensis sp. nov., novel acidobacteria from tundra soil. *International Journal of Systematic and Evolutionary Microbiology*, *62*(9), 2097–2106. doi:10.1099/ijs.0.031864-0

Massana, R., Murray, a E., Preston, C. M., & DeLong, E. F. (1997). Vertical distribution and phylogenetic characterization of marine planktonic Archaea in the Santa Barbara Channel. *Applied and Environmental Microbiology*, *63*(1), 50–56.

Mathai, J. C., Sprott, G. D., & Zeidel, M. L. (2001). Molecular Mechanisms of Water and Solute Transport across Archaebacterial Lipid Membranes. *Journal of Biological Chemistry*, *276*(29), 27266–27271. doi:10.1074/jbc.M103265200

McCullough, G. K., Barber, D., & Cooley, P. M. (2007). The Vertical Distribution of Runoff and its Suspended Load in Lake Malawi. *Journal of Great Lakes Research, 33,* 449–465.

Milliman, J. D., & Syvitski, J. P. M. (1992). Geomorphic/Tectonic Control of Sediment Discharge to the Ocean: The Importance of Small Mountainous Rivers. *The Journal of Geology*, *100*(5), 525–544. doi:10.1086/629606

Morrissey, A., Scholz, C. A., & Russell, J. M. (2017). Late Quaternary TEX_{86} paleotemperatures from the world???s largest desert lake, Lake Turkana, Kenya. *Journal of Paleolimnology*, 1–15. doi:10.1007/s10933-016-9939-6

Mueller-Niggemann, C., Utami, S. R., Marxen, A., Mangelsdorf, K., Bauersachs, T., & Schwark, L. (2016). Distribution of tetraether lipids in agricultural soils - Differentiation between paddy and upland management. *Biogeosciences*, *13*(5), 1647–1666. doi:10.5194/bg-13-1647-2016

Muñoz Ucros, J. (2014). Planktonic Archaeal Diversity and Ammonia-Oxidizer Abundance Change with Depth in Lakes Malawi, Kivu and Superior. Ph.D. Thesis, University of Minnesota Duluth.

Naeher, S., Peterse, F., Smittenberg, R. H., Niemann, H., Zigah, P. K., & Schubert, C. J. (2014). Sources of glycerol dialkyl glycerol tetraethers (GDGTs) in catchment soils, water column and sediments of Lake Rotsee (Switzerland) - Implications for the application of GDGT-based proxies for lakes. *Organic Geochemistry*, *66*, 164–173. doi:10.1016/j.orggeochem.2013.10.017

Nichols, B. W., & Wood, B. J. B. (1968). New glycolipid specific to nitrogen-fixing blue-green algae. *Nature*, *217*(5130), 767–768.

Nicholson, S. E. & Yin, X. (1996). Mesoscale Patterns of rainfall, Cloudiness and Evaporation Over the Great Lakes of East Africa. In: Odada, E. O., Olago, D. O. (Eds.), The East African Great Lakes: Limnology, Palaeolimnology and Biodiversity. Kluwer Academic Publishers, The Netherlands, pp. 393-414.

Northern Rhodesia, Joint Fisheries Research Organization Annual Reports. 1958, No.8; 1959, No.9; 1960, No.10; 1961, No.11.

Oscar Kisaka, M., Mucheru-Muna, M., Ngetich, F. K., Mugwe, J. N., Mugendi, D., & Mairura, F. (2015). Rainfall variability, drought characterization, and efficacy of rainfall data reconstruction: Case of Eastern Kenya. *Advances in Meteorology*, *2015*. doi:10.1155/2015/380404

Owen, R. B., & Crossley, R. (1989). Rift structures and facies distributions in Lake Malawi. *Journal of African Earth Sciences (and the Middle East)*, *8*(2), 415–427. doi:10.1016/S0899-5362(89)80035-1

Pancost, R. D., Hopmans, E. C., & Sinninghe Damsté, J. S. (2001). Archaeal lipids in mediterranean cold seeps: Molecular proxies for anaerobic methane oxidation. *Geochimica et Cosmochimica Acta*, *65*(10), 1611–1627. doi:10.1016/S0016-7037(00)00562-7

Patterson, G., & Kachinjika, O. (1995). Limnology and phytoplankton ecology. In: Menz, A. (Ed.), The Fishery Potential and Productivity of the Pelagic Zone of Lake Malawi/Niassa. Natural Resources Institute, pp. 1-67.

Patwardhan, A. P., & Thompson, D. H. (1999). Efficient synthesis of 40- and 48-membered tetraether macrocyclic bisphosphocholines. *Organic Letters*, *1*(2), 241–243.

Pearson, E. J., Juggins, S., Talbot, H. M., Weckström, J., Rosén, P., Ryves, D. B., Roberts, S. J., Schmidt, R. (2011). A lacustrine GDGT-temperature calibration from the Scandinavian Arctic to Antarctic: Renewed potential for the application of GDGT-paleothermometry in lakes. *Geochimica et Cosmochimica Acta*, *75*(20), 6225–6238. doi:10.1016/j.gca.2011.07.042

Pester, M., Schleper, C., & Wagner, M. (2011). The Thaumarchaeota: An emerging view of their phylogeny and ecophysiology. *Current Opinion in Microbiology*, *14*(3), 300–306. doi:10.1016/j.mib.2011.04.007

Peterse, F., Schouten, S., van der Meer, J., van der Meer, M. T. J., & Sinninghe Damsté, J. S. (2009). Distribution of branched tetraether lipids in geothermally heated soils: Implications for the MBT/CBT temperature proxy. *Organic Geochemistry*, *40*(2), 201–205. doi:10.1016/j.orggeochem.2008.10.010

Peterse, F., Nicol, G. W., Schouten, S., & Sinninghe Damsté, J. S. (2010). Influence of soil pH on the abundance and distribution of core and intact polar lipid-derived branched GDGTs in soil. *Organic Geochemistry*, *41*(10), 1171–1175. doi:10.1016/j.orggeochem.2010.07.004

Peterse, F., van der Meer, J., Schouten, S., Weijers, J. W. H., Fierer, N., Jackson, R. B., Kim, J. H., Sinninghe Damsté, J. S. (2012). Revised calibration of the MBT-CBT paleotemperature proxy based on branched tetraether membrane lipids in surface soils. *Geochimica et Cosmochimica Acta*, *96*, 215–229. doi:10.1016/j.gca.2012.08.011

Peterse, F., Moy, C. M., & Eglinton, T. I. (2015). A laboratory experiment on the behaviour of soil-derived core and intact polar GDGTs in aquatic environments. *Biogeosciences*, *12*(4), 933–943. doi:10.5194/bg-12-933-2015

Pilskaln, C. H., & Johnson, T. C. (1991). Seasonal signals in Lake Malawi sediments. *Limnology and Oceanography*, *36*(3), 544–557. doi:10.4319/lo.1991.36.3.0544

Pilskaln, C. H. (2004). Seasonal and interannual particle export in an African rift valley lake: A 5-year record from Lake Malawi, southern East Africa. *Limnology and Oceanography*, *49*(4), 964–977. doi:10.4319/lo.2004.49.4.0964

Pitcher, A. M., Schouten, S., & Sinninghe Damsté, J. S. (2009). In situ production of crenarchaeol in two California hot springs. *Applied and Environmental Microbiology*, *75*(13), 4443–4451. doi:10.1128/AEM.02591-08

Pitcher, A. M., Rychlik, N., Hopmans, E. C., Spieck, E., Rijpstra, W. I. C., Ossebaar, J., Schouten, S., Wagner, M., Sinninghe Damsté, J. S. (2010). Crenarchaeol dominates the membrane lipids of Candidatus Nitrososphaera gargensis, a thermophilic Group I.1b Archaeon. *The ISME Journal*, *4*(4), 542–552. doi:10.1038/ismej.2009.138

Pitcher, A. M., Hopmans, E. C., Mosier, A. C., Park, S. J., Rhee, S. K., Francis, C. A., Schouten, S., Sinninghe Damsté, J. S. (2011). Core and intact polar glycerol dibiphytanyl glycerol tetraether lipids of ammonia-oxidizing Archaea enriched from marine and estuarine sediments. *Applied and Environmental Microbiology*, *77*(10), 3468–3477. doi:10.1128/AEM.02758-10

Powers, L. A., Werne, J. P., Johnson, T. C., Hopmans, E. C., Sinninghe Damsté, J. S., & Schouten, S. (2004). Crenarchaeotal membrane lipids in lake sediments: A new paleotemperature proxy continental paleoclimate reconstruction? *Geology*, *32*(7), 613–616. doi:10.1130/G20434.1

Powers, L. A., Johnson, T. C., Werne, J. P., Castañeda, I. S., Hopmans, E. C., Sinninghe Damsté, J. S., & Schouten, S. (2005). Large temperature variability in the southern African tropics since the Last Glacial Maximum. *Geophysical Research Letters*, *32*(8), 1–4. doi:10.1029/2004GL022014

Powers, L. A., Werne, J. P., Vanderwoude, A. J., Sinninghe Damsté, J. S., Hopmans, E. C., & Schouten, S. (2010). Applicability and calibration of the TEX_{86} paleothermometer in lakes. *Organic Geochemistry*, *41*(4), 404–413. doi:10.1016/j.orggeochem.2009.11.009

Rampen, S. W., Willmott, V., Kim, J.-H., Rodrigo-Gámiz, M., Uliana, E., Mollenhauer, G., Schefuβ, E., Sinninghe Damsté, J. S., Schouten, S. (2014). Evaluation of long chain 1,14-alkyl diols in marine sediments as indicators for upwelling and temperature. *Organic Geochemistry*, *76*, 39–47. doi:10.1016/j.orggeochem.2014.07.012

Rogelj, J., Meinshausen, M., & Knutti, R. (2012). Global warming under old and new scenarios using IPCC climate sensitivity range estimates. *Nature Clim. Change*, *2*(4), 248–253. doi:10.1038/nclimate1385

Sanchi, L., Ménot, G., & Bard, E. (2014). Insights into continental temperatures in the northwestern Black Sea area during the Last Glacial period using branched tetraether lipids. *Quaternary Science Reviews*, *84*, 98–108. doi:10.1016/j.quascirev.2013.11.013

Sandercock, S. P., & Russell, N. J. (1980). The elongation of exogenous fatty acids and the control of phospholipid acyl chain length in Micrococcus cryophilus. *The Biochemical Journal*, *188*(3), 585–92.

Schoon, P. L., De Kluijver, A., Middelburg, J. J., Downing, J. A., Sinninghe Damsté, J. S., & Schouten, S. (2013). Influence of lake water pH and alkalinity on the distribution of core and intact polar branched glycerol dialkyl glycerol tetraethers (GDGTs) in lakes. *Organic Geochemistry*, *60*, 72–82. doi:10.1016/j.orggeochem.2013.04.015

Schouten, S., Hoefs, M. J. L., Koopmans, M. P., Bosch, H. J., & Sinninghe Damsté, J. S. (1998). Structural characterization, occurrence and fate of archaeal ether-bound acyclic and cyclic biphytanes and corresponding diols in sediments. *Organic Geochemistry*, *29*(5–7–7 pt 2), 1305–1319. doi:10.1016/S0146-6380(98)00131-4

Schouten, S., Hopmans, E. C., Pancost, R. D., & Sinninghe Damsté, J. S. (2000). Widespread occurrence of structurally diverse tetraether membrane lipids: Evidence for the ubiquitous presence of low-temperature relatives of hyperthermophiles. *Proceedings of the National Academy of Sciences*, *97*(26), 14421–14426. doi:10.1073/pnas.97.26.14421

Schouten, S., Hopmans, E. C., Schefuß, E., & Sinninghe Damsté, J. S. (2002). Distributional variations in marine crenarchaeotal membrane lipids: A new tool for reconstructing ancient sea water temperatures? *Earth and Planetary Science Letters*, *204*(1–2), 265–274. doi:10.1016/S0012-821X(02)00979-2

Schouten, S., Huguet, C., Hopmans, E. C., Kienhuis, M. V. M., & Sinninghe Damsté, J. S. (2007a). Analytical Methodology for TEX_{86} Paleothermometry by High-Performance Liquid Chromatography / Atmospheric Pressure Chemical Ionization-Mass Spectrometry. *Analytical Chemistry*, *79*(7), 2940–2944. doi:10.1029/2004PA001110.This

Schouten, S., Van Der Meer, M. T. J., Hopmans, E. C., Rijpstra, W. I. C., Reysenbach, A. L., Ward, D. M., & Damsté, J. S. S. (2007b). Archaeal and bacterial glycerol dialkyl glycerol tetraether lipids in hot springs of Yellowstone National Park. *Applied and Environmental Microbiology*, *73*(19), 6181–6191. doi:10.1128/AEM.00630-07

Schouten, S., Hopmans, E. C., Baas, M., Boumann, H., Standfest, S., Könneke, M., Stahl, D., Sinninghe Damsté, J. S. (2008). Intact membrane lipids of "Candidatus Nitrosopumilus maritimus," a cultivated representative of the cosmopolitan mesophilic group I crenarchaeota. *Applied and Environmental Microbiology*, *74*(8), 2433–2440. doi:10.1128/AEM.01709-07

Schouten, S., Hopmans, E. C., et al. (2009). An interlaboratory study of TEX_{86} and BIT analysis using high-performance liquid chromatography-mass spectrometry. *Geochemistry, Geophysics, Geosystems*, *10*(3), 1–13. doi:10.1029/2008GC002221

Schouten, S., Rijpstra, W. I. C., Durisch-Kaiser, E., Schubert, C. J., & Sinninghe Damsté, J. S. (2012). Distribution of glycerol dialkyl glycerol tetraether lipids in the water column of Lake Tanganyika. *Organic Geochemistry*, *53*, 34–37. doi:10.1016/j.orggeochem.2012.01.009

Schouten, S., Hopmans, E. C., & Sinninghe Damsté, J. S. (2013a). The organic geochemistry of glycerol dialkyl glycerol tetraether lipids: A review. *Organic Geochemistry*, *54*, 19–61. doi:10.1016/j.orggeochem.2012.09.006

Schouten, S., Hopmans, E. C., et al. (2013b). An interlaboratory study of TEX_{86} and BIT analysis of sediments, extracts, and standard mixtures. *Geochemistry, Geophysics, Geosystems*, *14*(12), 5263–5285. doi:10.1002/2013GC004904

Schreuder, L. T., Beets, C. J., Prins, M. A., Hatté, C., & Peterse, F. (2016). Late Pleistocene climate evolution in Southeastern Europe recorded by soil bacterial membrane lipids in Serbian loess. *Palaeogeography, Palaeoclimatology, Palaeoecology*, *449*, 141–148. doi:10.1016/j.palaeo.2016.02.013

Simpson, J. H., Lucas, N. S., Powell, B., & Maberly, S. C. (2015). Dissipation and mixing during the onset of stratification in a temperate lake, Windermere. *Limnology and Oceanography*, *60*(1), 29–41. doi:10.1002/lno.10008

Sinninghe Damsté, J. S., Hopmans, E. C., Pancost, R. D., Schouten, S., & Geenevasen, J. A. J. (2000). Newly discovered non-isoprenoid glycerol dialkyl glycerol tetraether lipids in sediments. *Chemical Communications*, (17), 1683–1684. doi:10.1039/b004517i

Sinninghe Damsté, J. S., Schouten, S., Hopmans, E. C., van Duin, A. C. T., & Geenevasen, J. A. J. (2002). Crenarchaeol: the characteristic core glycerol dibiphytanyl glycerol tetraether membrane lipid of cosmopolitan pelagic crenarchaeota. *The Journal of Lipid Research*, *43*(10), 1641–1651. doi:10.1194/jlr.M200148-JLR200

Sinninghe Damsté, J. S., Ossebaar, J., Abbas, B., Schouten, S., & Verschuren, D. (2009). Fluxes and distribution of tetraether lipids in an equatorial African lake: Constraints on the application of the TEX86 palaeothermometer and BIT index in lacustrine settings. *Geochimica et Cosmochimica Acta*, *73*(14), 4232–4249. doi:10.1016/j.gca.2009.04.022

Sinninghe Damsté, J. S., Rijpstra, W. I. C., Hopmans, E. C., Weijers, J. W. H., Foesel, B. U., Overmann, J., & Dedysh, S. N. (2011). 13,16-Dimethyl octacosanedioic acid (iso-Diabolic Acid), a common membrane-spanning lipid of Acidobacteria subdivisions 1 and 3. *Applied and Environmental Microbiology*, *77*(12), 4147–4154. doi:10.1128/AEM.00466-11

Sinninghe Damsté, J. S., Ossebaar, J., Schouten, S., & Verschuren, D. (2012). Distribution of tetraether lipids in the 25-ka sedimentary record of Lake Challa: Extracting reliable TEX_{86} and MBT/CBT palaeotemperatures from an equatorial African lake. *Quaternary Science Reviews*, *50*, 43–54. doi:10.1016/j.quascirev.2012.07.001

Sinninghe Damsté, J. S., Rijpstra, W. I. C., Hopmans, E. C., Foesel, B. U., Wüst, P. K., Overmann, J., Stott, M. B. (2014). Ether- and ester-bound iso-diabolic acid and other lipids in members of Acidobacteria subdivision 4. *Applied and Environmental Microbiology*, *80*(17), 5207–5218. doi:10.1128/AEM.01066-14

Sinninghe Damsté, J. S. (2016). Spatial heterogeneity of sources of branched tetraethers in shelf systems: The geochemistry of tetraethers in the Berau River delta (Kalimantan, Indonesia). *Geochimica et Cosmochimica Acta*, *186*, 13–31. doi:10.1016/j.gca.2016.04.033

Smith, P. F., Langworthy, T. A., Mayberry, W. R., & Hougland, A. E. (1973). Characterization of the membranes of Thermoplasma acidophilum. *Journal of Bacteriology*, *116*(2), 1019–1028.

Smith, S. J., & Wigley, T. M. L. (2006). Multi-Gas Forcing Stabilization with Minicam. *The Energy Journal*, *27*, 373–391.

Soriente, A., Sodano, G., Cambacorta, A., & Trincone, A. (1992). Structure of the "heterocyst glycolipids" of the marine cyanobacterium Nodularia harveyana. *Tetrahedron*, *48*(25), 5375–5384. doi:10.1016/S0040-4020(01)89033-5

Staal, M., Meysman, F. J. R., & Stal, L. J. (2003). Temperature excludes N2-fixing heterocystous cyanobacteria in the tropical oceans. *Nature*, *425*(6957), 504–507. doi:10.1038/nature01999

Stahl, D. A., & de la Torre, J. R. (2012). Physiology and Diversity of Ammonia-Oxidizing Archaea. *Annual Review of Microbiology*, *66*(1), 83–101. doi:10.1146/annurev-micro-092611-150128

Stal, L. J. (1995). Physiological ecology of cyanobacteria in microbial mats and other communities. *New Phytologist*. doi:10.1111/j.1469-8137.1995.tb03051.x

Sturt, H. F., Summons, R. E., Smith, K., Elvert, M., & Hinrichs, K.-U. (2004). Intact polar membrane lipids in prokaryotes and sediments deciphered by high-performance liquid chromatography/electrospray ionization multistage mass spectrometry—new biomarkers for biogeochemistry and microbial ecology. *Rapid Communications in Mass Spectrometry*, *18*(6), 617–628. doi:10.1002/rcm.1378

Sun, Q., Chu, G., Liu, M., Xie, M., Li, S., Ling, Y., Wang, X., Shi, L., Jia, G., Lü, H. (2011). Distributions and temperature dependence of branched glycerol dialkyl glycerol tetraethers in recent lacustrine sediments from China and Nepal. *Journal of Geophysical Research: Biogeosciences*, *116*(1), 1–12. doi:10.1029/2010JG001365

Tierney, J. E., Russell, J. M., Huang, Y., Sinninghe Damsté, J. S., Hopmans, E. C., & Cohen, A. S. (2008). Northern Hemisphere Controls on Tropical Southeast African Climate During the Past 60,000 Years. *Science*, *322*(5899), 252–255. doi:10.1126/science.1160485

Tierney, J. E., & Russell, J. M. (2009). Distributions of branched GDGTs in a tropical lake system: Implications for lacustrine application of the MBT/CBT paleoproxy. *Organic Geochemistry*, *40*(9), 1032–1036. doi:10.1016/j.orggeochem.2009.04.014

Tierney, J. E., Mayes, M. T., Meyer, N., Johnson, C., Swarzenski, P. W., Cohen, A. S., & Russell, J. M. (2010a). Late-twentieth-century warming in Lake Tanganyika unprecedented since AD 500. *Nature Geoscience*, *3*(6), 422–425. doi:10.1038/ngeo865

Tierney, J. E., Russell, J. M., Eggermont, H., Hopmans, E. C., Verschuren, D., & Sinninghe Damsté, J. S. (2010b). Environmental controls on branched tetraether lipid distributions in tropical East African lake sediments. *Geochimica et Cosmochimica Acta*, *74*(17), 4902–4918. doi:10.1016/j.gca.2010.06.002

Tierney, J. E., Schouten, S., Pitcher, A. M., Hopmans, E. C., & Sinninghe Damsté, J. S. (2012). Core and intact polar glycerol dialkyl glycerol tetraethers (GDGTs) in Sand Pond, Warwick, Rhode Island (USA): Insights into the origin of lacustrine GDGTs. *Geochimica et Cosmochimica Acta*, *77*, 561–581. doi:10.1016/j.gca.2011.10.018

Turich, C., Freeman, K. H., Bruns, M. A., Conte, M., Jones, A. D., & Wakeham, S. G. (2007). Lipids of marine Archaea: Patterns and provenance in the water-column and sediments. *Geochimica et Cosmochimica Acta*, *71*(13), 3272–3291. doi:10.1016/j.gca.2007.04.013

Verburg, P., Hecky, R. E., & Kling, H. (2003). Ecological Consequences of a Century of Warming in Lake Tanganyika. *Science*, *301*(5632), 505 LP-507.

Verdon-Kidd, D. C., & Kiem, A. S. (2010). Quantifying Drought Risk in a Nonstationary Climate. *Journal of Hydrometeorology*, *11*(4), 1019–1031. doi:10.1175/2010JHM1215.1

Villanueva, L., Schouten, S., & Sinninghe Damsté, J. S. (2014). Depth-related distribution of a key gene of the tetraether lipid biosynthetic pathway in marine Thaumarchaeota. *Environmental Microbiology*, *17*(10), 3527–3539. doi:10.1111/1462-2920.12508

Vollmer, M. K., Weiss, R. F., & Bootsma, H. A. (1999). Lake Malawi / Nyasa Deep Water Renewal. *Water Quality Report, Lake Malawi/Nyasa Biodiversity Conservation Project*, pp. 113–121.

Vollmer, M. K., Bootsma, H. A., Hecky, R. E., Patterson, G., Halfman, J. D., Edmond, J. M., Eccles, D. H., Weiss, R. F. (2005). Deep-water warming trend in Lake Malawi, East Africa. *Limnology and Oceanography*, *50*(2), 727–732. doi:10.4319/lo.2005.50.2.0727

Walsby, A. E. (1985). The permeability of heterocysts to the gases nitrogen and oxygen, *146*(923), 225–241.

Ward, N. L. et al. (2009). Three genomes from the phylum Acidobacteria provide insight into the lifestyles of these microorganisms in soils. *Applied and Environmental Microbiology*, *75*(7), 2046–2056. doi:10.1128/AEM.02294-08

Weber, Y., De Jonge, C., Rijpstra, W. I. C., Hopmans, E. C., Stadnitskaia, A., Schubert, C. J., Lehmann, M. F., Sinninghe Damsté, J. S., Niemann, H. (2015). Identification and carbon isotope composition of a novel branched GDGT isomer in lake sediments: Evidence for lacustrine branched GDGT production. *Geochimica et Cosmochimica Acta*, *154*, 118–129. doi:10.1016/j.gca.2015.01.032

Weijers, J. W. H., Schouten, S., Hopmans, E. C., Geenevasen, J. A. J., David, O. R. P., Coleman, J. M., Pancost, R. D., Sinninghe Damsté, J. S. (2006a). Membrane lipids of mesophilic anaerobic bacteria thriving in peats have typical archaeal traits. *Environmental Microbiology*, *8*(4), 648–657. doi:10.1111/j.1462-2920.2005.00941.x

Weijers, J. W. H., Schouten, S., Spaargaren, O. C., & Sinninghe Damsté, J. S. (2006b). Occurrence and distribution of tetraether membrane lipids in soils: Implications for the use of the TEX_{86} proxy and the BIT index. *Organic Geochemistry*, *37*(12), 1680–1693. doi:10.1016/j.orggeochem.2006.07.018

Weijers, J. W. H., Schouten, S., van den Donker, J. C., Hopmans, E. C., & Sinninghe Damsté, J. S. (2007). Environmental controls on bacterial tetraether membrane lipid distribution in soils. *Geochimica et Cosmochimica Acta*, *71*(3), 703–713. doi:10.1016/j.gca.2006.10.003

Weijers, J. W. H., Panoto, E., van Bleijswijk, J., Schouten, S., Rijpstra, W. I. C., Balk, M., Stams, A. J. M., Sinninghe Damsté, J. S. (2009). Constraints on the Biological Source(s) of the Orphan Branched Tetraether Membrane Lipids. *Geomicrobiology Journal*, *26*(6), 402–414. doi:10.1080/01490450902937293

White, D. C., Davis, W. M., Nickels, J. S., King, J. D., & Bobbie, R. J. (1979). Determination of the sedimentary microbial biomass by extractible lipid phosphate. *Oecologia*, *40*(1), 51–62.

Winkenbach, F., Wolk, C. P., & Jost, M. (1972). Lipids of membranes and of the cell envelope in heterocysts of a blue-green alga. *Planta*, *107*(1), 69–80. doi:10.1007/BF00398015

Wise, M., Calvin, K., Thomson, A., Clarke, L., Bond-Lamberty, B., Sands, R., Smith, S. J., Janetos, A., Edmonds, J. (2009). Implications of Limiting CO_2 Concentrations for Land Use and Energy. *Science*, *324*(5931), 1183 LP-1186.

Woese, C. R., Kandler, O., & Wheelis, M. L. (1990). Towards a natural system of organisms: proposal for the domains Archaea, Bacteria, and Eucarya. *Proceedings of the National Academy of Sciences of the United States of America*, *87*(12), 4576–4579. doi:10.1073/pnas.87.12.4576

Woese, C. R., Magrum, L. J., & Fox, G. E. (1978). Archaebacteria. *Journal of Molecular Evolution*, *11*(3), 245–252. doi:10.1007/BF01734485

Wolk, C. P. (1973). Nitrogen Fixation by Cyanobacterial Heterocysts BT - Genetic Engineering of Symbiotic Nitrogen Fixation and Conservation of Fixed Nitrogen. In J. M. Lyons, R. C. Valentine, D. A. Phillips, D. W. Rains, & R. C. Huffaker (Eds.) (pp. 315–331). Boston, MA: Springer US. doi:10.1007/978-1-4684-3953-3_27

Woltering, M. (2011). Thaumarchaeota Distribution in the Water Columns of Lakes Superior and Malawi : Implications for the TEX86 Lacustrine Temperature Proxy. Ph.D. Thesis, University of Minnesota Duluth.

Woltering, M., Johnson, T. C., Werne, J. P., Schouten, S., & Sinninghe Damsté, J. S. (2011). Late Pleistocene temperature history of Southeast Africa: A TEX_{86} temperature record from Lake Malawi. *Palaeogeography, Palaeoclimatology, Palaeoecology*, *303*(1–4), 93–102. doi:10.1016/j.palaeo.2010.02.013

Woltering, M., Werne, J. P., Kish, J. L., Hicks, R., Sinninghe Damsté, J. S., & Schouten, S. (2012). Vertical and temporal variability in concentration and distribution of thaumarchaeotal tetraether lipids in Lake Superior and the implications for the application of the TEX_{86} temperature proxy. *Geochimica et Cosmochimica Acta*, *87*, 136–153. doi:10.1016/j.gca.2012.03.024

Wörmer, L., Cirés, S., Velázquez, D., Quesada, A., & Hinrichs, K.-U. (2012). Cyanobacterial heterocyst glycolipids in cultures and environmental samples: Diversity and biomarker potential. *Limnology and Oceanography*, *57*(6), 1775–1788. doi:10.4319/lo.2012.57.6.1775

Wuchter, C., Schouten, S., Coolen, M. J. L., & Sinninghe Damsté, J. S. (2004). Temperature-dependent variation in the distribution of tetraether membrane lipids of marine Crenarchaeota: Implications for TEX_{86} paleothermometry. *Paleoceanography*, *19*(4), 1–10. doi:10.1029/2004PA001041

Wuchter, C., Schouten, S., Wakeham, S. G., & Sinninghe Damsté, J. S. (2005). Temporal and spatial variation in tetraether membrane lipids of marine Crenarchaeota in particulate organic matter: Implications for TEX_{86} paleothermometry. *Paleoceanography*, *20*(3), 1–11. doi:10.1029/2004PA001110

Wuchter, C., Schouten, S., Wakeham, S. G., & Sinninghe Damsté, J. S. (2006). Archaeal tetraether membrane lipid fluxes in the northeastern Pacific and the Arabian Sea: Implications for TEX_{86} paleothermometry. *Paleoceanography*, *21*(4), 1–9. doi:10.1029/2006PA001279

Wüest, A., Piepke, G., & Halfman, J. D. (1996). Combined effects of dissolved solids and temperature on the density stratification of Lake Malawi. *Climatology and Paleoclimatology of the East African Lakes*, 183.

Xiao, W., Xu, Y., Ding, S., Wang, Y., Zhang, X., Yang, H., Wang, G., Hou, J. (2015). Global calibration of a novel, branched GDGT-based soil pH proxy. *Organic Geochemistry*, *89–90*, 56–60. doi:10.1016/j.orggeochem.2015.10.005

Yamamoto, M., Shimamoto, A., Fukuhara, T., Tanaka, Y., & Ishizaka, J. (2012). Glycerol dialkyl glycerol tetraethers and TEX_{86} index in sinking particles in the western North Pacific. *Organic Geochemistry*, *53*, 52–62. doi:10.1016/j.orggeochem.2012.04.010

Yang, H., Lü, X., Ding, W., Lei, Y., Dang, X., & Xie, S. (2015). The 6-methyl branched tetraethers significantly affect the performance of the methylation index (MBT') in soils from an altitudinal transect at Mount Shennongjia. *Organic Geochemistry*, *82*, 42–53. doi:10.1016/j.orggeochem.2015.02.003

Yang, W., Seager, R., Cane, M. A., & Lyon, B. (2015). The rainfall annual cycle bias over East Africa in CMIP5 coupled climate models. *Journal of Climate*, *28*(24), 9789–9802. doi:10.1175/JCLI-D-15-0323.1

Zhang, Y. G., Pagani, M., & Wang, Z. (2016). Ring Index: A new strategy to evaluate the integrity of TEX_{86} paleothermometry. *Paleoceanography*, *31*(2), 220–232. doi:10.1002/2015PA002848

Zhang, Y. G., Zhang, C. L., Liu, X. L., Li, L., Hinrichs, K.-U., & Noakes, J. E. (2011). Methane Index: A tetraether archaeal lipid biomarker indicator for detecting the instability of marine gas hydrates. *Earth and Planetary Science Letters*, *307*(3–4), 525–534. doi:10.1016/j.epsl.2011.05.031

APPENDIX A

Chemical structure of the C_{46} internal standard used in GDGT analyses. Patwardhan and Thompson (1999) were the first to synthesize the compound. Huguet et al. (2006) first described the use of the compound as an internal standard for quantification of GDGT lipids. C_{46} is an ideal standard for GDGT analyses as the compound is not naturally abundant but behaves like GDGTs during analysis due to the structural similarities.

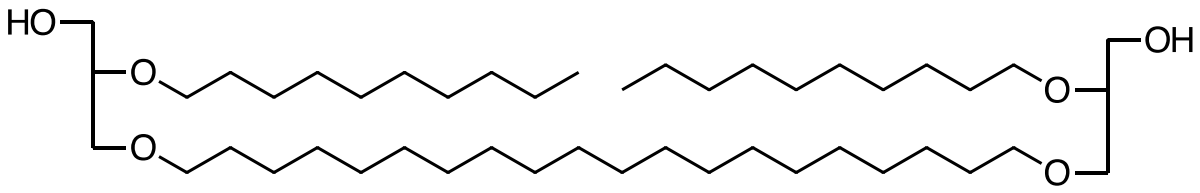

APPENDIX B

Table A.6.1: Concentration and isotopic composition of organic carbon and nitrogen in SPM.

Sample ID	Sample Date	C_{org} (%)	N_{org} (%)	C/N (wt.)	$\delta^{13}C_{org}$ (‰)	$\delta^{15}N_{org}$ (‰)
North Sediment Trap (170m)						
NST11-1	1/15/11 – 1/31/11	3.56	0.52	6.90	-24.83	2.34
NST11-2	2/1/11 – 2/17/11	3.48	0.42	8.35	-24.56	5.09
NST11-3	2/18/11 – 3/7/11	3.72	0.52	7.14	-24.90	2.15
NST11-4	3/7/11 – 3/24/11	3.02	0.33	9.02	-24.99	4.69
NST11-5	3/25/11 – 4/10/11	2.70	0.35	7.80	-24.73	2.55
NST11-6	4/11/11 – 4/27/11	2.64	0.37	7.12	-24.26	0.66
NST11-7	4/28/11 – 5/14/11	2.49	0.32	7.86	-24.11	0.43
NST11-8	5/15/11 – 6/1/11	2.52	0.31	8.10	-24.13	0.42
NST11-9	6/2/11 – 6/18/11	2.67	0.26	10.27	-24.35	0.23
NST11-10	6/19/11 – 7/5/11	2.60	0.34	7.52	-24.18	3.33
NST11-11	7/6/11 – 7/22/11	2.73	0.38	7.12	-24.33	1.80
NST11-12	7/21/11 – 8/8/11	3.03	0.38	8.03	-24.68	1.83
NST11-13	8/9/11 – 8/25/11	2.96	0.37	8.08	-24.73	1.52
NST11-14	8/26/11 – 9/12/11	3.20	0.38	8.37	-25.38	2.31
NST11-15	9/13/11 – 9/29/11	4.05	0.58	7.02	-26.51	2.05
NST11-16	9/30/11 – 10/16/11	3.83	0.53	7.28	-26.08	0.02
NST11-17	10/17/11 – 11/2/11	3.78	0.50	7.63	-25.73	-1.30
NST11-18	11/3/11 – 11/19/11	4.28	0.62	6.86	-26.14	0.73
NST11-19	11/20/11 – 12/7/11	4.24	0.57	7.37	-25.83	-1.83
NST11-20	12/8/11 – 12/24/11	4.53	0.57	7.92	-26.12	-1.60
NST11-21	12/25/11 – 1/10/12	4.53	0.58	7.82	-26.15	-5.23
NST12-1	1/11/12 – 1/30/12	4.95	0.53	9.41	-25.52	0.10
NST12-2	1/31/12 – 2/16/12	5.38	0.64	8.37	-25.17	1.11
NST12-3	2/17/12 – 3/4/12	4.66	0.58	8.03	-25.53	2.26
NST12-4	3/5/12 – 3/21/12	4.87	0.59	8.23	-25.71	4.80
NST12-5	3/22/12 – 4/6/12	3.39	0.40	8.57	-25.42	1.02
NST12-6	4/7/12 – 4/23/12	3.04	0.35	8.64	-24.81	2.50
NST12-7	4/24/12 – 5/10/12	2.83	0.36	7.78	-24.64	3.21

Sample ID	Sample Date	C_{org} (%)	N_{org} (%)	C/N (wt.)	$\delta^{13}C_{org}$ (‰)	$\delta^{15}N_{org}$ (‰)
NST12-8	5/11/12 – 5/27/12	2.82	0.35	8.16	-24.90	3.27
NST12-9	5/28/12 – 6/12/12	2.94	0.34	8.55	-24.63	2.21
NST12-10	6/13/12 – 6/29/12	2.91	0.35	8.35	-24.69	3.25
NST12-11	6/30/12 – 7/16/12	3.01	0.35	8.50	-24.97	1.53
NST12-12	7/17/12 – 8/2/12	3.52	0.41	8.67	-25.44	1.25
NST12-13	8/3/12 – 8/18/12	3.56	0.41	8.59	-23.60	-0.06
NST12-14	8/19/12 – 9/4/12	4.42	0.51	8.65	-25.07	1.32
NST12-15	9/5/12 – 9/21/12	4.23	0.52	8.09	-24.79	0.04
NST12-16	9/22/12 – 10/8/12	1.31	0.17	7.56	-24.52	-2.58
NST12-17	10/9/12 – 10/24/12	0.86	0.09	9.71	-26.12	-1.54
NST12-18	10/25/12 – 11/10/12	2.30	0.19	11.97	-20.75	0.62
NST12-19	11/11/12 – 11/27/12	1.53	0.08	18.21	-18.21	0.18
NST12-20	11/28/12 – 12/14/12	4.48	0.48	9.35	-25.28	-0.31
NST12-21	12/15/12 – 12/30/12	1.42	0.15	9.76	-20.50	-3.41
South Sediment Trap (125m)						
SST11-D-1	1/15/11 – 1/31/11	6.36	0.66	9.65	-23.70	-5.03
SST11-D-2	2/1/11 – 2/17/11	5.06	0.54	9.43	-23.26	-6.74
SST11-D-3	2/18/11 – 3/7/11	4.71	0.51	9.27	-23.00	-4.86
SST11-D-4	3/7/11 – 3/24/11	4.49	0.56	7.96	-22.72	1.13
SST11-D-5	3/25/11 – 4/10/11	4.83	0.44	10.94	-22.85	0.89
SST11-D-6	4/11/11 – 4/27/11	4.69	0.54	8.71	-22.59	-4.14
SST11-D-7	4/28/11 – 5/14/11	4.68	0.54	8.65	-22.95	-5.48
SST11-D-8	5/15/11 – 6/1/11	4.91	0.63	7.76	-22.91	-2.75
SST11-D-9	6/2/11 – 6/18/11	5.03	0.66	7.66	-22.58	-1.39
SST11-D-10	6/19/11 – 7/5/11	5.31	0.64	8.30	-22.80	-0.95
SST11-D-11	7/6/11 – 7/22/11	5.19	0.61	8.56	-23.12	-4.99
SST11-D-12	7/21/11 – 8/8/11	5.06	0.68	7.48	-23.29	-2.18
SST12-D-1	1/13/12 – 1/28/12	4.92	0.50	9.81	-24.06	1.58
SST12-D-2	1/29/12 – 2/15/12	5.14	0.53	9.69	-23.96	2.92
SST12-D-3	2/16/12 – 3/2/12	4.65	0.51	9.08	-23.44	3.00
SST12-D-4	3/3/12 – 3/19/12	4.76	0.48	9.91	-23.57	0.74
SST12-D-5	3/20/12 – 4/5/12	4.51	0.47	9.60	-23.72	0.14
SST12-D-6	4/6/12 – 4/22/12	3.73	0.38	9.85	-23.16	1.49
SST12-D-7	4/23/12 – 5/8/12	4.32	0.44	9.77	-23.29	0.88
SST12-D-8	5/9/12 – 5/25/12	4.36	0.48	9.17	-23.29	1.37
SST12-D-9	5/26/12 – 6/11/12	4.52	0.54	8.42	-23.26	2.06
SST12-D-10	6/12/12 – 6/28/12	4.85	0.59	8.24	-23.75	3.80
SST12-D-11	6/29/12 – 7/15/12	4.76	0.51	9.34	-23.67	1.13

Sample ID	Sample Date	C_{org} (%)	N_{org} (%)	C/N (wt.)	$\delta^{13}C_{org}$ (‰)	$\delta^{15}N_{org}$ (‰)
SST12-D-12	7/16/12 – 8/1/12	4.18	0.49	8.62	-23.58	2.49
SST12-D-13	8/2/12 - 8/18/12	4.25	0.47	9.02	-23.71	2.15
SST12-D-14	8/19/12 - 9/3/12	3.92	0.46	8.49	-23.48	3.06
SST12-D-15	9/4/12 - 9/20/12	3.06	0.81	3.76	-13.36	4.48
SST12-D-16	9/21/12 - 10/7/12	3.38	0.51	6.65	-26.03	3.78
SST12-D-17	10/8/12 - 10/24/12	4.57	0.59	7.72	-25.57	2.37
SST12-D-18	10/25/12 - 11/10/12	4.98	0.63	7.88	-24.18	3.19
SST12-D-19	11/11/12 - 11/27/12	3.83	0.49	7.80	-24.42	2.69
SST12-D-20	11/28/12 - 12/14/12	3.34	0.45	7.40	-23.70	3.28
SST12-D-21	12/15/12 - 12/31/12	2.60	0.35	7.40	-23.14	4.42
South Sediment Trap (110m)						
SST13-D-1	1/14/13 – 1/29/13	5.51	0.58	9.44	-24.74	2.33
SST13-D-2	1/30/13 – 2/15/13	3.22	0.40	8.06	-21.99	3.59
SST13-D-3	2/16/13 – 3/4/13	3.04	0.34	9.00	-22.12	2.31
SST13-D-4	3/5/13 – 3/21/13	2.96	0.38	7.90	-22.65	2.72
SST13-D-5	3/22/13 – 4/6/13	3.13	0.39	8.01	-22.71	3.24
SST13-D-6	4/7/13 – 4/23/13	5.48	0.80	6.85	-22.11	7.77
SST13-D-7	4/24/13 – 5/10/13	3.70	0.47	7.87	-23.36	2.78
SST13-D-8	5/11/13 – 5/27/13	4.26	0.51	8.39	-23.17	2.22
SST13-D-9	5/28/13 – 6/12/13	4.27	0.54	7.98	-23.39	2.71
SST13-D-10	6/13/13 – 6/29/13	6.05	0.93	6.48	-23.10	12.88
SST13-D-11	6/30/13 – 7/16/13	4.66	0.64	7.29	-23.58	4.55
SST13-D-12	7/17/13 – 8/2/13	4.86	0.64	7.63	-23.62	9.17
SST13-D-13	8/3/13 – 8/18/13	5.02	0.62	8.12	-23.72	4.19
SST13-D-14	8/19/13 – 9/4/13	5.27	1.79	2.94	n.a	3.81
SST13-D-15	9/5/13 – 9/21/13	4.87	1.00	4.88	n.a	3.52
SST13-D-16	9/22/13 –10/8/13	3.97	1.12	3.56	n.a	4.34
SST13-D-17	10/9/13 – 10/24/13	3.29	1.40	2.35	n.a	6.65
SST13-D-18	10/25/13 – 11/10/13	2.86	0.57	5.03	n.a	4.74
SST13-D-19	11/11/13 – 11/27/13	4.18	0.97	4.30	n.a	4.29
SST13-D-20	11/28/13 – 12/14/13	4.31	0.56	7.76	n.a	8.77
SST13-D-21	12/15/13 – 12/30/13	4.81	0.27	17.98	n.a	5.21
South Sediment Trap (50m)						
SST13-S-1	1/14/13 – 1/29/13	8.81	1.29	6.86	-22.97	6.10
SST13-S-2	1/30/13 – 2/15/13	2.91	0.31	9.49	-21.36	1.83
SST13-S-3	2/16/13 – 3/4/13	2.97	0.40	7.34	-22.00	4.92
SST13-S-4	3/5/13 – 3/21/13	2.78	0.31	8.86	-22.39	1.21

Sample ID	Sample Date	C_{org} (%)	N_{org} (%)	C/N (wt.)	$\delta^{13}C_{org}$ (‰)	$\delta^{15}N_{org}$ (‰)
SST13-S-5	3/22/13 – 4/6/13	2.92	0.32	9.18	-22.47	0.99
SST13-S-6	4/7/13 – 4/23/13	3.02	0.35	8.60	-22.75	2.09
SST13-S-7	4/24/13 – 5/10/13	3.31	0.37	8.91	-24.55	2.55
SST13-S-8	5/11/13 – 5/27/13	4.57	0.50	9.14	-24.28	4.76
SST13-S-10	6/13/13 – 6/29/13	8.67	1.32	6.55	-22.46	9.30
SST13-S-11	6/30/13 – 7/16/13	5.24	0.68	7.68	-23.67	6.14
SST13-S-12	7/17/13 – 8/2/13	4.81	0.67	7.20	-23.41	8.70
SST13-S-13	8/3/13 – 8/18/13	5.67	0.77	7.33	-23.68	5.46
SST13-S-14	8/19/13 – 9/4/13	6.89	1.03	6.72	-23.93	4.92
SST13-S-15	9/5/13 – 9/21/13	5.45	0.91	5.97	-22.42	4.33
SST13-S-16	9/22/13 –10/8/13	5.38	0.80	6.69	-23.49	2.73
SST13-S-17	10/9/13 – 10/24/13	6.60	1.00	6.61	-23.19	2.14
SST13-S-18	10/25/13 – 11/10/13	7.03	1.02	6.90	-23.86	5.24
SST13-S-19	11/11/13 – 11/27/13	8.92	1.10	8.11	-24.75	1.34
SST13-S-20	11/28/13 – 12/14/13	12.62	1.92	6.59	-23.28	5.18
SST13-S-21	12/15/13 – 12/30/13	14.27	2.38	5.99	-23.09	4.84

n.a. = not analyzed

APPENDIX C

Table A.6.2: Relative abundances (% of total) of isoGDGTs in Lake Malawi SPM.

Sample ID	GDGT 0 (%)	GDGT 1 (%)	GDGT 2 (%)	GDGT 3 (%)	Cren. (%)	Cren.' (%)
North Sediment Trap (170m)						
NST11-1	6.3	8.9	6.1	67.3	3.5	8.0
NST11-2	6.3	8.9	6.2	67.6	3.8	7.2
NST11-3	6.0	8.8	6.2	69.3	3.7	5.9
NST11-4	6.2	9.0	6.3	69.1	3.7	5.7
NST11-5	5.8	9.0	6.4	69.5	4.1	5.2
NST11-6	5.8	8.6	6.3	70.5	4.0	4.9
NST11-7	5.6	8.2	6.3	71.1	4.0	4.8
NST11-8	5.7	8.1	6.3	71.0	4.1	4.8
NST11-9	5.8	8.3	6.3	70.8	4.0	4.9
NST11-10	5.8	8.3	6.3	70.3	3.9	5.3
NST11-11	5.7	8.2	6.3	70.5	4.0	5.4
NST11-12	5.7	8.2	6.3	70.8	4.0	5.2
NST11-13	5.6	8.0	6.2	70.6	4.3	5.2
NST11-14	5.4	8.1	6.0	70.8	4.4	5.4
NST11-15	5.3	8.4	5.5	70.2	4.6	6.0
NST11-16	5.4	8.5	5.8	70.0	4.4	5.9
NST11-17	5.5	8.7	5.8	69.9	4.3	5.9
NST11-18	5.5	8.8	5.6	69.7	4.4	6.0
NST11-19	5.9	8.4	5.9	69.7	4.3	5.9
NST11-20	5.7	8.6	5.7	69.8	4.3	5.9
NST11-21	6.0	8.5	5.8	69.5	4.2	6.0
NST12-1	4.5	6.1	5.5	74.4	5.2	4.5
NST12-2	3.8	4.9	4.7	63.6	4.0	19.0
NST12-3	4.7	5.7	5.6	71.2	5.3	7.4
NST12-4	4.5	6.0	5.7	74.9	4.7	4.2
NST12-5	4.6	5.9	5.7	75.0	4.7	4.0
NST12-6	4.8	5.8	5.9	74.9	4.4	4.2
NST12-7	4.5	5.8	5.7	76.0	4.5	3.6

Sample ID	GDGT 0 (%)	GDGT 1 (%)	GDGT 2 (%)	GDGT 3 (%)	Cren. (%)	Cren.' (%)
NST12-8	4.4	5.9	5.6	75.8	4.5	3.7
NST12-9	4.5	5.6	5.7	75.8	4.4	3.9
NST12-10	4.4	5.5	5.4	76.3	4.8	3.6
NST12-11	4.3	5.4	5.4	76.7	4.7	3.5
NST12-12	4.1	5.4	5.4	76.6	5.1	3.5
NST12-13	4.1	5.5	5.5	76.0	5.3	3.6
NST12-14	4.1	5.2	5.4	76.3	5.2	3.8
NST12-15	4.1	5.3	5.2	76.2	5.4	3.8
NST12-16	4.4	5.9	5.1	74.5	5.5	4.6
NST12-17	4.3	5.5	5.1	75.3	5.4	4.4
NST12-18	4.5	6.0	5.2	74.3	5.4	4.6
NST12-19	4.6	6.6	5.1	73.8	5.0	4.8
NST12-20	4.6	6.8	5.2	73.7	5.0	4.7
NST12-21	4.6	6.5	5.2	74.0	4.9	4.8
South Sediment Trap (125m)						
SST11-D-1	7.7	8.4	6.8	67.3	2.5	7.2
SST11-D-2	7.7	9.1	7.3	67.4	2.7	5.7
SST11-D-3	7.6	8.9	7.2	68.4	2.8	5.1
SST11-D-4	7.1	8.8	7.1	69.6	2.8	4.7
SST11-D-5	7.3	9.1	7.3	68.5	2.7	5.0
SST11-D-6	7.2	9.1	7.3	68.5	2.8	5.2
SST11-D-7	6.9	9.0	7.2	69.2	2.9	4.8
SST11-D-8	6.9	8.7	7.1	69.3	2.9	5.1
SST11-D-9	7.0	8.8	7.0	68.9	2.9	5.4
SST11-D-10	6.8	8.7	6.8	69.3	2.8	5.6
SST11-D-11	6.5	8.8	6.7	69.6	3.0	5.4
SST11-D-12	6.5	8.8	6.6	69.6	3.1	5.4
SST12-D-1	6.4	6.3	6.1	73.7	2.6	4.9
SST12-D-3	6.2	6.3	6.3	74.4	2.7	4.1
SST12-D-4	6.2	6.6	6.5	73.9	2.7	4.2
SST12-D-6	5.8	6.8	6.8	73.9	3.0	3.8
SST12-D-7	5.5	6.5	6.2	74.9	2.9	4.0
SST12-D-8	5.1	6.2	6.0	75.6	3.1	4.0
SST12-D-9	6.0	6.6	6.3	72.8	3.0	5.3
SST12-D-10	5.8	6.5	6.0	73.8	3.0	4.8
SST12-D-11	5.6	6.2	5.8	74.9	2.9	4.5
SST12-D-12	5.3	6.5	5.3	75.1	3.1	4.8

Sample ID	GDGT 0 (%)	GDGT 1 (%)	GDGT 2 (%)	GDGT 3 (%)	Cren. (%)	Cren.' (%)
South Sediment Trap (110m)						
SST13-D-1	6.4	6.5	6.2	73.8	2.3	4.9
SST13-D-2	6.2	6.1	6.1	74.5	2.6	4.5
SST13-D-3	5.6	5.7	6.1	76.3	2.5	3.8
SST13-D-4	5.3	6.1	6.3	76.2	2.6	3.5
SST13-D-5	5.3	6.1	6.4	76.1	2.7	3.5
SST13-D-6	4.3	5.1	5.3	59.0	2.3	24.0
SST13-D-7	5.6	6.6	6.7	74.3	2.8	4.0
SST13-D-8	5.8	6.4	6.2	74.3	2.7	4.5
SST13-D-9	5.8	6.4	6.0	74.4	2.8	4.4
SST13-D-10	5.6	6.4	6.1	74.0	2.8	5.1
SST13-D-11	6.0	6.1	5.9	73.6	2.9	5.5
SST13-D-12	6.8	6.1	5.6	72.2	2.7	6.6
SST13-D-13	6.9	5.7	5.4	72.7	2.4	6.9
South Sediment Trap (50m)						
SST13-S-1	4.7	4.9	5.9	79.0	2.0	3.4
SST13-S-2	4.7	5.0	6.0	78.9	2.2	3.2
SST13-S-3	4.5	5.1	6.3	77.8	2.5	3.8
SST13-S-4	6.2	5.6	6.4	69.2	0.0	12.6
SST13-S-5	6.1	5.3	6.0	75.4	2.2	5.0
SST13-S-6	6.6	5.7	6.0	70.7	2.2	8.9
SST13-S-7	6.9	5.4	5.8	73.0	2.0	6.9
SST13-S-8	6.9	5.2	5.8	74.1	2.2	5.9
SST13-S-10	7.8	5.2	5.8	71.9	1.9	7.4
SST13-S-11	7.9	5.3	5.8	72.0	1.9	7.0
SST13-S-12	8.4	5.3	5.7	70.8	2.3	7.6
SST13-S-13	8.3	5.3	6.2	71.0	2.0	7.2
SST13-S-14	8.6	5.4	6.0	70.2	2.0	7.8
SST13-S-15	8.7	5.4	6.0	71.2	2.1	6.6
SST13-S-16	9.0	5.5	6.1	70.7	1.8	6.9
SST13-S-17	9.1	5.8	6.2	70.6	1.9	6.4
SST13-S-18	8.9	6.0	6.4	70.6	1.7	6.3
SST13-S-19	6.9	9.0	5.5	6.1	70.7	1.8
SST13-S-20	6.4	9.1	5.8	6.2	70.6	1.9
SST13-S-21	6.3	8.9	6.0	6.4	70.6	1.7

APPENDIX D

Table A.6.3: IsoGDGT-based indices and TEX_{86} reconstructed temperatures.

Sample ID	2/2+3	TEX_{86}	LST[a]	BIT	GDGT-0 /cren.[b]	MI[c]
North Sediment Trap (170m)						
NST11-1	0.59	0.75	27.2	0.19	0.12	0.23
NST11-2	0.59	0.75	27.5	0.18	0.11	0.23
NST11-3	0.59	0.76	27.8	0.16	0.09	0.22
NST11-4	0.59	0.75	27.7	0.15	0.08	0.23
NST11-5	0.58	0.77	28.5	0.15	0.07	0.22
NST11-6	0.58	0.77	28.3	0.15	0.07	0.22
NST11-7	0.56	0.77	28.4	0.15	0.07	0.21
NST11-8	0.56	0.76	28.2	0.15	0.07	0.21
NST11-9	0.57	0.76	28.1	0.15	0.07	0.21
NST11-10	0.57	0.76	28.0	0.15	0.08	0.22
NST11-11	0.57	0.77	28.3	0.15	0.08	0.21
NST11-12	0.57	0.77	28.2	0.15	0.07	0.21
NST11-13	0.56	0.77	28.4	0.15	0.07	0.21
NST11-14	0.58	0.78	28.8	0.14	0.08	0.21
NST11-15	0.61	0.78	29.0	0.15	0.09	0.20
NST11-16	0.59	0.77	28.8	0.15	0.08	0.21
NST11-17	0.60	0.77	28.6	0.15	0.08	0.21
NST11-18	0.61	0.77	28.6	0.16	0.09	0.21
NST11-19	0.59	0.76	28.0	0.16	0.08	0.21
NST11-20	0.60	0.76	28.2	0.17	0.08	0.21
NST11-21	0.59	0.76	27.8	0.17	0.09	0.22
NST12-1	0.53	0.79	29.6	0.21	0.06	0.17
NST12-2	0.51	0.78	29.1	0.21	0.30	0.17
NST12-3	0.51	0.78	29.2	0.24	0.10	0.17
NST12-4	0.51	0.78	29.3	0.23	0.06	0.17
NST12-5	0.51	0.78	29.2	0.21	0.05	0.17
NST12-6	0.49	0.77	28.6	0.15	0.06	0.17
NST12-7	0.51	0.78	28.9	0.16	0.05	0.17

Sample ID	2/2+3	TEX_{86}	LST[a]	BIT	GDGT-0 /cren.[b]	MI[c]
NST12-8	0.52	0.78	29.2	0.19	0.05	0.17
NST12-9	0.49	0.78	28.9	0.16	0.05	0.16
NST12-10	0.51	0.78	29.2	0.18	0.05	0.16
NST12-11	0.50	0.78	29.2	0.19	0.05	0.16
NST12-12	0.50	0.80	29.9	0.18	0.05	0.15
NST12-13	0.50	0.80	30.1	0.17	0.05	0.16
NST12-14	0.49	0.80	29.9	0.15	0.05	0.15
NST12-15	0.50	0.79	29.8	0.20	0.05	0.15
NST12-16	0.53	0.79	29.6	0.16	0.06	0.16
NST12-17	0.52	0.79	29.4	0.20	0.06	0.16
NST12-18	0.54	0.79	29.4	0.19	0.06	0.16
NST12-19	0.56	0.78	29.3	0.22	0.07	0.17
NST12-20	0.57	0.79	29.5	0.21	0.06	0.17
NST12-21	0.56	0.78	29.2	0.26	0.07	0.17
South Sediment Trap (125m)						
SST11-D-1	0.55	0.70	24.4	0.23	0.11	0.25
SST11-D-2	0.55	0.71	25.3	0.20	0.08	0.26
SST11-D-3	0.55	0.71	25.3	0.18	0.08	0.25
SST11-D-4	0.55	0.72	26.0	0.16	0.07	0.24
SST11-D-5	0.56	0.72	25.9	0.15	0.07	0.25
SST11-D-6	0.56	0.73	26.1	0.14	0.08	0.25
SST11-D-7	0.56	0.73	26.5	0.14	0.07	0.24
SST11-D-8	0.55	0.73	26.3	0.15	0.07	0.24
SST11-D-9	0.56	0.73	26.1	0.13	0.08	0.24
SST11-D-10	0.56	0.73	26.2	0.13	0.08	0.24
SST11-D-11	0.57	0.74	26.8	0.12	0.08	0.23
SST11-D-12	0.57	0.74	26.8	0.12	0.08	0.23
SST12-D-1	0.51	0.70	24.7	0.14	0.07	0.20
SST12-D-3	0.50	0.71	25.3	0.17	0.05	0.20
SST12-D-4	0.50	0.72	25.6	0.23	0.06	0.20
SST12-D-6	0.50	0.74	26.8	0.17	0.05	0.20
SST12-D-7	0.51	0.74	26.8	0.22	0.05	0.19
SST12-D-8	0.51	0.75	27.4	0.20	0.05	0.18
SST12-D-9	0.51	0.73	26.0	0.15	0.07	0.20
SST12-D-10	0.52	0.73	26.2	0.17	0.07	0.19
SST12-D-11	0.52	0.73	26.2	0.18	0.06	0.18
SST12-D-12	0.55	0.74	26.8	0.19	0.06	0.18

Sample ID	2/2+3	TEX_{86}	LST[a]	BIT	GDGT-0 /cren.[b]	MI[c]
South Sediment Trap (110m)						
SST13-D-1	0.51	0.70	24.6	0.17	0.07	0.20
SST13-D-2	0.50	0.70	24.9	0.18	0.06	0.19
SST13-D-3	0.48	0.72	25.6	0.16	0.05	0.18
SST13-D-4	0.49	0.74	26.8	0.14	0.05	0.18
SST13-D-5	0.49	0.74	27.0	0.13	0.05	0.18
SST13-D-6	0.49	0.75	27.2	0.15	0.41	0.19
SST13-D-7	0.50	0.74	26.9	0.15	0.05	0.20
SST13-D-8	0.51	0.72	26.0	0.17	0.06	0.19
SST13-D-9	0.51	0.72	26.0	0.20	0.06	0.19
SST13-D-10	0.51	0.73	26.3	0.16	0.07	0.19
SST13-D-11	0.51	0.71	25.2	0.18	0.07	0.19
SST13-D-12	0.52	0.68	23.5	0.18	0.09	0.20
SST13-D-13	0.52	0.66	22.5	0.18	0.10	0.19
South Sediment Trap (50m)						
SST13-S-1	0.49	0.63	21.0	0.22	0.44	0.22
SST13-S-2	0.48	0.66	22.6	0.18	0.09	0.20
SST13-S-3	0.47	0.67	23.0	0.22	0.06	0.18
SST13-S-4	0.45	0.73	26.3	0.11	0.04	0.16
SST13-S-5	0.45	0.74	26.6	0.11	0.04	0.16
SST13-S-6	0.45	0.76	27.7	0.10	0.05	0.17
SST13-S-7	0.47	0.66	22.2	0.13	0.18	0.21
SST13-S-8	0.47	0.69	23.9	0.10	0.07	0.18
SST13-S-10	0.49	0.68	23.4	0.20	0.13	0.20
SST13-S-11	0.48	0.66	22.3	0.17	0.09	0.20
SST13-S-12	0.47	0.66	22.2	0.17	0.08	0.19
SST13-S-13	0.48	0.62	20.4	0.14	0.10	0.20
SST13-S-14	0.48	0.62	20.4	0.12	0.10	0.20
SST13-S-15	0.48	0.61	19.8	0.16	0.11	0.21
SST13-S-16	0.46	0.62	20.2	0.14	0.10	0.21
SST13-S-17	0.48	0.61	19.5	0.14	0.11	0.22
SST13-S-18	0.47	0.61	19.6	0.14	0.09	0.22
SST13-S-19	0.48	0.60	19.0	0.14	0.10	0.22
SST13-S-20	0.48	0.61	19.4	0.18	0.09	0.23
SST13-S-21	0.48	0.61	19.8	0.23	0.09	0.23

[a]LST calculated according to Powers et al. (2010).

[b]GDGT-0/crenarchaeol with values >2 are indicative of high contributions of GDGT-0 by methanogenic archaea.

[c]MI calculated according to Zhang et al. (2011). Values > 0.3 are indicative of substantial contributions of GDGT-1 -2 and -3 by methanotrophic *Euryarchaeota*.

APPENDIX E

Table A.6.4: Relative abundances (% of total) of brGDGTs in Lake Malawi SPM.

Sample ID	Ia	Ib	Ic	IIa	IIa’	IIb	IIb’	IIc	IIc’	IIIa	IIIa’	IIIb	IIIb’	IIIc	IIIc’
North Sediment Trap (170 m)															
NST11-1	39.8	0.0	0.0	49.0	0.0	0.0	0.0	0.0	0.0	11.2	0.0	0.0	0.0	0.0	0.0
NST11-2	39.9	0.0	0.0	49.0	0.0	0.0	0.0	0.0	0.0	11.1	0.0	0.0	0.0	0.0	0.0
NST11-3	40.3	0.0	0.0	48.2	0.0	0.0	0.0	0.0	0.0	11.5	0.0	0.0	0.0	0.0	0.0
NST11-4	40.0	0.0	0.0	48.5	0.0	0.0	0.0	0.0	0.0	11.5	0.0	0.0	0.0	0.0	0.0
NST11-5	39.7	0.0	0.0	48.9	0.0	0.0	0.0	0.0	0.0	11.5	0.0	0.0	0.0	0.0	0.0
NST11-6	40.7	0.0	0.0	48.1	0.0	0.0	0.0	0.0	0.0	11.2	0.0	0.0	0.0	0.0	0.0
NST11-7	41.9	0.0	0.0	47.3	0.0	0.0	0.0	0.0	0.0	10.9	0.0	0.0	0.0	0.0	0.0
NST11-8	42.8	0.0	0.0	46.8	0.0	0.0	0.0	0.0	0.0	10.4	0.0	0.0	0.0	0.0	0.0
NST11-9	43.1	0.0	0.0	46.6	0.0	0.0	0.0	0.0	0.0	10.3	0.0	0.0	0.0	0.0	0.0
NST11-10	42.8	0.0	0.0	46.8	0.0	0.0	0.0	0.0	0.0	10.4	0.0	0.0	0.0	0.0	0.0
NST11-11	43.0	0.0	0.0	46.6	0.0	0.0	0.0	0.0	0.0	10.4	0.0	0.0	0.0	0.0	0.0
NST11-12	43.1	0.0	0.0	46.5	0.0	0.0	0.0	0.0	0.0	10.5	0.0	0.0	0.0	0.0	0.0
NST11-13	43.2	0.0	0.0	46.5	0.0	0.0	0.0	0.0	0.0	10.3	0.0	0.0	0.0	0.0	0.0
NST11-14	42.2	0.0	0.0	47.2	0.0	0.0	0.0	0.0	0.0	10.6	0.0	0.0	0.0	0.0	0.0
NST11-15	40.8	0.0	0.0	49.6	0.0	0.0	0.0	0.0	0.0	9.7	0.0	0.0	0.0	0.0	0.0
NST11-16	41.4	0.0	0.0	48.7	0.0	0.0	0.0	0.0	0.0	9.8	0.0	0.0	0.0	0.0	0.0
NST11-17	40.3	0.0	0.0	49.2	0.0	0.0	0.0	0.0	0.0	10.5	0.0	0.0	0.0	0.0	0.0
NST11-18	39.7	0.0	0.0	49.5	0.0	0.0	0.0	0.0	0.0	10.8	0.0	0.0	0.0	0.0	0.0
NST11-19	40.1	0.0	0.0	49.4	0.0	0.0	0.0	0.0	0.0	10.5	0.0	0.0	0.0	0.0	0.0
NST11-20	39.8	0.0	0.0	49.3	0.0	0.0	0.0	0.0	0.0	10.9	0.0	0.0	0.0	0.0	0.0
NST11-21	40.3	0.0	0.0	49.1	0.0	0.0	0.0	0.0	0.0	10.6	0.0	0.0	0.0	0.0	0.0
NST12-1	40.9	3.5	0.5	8.9	32.7	1.3	2.8	0.0	0.0	1.3	8.1	0.0	0.0	0.0	0.0
NST12-2	42.1	3.1	0.5	7.5	33.0	1.2	2.8	0.0	0.0	1.0	8.7	0.0	0.0	0.0	0.0
NST12-3	43.9	4.0	0.6	6.0	34.2	0.0	3.3	0.0	0.0	0.0	8.0	0.0	0.0	0.0	0.0
NST12-4	43.2	3.5	0.5	4.3	35.5	0.8	2.5	0.0	0.0	0.7	8.9	0.0	0.0	0.0	0.0
NST12-5	41.4	3.6	0.5	4.6	36.8	0.8	3.0	0.0	0.0	0.7	8.7	0.0	0.0	0.0	0.0
NST12-6	40.5	3.5	0.0	4.9	37.3	1.1	3.0	0.0	0.0	0.0	9.7	0.0	0.0	0.0	0.0
NST12-7	39.2	3.5	0.6	4.1	37.8	0.7	3.5	0.2	0.2	0.7	9.3	0.2	0.0	0.0	0.0

Sample ID	Ia	Ib	Ic	IIa	IIa'	IIb	IIb'	IIc	IIc'	IIIa	IIIa'	IIIb	IIIb'	IIIc	IIIc'
NST12-9	43.5	3.8	0.6	3.8	35.2	0.8	3.4	0.0	0.0	0.6	8.2	0.0	0.0	0.0	0.0
NST12-10	43.2	3.8	0.7	4.2	34.9	1.0	3.3	0.3	0.2	0.7	7.5	0.2	0.1	0.0	0.0
NST12-11	42.3	4.1	0.8	4.8	34.5	1.3	3.5	0.4	0.0	0.7	7.6	0.0	0.0	0.0	0.0
NST12-12	41.8	4.3	0.9	4.6	34.1	1.6	3.6	0.4	0.2	0.8	7.4	0.2	0.1	0.0	0.0
NST12-13	41.4	4.7	1.0	4.9	33.3	1.8	3.7	0.5	0.2	0.9	7.1	0.2	0.1	0.1	0.0
NST12-14	41.7	4.8	1.1	5.1	32.5	1.8	3.9	0.5	0.2	0.9	7.2	0.3	0.1	0.0	0.0
NST12-15	41.2	5.0	1.1	6.4	31.5	1.9	4.2	0.5	0.0	1.0	6.9	0.3	0.0	0.0	0.0
NST12-16	38.1	5.2	1.1	7.7	31.2	2.6	4.1	0.6	0.3	1.2	7.2	0.3	0.2	0.1	0.0
NST12-17	38.2	5.3	1.0	7.3	31.6	2.4	4.3	0.5	0.3	1.1	7.2	0.3	0.2	0.1	0.0
NST12-18	36.8	5.1	1.0	7.6	32.4	2.1	4.7	0.5	0.3	1.2	7.8	0.3	0.2	0.1	0.0
NST12-19	33.1	4.5	0.8	7.5	31.4	6.5	6.2	0.4	0.3	1.2	7.5	0.3	0.2	0.1	0.0
NST12-20	35.1	4.9	0.9	7.6	33.9	1.7	5.3	0.4	0.3	1.3	8.0	0.3	0.2	0.1	0.0
NST12-21	36.1	4.9	0.9	8.0	32.9	1.9	4.9	0.4	0.3	1.2	7.8	0.3	0.2	0.1	0.0
South Sediment Trap (125 m)															
SST11-D-1	42.1	0.0	0.0	47.2	0.0	0.0	0.0	0.0	0.0	10.7	0.0	0.0	0.0	0.0	0.0
SST11-D-2	39.2	0.0	0.0	49.2	0.0	0.0	0.0	0.0	0.0	11.5	0.0	0.0	0.0	0.0	0.0
SST11-D-3	40.5	0.0	0.0	48.3	0.0	0.0	0.0	0.0	0.0	11.2	0.0	0.0	0.0	0.0	0.0
SST11-D-4	41.5	0.0	0.0	47.8	0.0	0.0	0.0	0.0	0.0	10.7	0.0	0.0	0.0	0.0	0.0
SST11-D-5	41.3	0.0	0.0	47.8	0.0	0.0	0.0	0.0	0.0	10.9	0.0	0.0	0.0	0.0	0.0
SST11-D-6	41.4	0.0	0.0	47.7	0.0	0.0	0.0	0.0	0.0	10.9	0.0	0.0	0.0	0.0	0.0
SST11-D-7	43.9	0.0	0.0	46.2	0.0	0.0	0.0	0.0	0.0	9.9	0.0	0.0	0.0	0.0	0.0
SST11-D-8	44.2	0.0	0.0	46.1	0.0	0.0	0.0	0.0	0.0	9.7	0.0	0.0	0.0	0.0	0.0
SST11-D-9	45.7	0.0	0.0	45.3	0.0	0.0	0.0	0.0	0.0	8.9	0.0	0.0	0.0	0.0	0.0
SST11-D-10	45.9	0.0	0.0	45.6	0.0	0.0	0.0	0.0	0.0	8.5	0.0	0.0	0.0	0.0	0.0
SST11-D-11	45.8	0.0	0.0	45.8	0.0	0.0	0.0	0.0	0.0	8.4	0.0	0.0	0.0	0.0	0.0
SST11-D-12	45.4	0.0	0.0	45.9	0.0	0.0	0.0	0.0	0.0	8.7	0.0	0.0	0.0	0.0	0.0
SST12-D-1	38.3	4.5	1.1	3.0	38.0	1.0	3.4	0.0	0.0	0.7	10.1	0.0	0.0	0.0	0.0
SST12-D-3	36.6	4.6	1.2	3.2	37.3	0.9	4.3	0.3	0.3	0.6	10.3	0.2	0.2	0.0	0.0
SST12-D-4	36.2	4.9	1.2	3.2	36.9	1.1	4.8	0.3	0.4	0.6	9.9	0.2	0.3	0.0	0.0

Sample ID	Ia	Ib	Ic	IIa	IIa'	IIb	IIb'	IIc	IIc'	IIIa	IIIa'	IIIb	IIIb'	IIIc	IIIc'
SST12-D-6	36.3	5.1	1.3	3.0	36.4	1.4	5.4	0.5	0.4	0.6	8.8	0.2	0.3	0.0	0.1
SST12-D-7	38.8	6.6	1.9	4.0	31.9	1.8	5.5	0.7	0.4	0.8	7.1	0.2	0.3	0.0	0.0
SST12-D-8	42.8	6.6	2.0	4.6	29.3	2.4	4.6	0.8	0.4	0.8	5.4	0.0	0.3	0.0	0.0
SST12-D-9	39.1	8.0	2.4	4.2	29.1	2.5	6.3	1.0	0.6	0.9	5.3	0.3	0.3	0.1	0.1
SST12-D-10	37.9	7.9	2.4	4.2	29.1	2.6	6.9	1.0	0.6	0.9	5.7	0.3	0.4	0.1	0.1
SST12-D-11	38.2	7.7	2.4	4.5	28.8	2.4	7.0	0.9	0.7	0.9	5.8	0.3	0.4	0.0	0.0
SST12-D-12	38.2	9.3	3.0	7.9	23.9	3.5	6.3	1.0	0.8	1.1	4.4	0.3	0.4	0.0	0.0
South Sediment Trap (110 m)															
SST13-D-1	37.1	4.2	0.9	2.1	39.6	0.6	4.6	0.3	0.2	0.4	9.6	0.2	0.1	0.0	0.0
SST13-D-2	37.2	4.2	0.9	2.5	38.7	1.1	3.8	0.3	0.2	0.6	10.0	0.2	0.1	0.0	0.0
SST13-D-3	36.0	4.4	1.1	3.1	38.0	0.9	4.6	0.4	0.3	0.6	10.4	0.2	0.0	0.0	0.0
SST13-D-4	36.7	4.4	1.2	3.2	37.7	0.8	4.5	0.4	0.3	0.6	9.8	0.2	0.2	0.0	0.0
SST13-D-5	36.3	4.2	1.2	2.2	38.4	1.0	4.8	0.6	0.3	0.5	10.1	0.3	0.2	0.0	0.0
SST13-D-6	39.0	5.1	1.3	3.8	35.0	2.0	5.0	0.8	0.0	0.0	8.2	0.0	0.0	0.0	0.0
SST13-D-7	38.6	5.5	1.6	2.3	34.9	2.1	5.5	1.0	0.3	0.5	6.9	0.3	0.3	0.1	0.1
SST13-D-8	37.5	7.0	2.3	2.7	31.7	3.2	6.1	1.3	0.5	0.7	6.0	0.4	0.3	0.2	0.2
SST13-D-9	37.7	6.9	2.3	2.8	31.9	3.2	6.4	1.4	0.5	0.7	6.2	0.0	0.0	0.0	0.0
SST13-D-10	35.8	7.4	2.6	3.6	29.9	3.5	6.9	1.5	0.6	0.9	6.0	0.5	0.5	0.3	0.0
SST13-D-11	36.8	7.6	2.6	3.5	29.6	3.5	7.0	1.6	0.6	0.8	5.4	0.4	0.4	0.2	0.0
SST13-D-12	36.3	8.2	2.8	4.4	28.4	3.9	6.7	1.5	0.7	0.9	5.2	0.5	0.4	0.2	0.0
SST13-D-13	37.1	8.1	2.7	5.8	26.7	3.7	6.4	1.4	0.6	1.1	5.1	0.4	0.4	0.3	0.2
South Sediment Trap (50 m)															
SST13-S-1	37.5	3.2	0.0	3.2	40.5	0.0	2.1	0.0	0.0	0.0	13.5	0.0	0.0	0.0	0.0
SST13-S-2	39.8	4.6	0.0	3.5	37.5	0.0	2.3	0.0	0.0	0.0	12.2	0.0	0.0	0.0	0.0
SST13-S-3	35.9	3.8	0.7	3.4	39.5	0.9	2.7	0.0	0.2	0.6	12.1	0.2	0.0	0.0	0.0
SST13-S-4	36.6	4.0	0.9	3.1	38.9	0.4	3.2	0.0	0.3	0.5	11.9	0.2	0.0	0.0	0.0
SST13-S-5	41.1	4.3	0.0	3.1	37.9	0.0	3.4	0.0	0.0	0.0	10.2	0.0	0.0	0.0	0.0
SST13-S-6	43.2	5.3	0.0	2.8	35.5	0.0	4.6	0.0	0.0	0.0	8.6	0.0	0.0	0.0	0.0

Sample ID	Ia	Ib	Ic	IIa	IIa’	IIb	IIb’	IIc	IIc’	IIIa	IIIa’	IIIb	IIIb’	IIIc	IIIc’
SST13-S-7	60.9	0.0	0.0	0.0	39.1	0.0	0.0	0.0	0.0	0.0	0.0	0.0	0.0	0.0	0.0
SST13-S-8	43.5	7.6	1.9	1.3	32.2	1.3	7.1	0.0	0.0	0.0	5.1	0.0	0.0	0.0	0.0
SST13-S-10	39.6	7.8	2.2	2.7	30.6	1.4	8.2	0.6	0.7	0.4	5.1	0.2	0.4	0.0	0.0
SST13-S-11	36.6	9.1	2.2	3.7	28.7	1.7	10.4	0.6	0.9	0.6	4.9	0.0	0.5	0.0	0.0
SST13-S-12	34.1	10.3	2.2	2.5	28.2	1.7	13.0	0.5	1.2	0.5	5.1	0.1	0.6	0.0	0.0
SST13-S-13	37.3	8.7	2.1	4.4	27.9	2.0	10.1	0.7	0.9	0.7	4.7	0.2	0.4	0.0	0.0
SST13-S-14	35.7	9.1	2.0	3.3	30.1	1.8	10.5	0.6	1.0	0.5	4.9	0.0	0.4	0.0	0.0
SST13-S-15	36.6	7.6	1.9	5.2	31.5	2.3	6.9	0.7	0.6	0.7	6.0	0.0	0.0	0.0	0.0
SST13-S-16	38.2	4.9	1.0	2.3	37.6	0.9	5.2	0.3	0.4	0.4	8.8	0.0	0.0	0.0	0.0
SST13-S-17	37.4	4.5	1.0	2.1	39.1	0.7	4.7	0.3	0.4	0.3	9.5	0.0	0.0	0.0	0.0
SST13-S-18	34.3	4.4	1.0	2.8	40.1	0.7	4.7	0.0	0.4	0.0	11.6	0.0	0.0	0.0	0.0
SST13-S-19	33.8	4.2	0.9	2.0	41.0	0.8	4.2	0.0	0.0	0.0	13.2	0.0	0.0	0.0	0.0
SST13-S-20	32.6	4.1	0.8	1.0	42.1	0.4	4.5	0.0	0.4	0.0	14.0	0.0	0.0	0.0	0.0
SST13-S-21	28.6	3.9	0.0	0.0	37.3	2.0	3.1	0.0	0.0	12.6	12.5	0.0	0.0	0.0	0.0

APPENDIX F

Table A.6.5: Reconstructed temperatures using various brGDGT-based calibrations.

Sample ID	MAAT[a] (°C) (5_{me} + 6_{me})	MAAT[a] (°C) (5_{me} only)	MAAT[b] (°C) (5_{me} + 6_{me})	MAAT[b] (°C) (5_{me} only)	MAT_{mr}[c] (°C) (5_{me} only)
North Sediment Trap (170m)					
NST12-1	16.1	32.5	17.2	24.2	12.7
NST12-2	15.8	32.7	17.0	24.2	13.2
NST12-3	16.6	33.3	18.4	25.5	14.2
NST12-4	15.8	33.6	17.4	25.0	14.4
NST12-5	16.1	34.2	17.4	25.0	14.1
NST12-6	15.9	34.9	17.1	25.2	13.6
NST12-7	16.2	35.1	15.5	24.3	13.8
NST12-8	16.9	33.6	16.8	24.6	14.8
NST12-9	16.5	33.7	18.1	25.4	14.7
NST12-10	17.0	33.7	16.4	24.1	14.6
NST12-11	17.2	33.7	17.0	24.0	14.4
NST12-12	17.7	33.9	16.2	23.9	14.4
NST12-13	18.1	33.9	16.2	23.9	14.4
NST12-14	18.1	33.7	16.1	23.7	14.4
NST12-15	18.4	33.4	17.3	23.6	14.1
NST12-16	18.7	33.9	15.6	23.3	13.2
NST12-17	18.7	34.1	16.0	23.7	13.3
NST12-18	18.4	34.4	15.6	23.6	12.9
NST12-19	20.2	35.7	15.8	23.6	12.1
NST12-20	18.3	35.0	15.4	23.8	12.6
NST12-21	18.3	34.5	15.6	23.8	12.6
South Sediment Trap (125m)					
SST12-D-1	16.2	35.7	17.8	26.0	14.4
SST12-D-3	16.9	36.3	15.3	25.0	14.1
SST12-D-4	17.4	36.4	15.3	25.0	14.2
SST12-D-6	18.4	36.4	15.3	24.6	14.3
SST12-D-7	19.8	35.2	16.5	24.9	15.0
SST12-D-8	20.3	33.6	17.2	24.4	15.6
SST12-D-9	21.8	34.9	17.0	24.8	15.6
SST12-D-10	21.9	35.4	16.4	24.6	15.3

Sample ID	MAAT[a] (°C) (5_{me} + 6_{me})	MAAT[a] (°C) (5_{me} only)	MAAT[b] (°C) (5_{me} + 6_{me})	MAAT[b] (°C) (5_{me} only)	MAT_{mr}[c] (°C) (5_{me} only)
SST12-D-11	21.7	35.2	16.2	24.6	15.3
SST12-D-12	23.0	33.9	17.4	25.1	14.9
South Sediment Trap (110m)					
SST13-D-1	17.0	36.6	15.4	24.6	14.3
SST13-D-2	16.7	36.3	15.2	24.5	14.2
SST13-D-3	16.8	36.6	14.8	24.4	14.0
SST13-D-4	17.1	36.3	14.9	24.3	14.1
SST13-D-6	17.2	36.8	14.0	23.6	14.2
SST13-D-7	18.6	35.8	16.0	23.3	14.5
SST13-D-8	19.8	36.0	14.7	22.8	15.1
SST13-D-9	21.6	36.1	14.5	22.6	15.4
SST13-D-10	21.3	36.0	13.9	22.3	15.4
SST13-D-11	22.3	36.3	13.5	22.1	15.1
SST13-D-12	22.6	36.0	14.1	22.1	15.3
SST13-D-13	22.9	35.8	14.6	22.7	15.2
South Sediment Trap (50m)					
SST13-S-1	13.6	36.4	15.3	25.1	13.5
SST13-S-2	14.6	35.6	17.3	26.3	14.2
SST13-S-3	15.1	36.5	15.5	25.5	13.6
SST13-S-4	15.3	36.4	15.6	25.7	13.9
SST13-S-5	15.7	35.2	17.8	26.1	14.4
SST13-S-6	17.0	34.6	19.5	27.0	15.1
SST13-S-7	17.0	29.3	17.7	22.8	17.6
SST13-S-8	21.0	35.0	23.3	29.2	16.8
SST13-S-10	22.1	35.6	17.6	26.3	16.0
SST13-S-11	23.4	36.1	18.3	27.5	15.5
SST13-S-12	24.8	37.5	18.7	29.0	15.7
SST13-S-13	23.4	35.6	17.8	26.8	15.3
SST13-S-14	23.5	36.6	18.0	27.5	15.4
SST13-S-15	21.2	35.6	16.9	25.6	14.5
SST13-S-16	17.8	36.2	16.1	25.4	14.7
SST13-S-18	17.2	36.6	15.4	25.2	14.5
SST13-S-19	16.4	37.7	15.5	26.2	13.7
SST13-S-20	15.4	38.1	16.4	26.1	13.8
SST13-S-21	15.1	38.8	14.5	26.2	13.8

[a] MAAT calculated according to Tierney et al., 2010.
[b] MAAT calculated according to Loomis et al., 2012.
[c] MAT calculated according to De Jonge et al., 2014.

APPENDIX G

Table A.6.6: Total mass fluxes, crenarchaeol IPL fluxes, isoprenoid and branched GDGT fluxes, and HG fluxes. Lipid fluxes are normalized to TOC.

Sample ID	Collection Range	Bulk Flux $g/m^2/d$	Cren. IPL Flux $area/m^2/d$	Total isoGDGT Flux $\mu g/m^2/d$	Major brGDGT Flux $\mu g/m^2/d$	Total brGDGT Flux $\mu g/m^2/d$	Total HG Flux $area/m^2/d$
North Sediment Trap (170m)							
NST11-1	1/15/11 – 1/31/11	0.37	2.5E+06	19.5	3.1	n.a.	5.9E+07
NST11-2	2/1/11 – 2/17/11	0.22	1.9E+06	12.1	1.8	n.a.	9.5E+06
NST11-3	2/18/11 – 3/7/11	0.45	1.8E+06	17.1	2.3	n.a.	1.3E+07
NST11-4	3/7/11 – 3/24/11	0.16	2.3E+06	6.9	0.8	n.a.	6.3E+06
NST11-5	3/25/11 – 4/10/11	0.51	3.1E+06	29.4	3.6	n.a.	8.6E+06
NST11-6	4/11/11 – 4/27/11	2.36	1.8E+06	26.1	3.3	n.a.	1.3E+07
NST11-7	4/28/11 – 5/14/11	2.65	2.0E+06	38.5	4.7	n.a.	1.5E+07
NST11-8	5/15/11 – 6/1/11	1.47	3.3E+06	47.6	6.1	n.a.	9.9E+07
NST11-9	6/2/11 – 6/18/11	0.75	3.5E+06	26.3	3.3	n.a.	1.1E+08
NST11-10	6/19/11 – 7/5/11	0.30	3.1E+06	12.2	1.5	n.a.	1.4E+07
NST11-11	7/6/11 – 7/22/11	0.59	3.5E+06	26.3	3.3	n.a.	5.2E+07
NST11-12	7/21/11 – 8/8/11	0.17	3.8E+06	8.1	1.0	n.a.	4.7E+07
NST11-13	8/9/11 – 8/25/11	0.37	3.5E+06	22.0	2.8	n.a.	4.9E+07
NST11-14	8/26/11 – 9/12/11	0.27	4.2E+06	12.7	1.5	n.a.	5.7E+07
NST11-15	9/13/11 – 9/29/11	0.84	6.0E+06	46.0	5.6	n.a.	8.3E+07
NST11-16	9/30/11 – 10/16/11	0.75	1.7E+06	13.9	1.7	n.a.	2.4E+07
NST11-17	10/17/11 – 11/2/11	0.60	4.5E+06	24.6	3.0	n.a.	1.1E+07
NST11-18	11/3/11 – 11/19/11	2.75	7.7E+06	97.3	12.4	n.a.	1.1E+08
NST11-19	11/20/11 – 12/7/11	1.50	1.2E+07	48.5	6.7	n.a.	1.9E+08
NST11-20	12/8/11 – 12/24/11	1.37	3.6E+06	53.9	7.7	n.a.	1.2E+08
NST11-21	12/25/11 – 1/10/12	0.52	3.4E+06	30.6	4.2	n.a.	8.9E+07
NST12-1	1/11/12 – 1/30/12	0.07	n.a.	3.8	1.4	1.5	6.3E+10
NST12-2	1/31/12 – 2/16/12	0.07	n.a.	0.7	0.2	0.2	8.0E+10
NST12-3	2/17/12 – 3/4/12	0.08	n.a.	0.0	0.0	0.0	1.1E+11
NST12-4	3/5/12 – 3/21/12	0.27	n.a.	2.4	1.0	1.1	1.1E+11
NST12-5	3/22/12 – 4/6/12	0.16	n.a.	8.5	3.3	3.6	7.6E+10
NST12-6	4/7/12 – 4/23/12	0.10	n.a.	3.9	1.0	1.1	2.8E+10

Sample ID	Collection Range	Bulk Flux g/m^2/d	Cren. IPL Flux area/m^2/d	Total isoGDGT Flux µg/m^2/d	Major brGDGT Flux µg/m^2/d	Total brGDGT Flux µg/m^2/d	Total HG Flux area/m^2/d
NST12-7	4/24/12 – 5/10/12	1.10	n.a.	8.4	2.5	2.7	1.6E+11
NST12-8	5/11/12 – 5/27/12	0.25	n.a.	4.1	1.3	1.5	5.4E+10
NST12-9	5/28/12 – 6/12/12	0.17	n.a.	10.2	2.7	3.0	5.7E+10
NST12-10	6/13/12 – 6/29/12	0.48	n.a.	7.3	2.4	2.6	9.3E+10
NST12-11	6/30/12 – 7/16/12	1.15	n.a.	20.8	7.2	8.0	7.3E+10
NST12-12	7/17/12 – 8/2/12	0.83	n.a.	14.7	4.5	5.1	8.0E+10
NST12-13	8/3/12 – 8/18/12	0.72	n.a.	42.3	12.0	13.6	6.0E+10
NST12-14	8/19/12 – 9/4/12	0.32	n.a.	6.7	1.6	1.8	3.7E+10
NST12-15	9/5/12 – 9/21/12	0.63	n.a.	7.4	2.5	2.8	4.1E+10
NST12-16	9/22/12 – 10/8/12	1.08	n.a.	24.6	6.3	7.3	3.1E+10
NST12-17	10/9/12 – 10/24/12	1.95	n.a.	27.8	9.5	11.2	4.1E+10
NST12-18	10/25/12 – 11/10/12	3.35	n.a.	56.3	18.0	20.9	1.3E+11
NST12-19	11/11/12 – 11/27/12	1.28	n.a.	n.a.	n.a.	n.a.	n.a.
NST12-20	11/28/12 – 12/14/12	1.57	n.a.	29.6	11.1	13.0	9.0E+11
NST12-21	12/15/12 – 12/30/12	0.17	n.a.	2.0	1.0	1.1	4.2E+11
South Sediment Trap (125m)							
SST11-D-1	1/15/11 – 1/31/11	0.16	1.1E+06	9.7	3.0	n.a.	4.7E+07
SST11-D-2	2/1/11 – 2/17/11	0.24	2.0E+06	17.8	5.7	n.a.	2.8E+07
SST11-D-3	2/18/11 – 3/7/11	0.53	2.4E+06	38.4	14.9	n.a.	2.2E+07
SST11-D-4	3/7/11 – 3/24/11	2.21	4.6E+06	116.4	3.0	n.a.	1.2E+07
SST11-D-5	3/25/11 – 4/10/11	0.35	4.1E+06	24.7	2.6	n.a.	7.7E+07
SST11-D-6	4/11/11 – 4/27/11	0.32	4.0E+06	23.6	2.4	n.a.	6.7E+07
SST11-D-7	4/28/11 – 5/14/11	0.32	5.2E+06	21.7	6.1	n.a.	6.6E+07
SST11-D-8	5/15/11 – 6/1/11	0.89	3.2E+06	52.0	9.5	n.a.	1.8E+07
SST11-D-9	6/2/11 – 6/18/11	2.18	5.8E+06	90.0	3.0	n.a.	9.9E+06
SST11-D-10	6/19/11 – 7/5/11	0.91	4.7E+06	52.8	5.4	n.a.	1.3E+07
SST11-D-11	7/6/11 – 7/22/11	0.46	3.0E+06	27.7	2.7	n.a.	2.0E+07
SST11-D-12	7/21/11 – 8/8/11	1.04	3.1E+06	49.1	4.8	n.a.	2.6E+07
SST12-D-1	1/13/12 – 1/28/12	0.14	n.a.	1.7	0.5	0.5	1.5E+11
SST12-D-2	1/29/12 – 2/15/12	n.a.	n.a.	n.a.	n.a.	n.a.	n.a.
SST12-D-3	2/16/12 – 3/2/12	0.40	n.a.	7.1	2.4	2.7	7.3E+10
SST12-D-4	3/3/12 – 3/19/12	0.86	n.a.	0.9	0.5	0.5	1.0E+11
SST12-D-5	3/20/12 – 4/5/12	n.a.	n.a.	n.a.	n.a.	n.a.	n.a.
SST12-D-6	4/6/12 – 4/22/12	1.43	n.a.	70.2	22.8	26.7	1.0E+11
SST12-D-7	4/23/12 – 5/8/12	0.38	n.a.	5.8	2.3	2.8	1.0E+11
SST12-D-8	5/9/12 – 5/25/12	0.16	n.a.	1.8	0.6	0.7	4.8E+10
SST12-D-9	5/26/12 – 6/11/12	0.32	n.a.	10.0	2.4	3.0	6.1E+10
SST12-D-10	6/12/12 – 6/28/12	0.87	n.a.	15.0	4.1	5.3	6.6E+10
SST12-D-11	6/29/12 – 7/15/12	0.89	n.a.	10.0	3.0	3.8	6.3E+10

Sample ID	Collection Range	Bulk Flux g/m^2/d	Cren. IPL Flux area/m^2/d	Total isoGDGT Flux µg/m^2/d	Major brGDGT Flux µg/m^2/d	Total brGDGT Flux µg/m^2/d	Total HG Flux area/m^2/d
SST12-D-12	7/16/12 – 8/1/12	0.19	n.a.	0.7	0.2	0.3	3.1E+10
SST12-D-13	8/2/12 - 8/18/12	0.01	n.a.	n.a.	n.a.	n.a.	n.a.
SST12-D-14	8/19/12 - 9/3/12	0.01	n.a.	n.a.	n.a.	n.a.	n.a.
SST12-D-15	9/4/12 - 9/20/12	0.01	n.a.	n.a.	n.a.	n.a.	n.a.
SST12-D-16	9/21/12 - 10/7/12	0.01	n.a.	n.a.	n.a.	n.a.	n.a.
SST12-D-17	10/8/12 - 10/24/12	0.01	n.a.	n.a.	n.a.	n.a.	n.a.
SST12-D-18	10/25/12 - 11/10/12	0.02	n.a.	n.a.	n.a.	n.a.	n.a.
SST12-D-19	11/11/12 - 11/27/12	0.03	n.a.	n.a.	n.a.	n.a.	n.a.
SST12-D-20	11/28/12 - 12/14/12	0.01	n.a.	n.a.	n.a.	n.a.	n.a.
SST12-D-21	12/15/12 - 12/31/12	0.01	n.a.	n.a.	n.a.	n.a.	n.a.
South Sediment Trap (110m)							
SST13-D-1	1/14/13 – 1/29/13	0.36	n.a.	6.8	2.3	2.6	1.1E+12
SST13-D-2	1/30/13 – 2/15/13	1.66	n.a.	12.0	4.5	5.0	4.2E+11
SST13-D-3	2/16/13 – 3/4/13	1.49	n.a.	11.4	3.7	4.2	2.9E+11
SST13-D-4	3/5/13 – 3/21/13	3.12	n.a.	20.1	5.6	6.3	2.3E+11
SST13-D-5	3/22/13 – 4/6/13	1.19	n.a.	11.6	3.0	3.4	2.1E+11
SST13-D-6	4/7/13 – 4/23/13	0.16	n.a.	4.5	0.9	1.1	6.7E+10
SST13-D-7	4/24/13 – 5/10/13	0.74	n.a.	8.6	2.3	2.7	1.3E+11
SST13-D-8	5/11/13 – 5/27/13	1.04	n.a.	11.6	3.4	4.4	2.2E+11
SST13-D-9	5/28/13 – 6/12/13	1.31	n.a.	5.1	1.8	2.3	2.3E+11
SST13-D-10	6/13/13 – 6/29/13	1.05	n.a.	10.9	3.0	3.9	4.4E+11
SST13-D-11	6/30/13 – 7/16/13	1.25	n.a.	9.8	2.9	3.8	3.9E+11
SST13-D-12	7/17/13 – 8/2/13	0.92	n.a.	9.3	2.6	3.4	3.4E+11
SST13-D-13	8/3/13 – 8/18/13	0.32	n.a.	3.7	1.0	1.4	2.2E+11
SST13-D-14	8/19/13 – 9/4/13	0.01	n.a.	n.a.	n.a.	n.a.	n.a.
SST13-D-15	9/5/13 – 9/21/13	0.01	n.a.	n.a.	n.a.	n.a.	n.a.
SST13-D-16	9/22/13 –10/8/13	0.01	n.a.	n.a.	n.a.	n.a.	n.a.
SST13-D-17	10/9/13 – 10/24/13	0.01	n.a.	n.a.	n.a.	n.a.	n.a.
SST13-D-18	10/25/13 – 11/10/13	0.01	n.a.	n.a.	n.a.	n.a.	n.a.
SST13-D-19	11/11/13 – 11/27/13	0.01	n.a.	n.a.	n.a.	n.a.	n.a.
SST13-D-20	11/28/13 – 12/14/13	0.01	n.a.	n.a.	n.a.	n.a.	n.a.
SST13-D-21	12/15/13 – 12/30/13	0.01	n.a.	n.a.	n.a.	n.a.	n.a.
South Sediment Trap (50m)							
SST13-S-1	1/14/13 – 1/29/13	0.20	n.a.	1.8	0.7	0.7	3.4E+11
SST13-S-2	1/30/13 – 2/15/13	0.31	n.a.	2.1	0.7	0.8	2.5E+11
SST13-S-3	2/16/13 – 3/4/13	2.74	n.a.	3.6	1.7	1.9	1.7E+11
SST13-S-4	3/5/13 – 3/21/13	1.42	n.a.	10.6	2.3	2.5	1.8E+11
SST13-S-5	3/22/13 – 4/6/13	0.64	n.a.	4.2	0.9	0.9	1.3E+11
SST13-S-6	4/7/13 – 4/23/13	0.38	n.a.	3.7	0.6	0.7	1.0E+11

Sample ID	Collection Range	Bulk Flux $g/m^2/d$	Cren. IPL Flux $area/m^2/d$	Total isoGDGT Flux $\mu g/m^2/d$	Major brGDGT Flux $\mu g/m^2/d$	Total brGDGT Flux $\mu g/m^2/d$	Total HG Flux $area/m^2/d$
SST13-S-7	4/24/13 – 5/10/13	0.07	n.a.	0.4	0.1	0.1	4.5E+10
SST13-S-8	5/11/13 – 5/27/13	0.07	n.a.	1.6	0.3	0.3	4.0E+10
SST13-S-10	6/13/13 – 6/29/13	0.28	n.a.	3.1	1.0	1.3	1.5E+11
SST13-S-11	6/30/13 – 7/16/13	0.42	n.a.	4.0	1.1	1.4	2.3E+11
SST13-S-12	7/17/13 – 8/2/13	1.71	n.a.	11.4	3.3	4.6	1.8E+11
SST13-S-13	8/3/13 – 8/18/13	0.24	n.a.	5.5	1.1	1.5	8.6E+10
SST13-S-14	8/19/13 – 9/4/13	0.12	n.a.	2.7	0.5	0.7	5.4E+10
SST13-S-15	9/5/13 – 9/21/13	0.09	n.a.	1.5	0.4	0.5	2.8E+10
SST13-S-16	9/22/13 –10/8/13	0.07	n.a.	1.5	0.4	0.4	5.9E+10
SST13-S-17	10/9/13 – 10/24/13	0.17	n.a.	2.8	0.7	0.8	1.0E+11
SST13-S-18	10/25/13 – 11/10/13	0.24	n.a.	7.6	2.2	2.4	1.1E+12
SST13-S-19	11/11/13 – 11/27/13	0.10	n.a.	3.0	0.9	1.0	3.6E+12
SST13-S-20	11/28/13 – 12/14/13	0.34	n.a.	7.8	3.2	3.6	1.5E+12
SST13-S-21	12/15/13 – 12/30/13	0.27	n.a.	3.3	1.5	1.7	4.5E+11

n.a. = Not Analyzed

APPENDIX H

Table A.6.7: Fractional abundances (% of total) of HGs, and HDI_{26}, HDI_{28}, and HTI_{28} values and temperatures.

Sample ID	HG_{26} Diol	HG_{26} Keto-ol	HG_{28} Diol	HG_{28} Keto-ol	HG_{28} Triol	HG_{28} Keto-diol	HDI_{26}[a]	LST_{HDI26}[a]	HDI_{28}[a]	LST_{HDI28}[a]
North Sediment Trap (170 m)										
NST11-1	46.4	0.1	49.2	4.1	0.2	0.0	1.00	25.0	0.92	21.8
NST11-2	57.7	0.4	35.2	6.7	0.0	0.0	0.99	24.8	0.84	19.7
NST11-3	56.3	0.4	35.8	7.4	0.0	0.0	0.99	24.8	0.83	19.5
NST11-4	54.4	0.0	37.5	8.1	0.0	0.0	1.00	25.1	0.82	19.3
NST11-5	54.1	0.0	39.6	6.3	0.0	0.0	1.00	25.1	0.86	20.3
NST11-6	62.1	1.0	31.9	5.0	0.0	0.0	0.98	24.4	0.87	20.4
NST11-7	61.1	1.3	32.4	5.2	0.0	0.0	0.98	24.2	0.86	20.3
NST11-8	58.6	0.7	36.5	3.9	0.3	0.0	0.99	24.6	0.90	21.3
NST11-9	57.2	0.6	38.3	3.7	0.3	0.0	0.99	24.7	0.91	21.5
NST11-10	38.4	0.3	31.4	29.8	0.0	0.0	0.99	24.7	0.51	11.7
NST11-11	54.4	0.6	41.1	3.7	0.3	0.0	0.99	24.6	0.92	21.7
NST11-12	60.1	0.5	35.5	3.6	0.3	0.0	0.99	24.7	0.91	21.4
NST11-13	65.5	0.6	30.9	3.0	0.0	0.0	0.99	24.7	0.91	21.5
NST11-14	70.7	0.5	26.6	2.1	0.2	0.0	0.99	24.8	0.93	21.9
NST11-15	80.0	0.6	17.7	1.7	0.1	0.0	0.99	24.8	0.91	21.5
NST11-16	73.2	0.5	23.7	2.5	0.2	0.0	0.99	24.8	0.91	21.4
NST11-17	60.5	0.7	32.2	6.6	0.0	0.0	0.99	24.6	0.83	19.5
NST11-18	32.5	0.2	58.2	9.1	0.0	0.0	0.99	24.8	0.86	20.4
NST11-19	28.0	0.2	60.9	10.8	0.1	0.0	0.99	24.8	0.85	20.0
NST11-20	14.2	0.1	75.8	9.9	0.0	0.0	0.99	24.7	0.88	20.9
NST11-21	19.2	0.1	71.9	8.8	0.0	0.0	0.99	24.7	0.89	21.0
NST12-1	3.2	0.0	89.6	6.8	0.2	0.1	1.00	25.0	0.93	22.0
NST12-2	2.7	0.0	89.4	7.7	0.2	0.0	0.99	24.6	0.92	21.7
NST12-3	3.2	0.0	88.5	8.0	0.2	0.1	0.99	24.5	0.92	21.7
NST12-4	3.0	0.0	87.9	8.7	0.3	0.1	0.99	24.6	0.91	21.5
NST12-5	3.4	0.0	88.1	8.1	0.3	0.1	0.99	24.6	0.92	21.6
NST12-6	7.4	0.1	84.6	7.6	0.2	0.1	0.99	24.5	0.92	21.7
NST12-7	16.5	0.2	76.8	5.9	0.5	0.1	0.99	24.5	0.93	21.9
NST12-8	19.7	0.2	73.5	6.0	0.4	0.1	0.99	24.6	0.92	21.8

Sample ID	HG_{26} Diol	HG_{26} Keto-ol	HG_{28} Diol	HG_{28} Keto-ol	HG_{28} Triol	HG_{28} Keto-diol	HDI_{26}[a]	LST_{HDI26}[a]	HDI_{28}[a]	LST_{HDI28}[a]
NST12-9	24.4	0.2	69.5	5.4	0.5	0.0	0.99	24.7	0.93	21.9
NST12-10	25.8	0.2	67.0	6.4	0.6	0.0	0.99	24.7	0.91	21.5
NST12-11	34.8	0.4	59.6	4.6	0.6	0.0	0.99	24.6	0.93	21.9
NST12-12	25.9	0.2	67.7	5.6	0.5	0.0	0.99	24.7	0.92	21.8
NST12-13	23.8	0.2	68.7	6.8	0.5	0.0	0.99	24.7	0.91	21.5
NST12-14	24.4	0.0	69.6	5.6	0.5	0.0	1.00	25.1	0.93	21.9
NST12-15	31.2	0.1	63.8	4.5	0.5	0.0	1.00	25.0	0.93	22.1
NST12-16	30.1	0.3	63.0	6.2	0.5	0.0	0.99	24.7	0.91	21.5
NST12-17	29.1	0.1	64.4	6.0	0.5	0.0	1.00	24.9	0.92	21.6
NST12-18	18.6	0.3	69.8	10.9	0.4	0.0	0.98	24.3	0.87	20.4
NST12-19	6.6	0.1	72.5	20.4	0.2	0.2	0.99	24.6	0.78	18.3
NST12-20	5.7	0.1	77.0	17.1	0.2	0.0	0.99	24.7	0.82	19.2
NST12-21	5.9	0.0	83.6	10.2	0.1	0.1	0.99	24.8	0.89	21.0
South Sediment Trap (125 m)										
SST11-D-1	56.9	0.4	37.3	4.6	0.5	0.3	0.99	24.8	0.89	21.0
SST11-D-2	54.4	0.4	41.2	4.0	0.0	0.0	0.99	24.8	0.91	21.5
SST11-D-3	57.7	0.5	37.8	4.0	0.0	0.0	0.99	24.7	0.90	21.3
SST11-D-4	52.6	0.8	41.3	4.7	0.6	0.0	0.98	24.4	0.90	21.2
SST11-D-5	52.9	0.5	41.8	4.1	0.6	0.0	0.99	24.7	0.91	21.5
SST11-D-6	59.6	0.9	33.8	5.2	0.5	0.0	0.98	24.4	0.87	20.4
SST11-D-7	56.4	0.5	38.7	3.8	0.6	0.0	0.99	24.7	0.91	21.5
SST11-D-8	59.3	0.4	36.4	3.2	0.7	0.0	0.99	24.8	0.92	21.7
SST11-D-9	50.7	0.5	41.6	7.2	0.0	0.0	0.99	24.7	0.85	20.0
SST11-D-10	60.6	0.0	33.7	5.7	0.0	0.0	1.00	25.1	0.86	20.2
SST11-D-11	67.5	0.3	28.1	4.1	0.0	0.0	1.00	24.9	0.87	20.5
SST11-D-12	73.1	0.6	21.2	5.0	0.1	0.0	0.99	24.7	0.81	19.0
SST12-D-1	6.1	0.0	84.4	7.7	1.8	0.0	1.00	25.1	0.92	21.6
SST12-D-3	7.3	0.1	84.0	6.6	1.9	0.1	0.99	24.6	0.93	21.9
SST12-D-4	10.2	0.2	81.3	6.4	1.8	0.1	0.98	24.3	0.93	21.9

Sample ID	HG_{26} Diol	HG_{26} Keto-ol	HG_{28} Diol	HG_{28} Keto-ol	HG_{28} Triol	HG_{28} Keto-diol	HDI_{26}[a]	LST_{HDI26}[a]	HDI_{28}[a]	LST_{HDI28}[a]
SST12-D-6	20.9	0.0	71.8	5.4	1.9	0.0	1.00	25.1	0.93	22.0
SST12-D-7	28.1	0.0	64.4	4.7	2.6	0.1	1.00	25.1	0.93	22.0
SST12-D-8	27.5	0.0	65.9	5.1	1.5	0.0	1.00	25.1	0.93	21.9
SST12-D-9	41.9	0.3	51.6	3.6	2.6	0.0	0.99	24.8	0.94	22.1
SST12-D-10	45.5	0.4	48.3	3.6	2.2	0.1	0.99	24.7	0.93	22.0
SST12-D-11	46.0	0.2	48.7	3.3	1.8	0.0	1.00	24.9	0.94	22.1
SST12-D-12	52.6	0.0	43.1	3.3	0.9	0.0	1.00	25.1	0.93	21.9
South Sediment Trap (110 m)										
SST13-D-1	6.2	0.0	87.1	6.3	0.4	0.0	0.99	24.8	0.93	22.0
SST13-D-2	6.0	0.1	88.3	5.4	0.3	0.0	0.99	24.5	0.94	22.3
SST13-D-3	8.4	0.1	85.4	5.8	0.4	0.0	0.99	24.6	0.94	22.1
SST13-D-4	18.3	0.3	75.7	5.1	0.5	0.0	0.98	24.4	0.94	22.1
SST13-D-5	27.6	0.3	67.7	3.9	0.4	0.0	0.99	24.6	0.95	22.4
SST13-D-6	23.0	0.1	72.2	4.3	0.4	0.0	1.00	24.9	0.94	22.3
SST13-D-7	25.6	0.1	69.3	4.6	0.4	0.0	0.99	24.8	0.94	22.2
SST13-D-8	31.9	0.2	61.9	5.7	0.3	0.0	0.99	24.8	0.92	21.6
SST13-D-9	54.2	0.3	42.0	3.3	0.2	0.0	1.00	24.9	0.93	21.9
SST13-D-10	88.0	0.2	10.8	0.9	0.1	0.0	1.00	25.0	0.92	21.7
SST13-D-11	86.4	0.3	12.3	0.9	0.1	0.0	1.00	24.9	0.93	22.0
SST13-D-12	83.0	0.3	15.4	1.2	0.1	0.0	1.00	24.9	0.93	21.9
SST13-D-13	84.4	0.2	14.2	1.1	0.1	0.0	1.00	25.0	0.93	22.0
SST12-D-6	20.9	0.0	71.8	5.4	1.9	0.0	1.00	25.1	0.93	22.0
SST12-D-7	28.1	0.0	64.4	4.7	2.6	0.1	1.00	25.1	0.93	22.0
SST12-D-8	27.5	0.0	65.9	5.1	1.5	0.0	1.00	25.1	0.93	21.9
SST12-D-9	41.9	0.3	51.6	3.6	2.6	0.0	0.99	24.8	0.94	22.1
SST12-D-10	45.5	0.4	48.3	3.6	2.2	0.1	0.99	24.7	0.93	22.0
SST12-D-11	46.0	0.2	48.7	3.3	1.8	0.0	1.00	24.9	0.94	22.1
SST12-D-12	52.6	0.0	43.1	3.3	0.9	0.0	1.00	25.1	0.93	21.9
SST13-D-13	84.4	0.2	14.2	1.1	0.1	0.0	1.00	25.0	0.93	22.0

Sample ID	HG_{26} Diol	HG_{26} Keto-ol	HG_{28} Diol	HG_{28} Keto-ol	HG_{28} Triol	HG_{28} Keto-diol	HDI_{26}[a]	LST_{HDI26}[a]	HDI_{28}[a]	LST_{HDI28}[a]
South Sediment Trap (50 m)										
SST13-S-1	8.5	0.0	85.8	5.0	0.6	0.0	0.99	24.8	0.94	22.3
SST13-S-2	6.6	0.0	89.2	3.7	0.4	0.0	0.99	24.8	0.96	22.7
SST13-S-3	12.6	0.2	83.1	3.7	0.4	0.0	0.99	24.5	0.96	22.6
SST13-S-4	26.6	0.4	69.0	3.5	0.5	0.0	0.99	24.5	0.95	22.5
SST13-S-5	32.2	0.4	63.6	3.1	0.8	0.0	0.99	24.6	0.95	22.6
SST13-S-6	20.4	0.2	74.6	4.1	0.6	0.0	0.99	24.6	0.95	22.4
SST13-S-7	26.4	0.1	68.7	4.3	0.5	0.0	1.00	24.9	0.94	22.2
SST13-S-8	33.4	0.1	61.3	4.8	0.5	0.0	1.00	25.0	0.93	21.9
SST13-S-10	87.6	0.0	11.5	0.7	0.1	0.0	1.00	25.1	0.94	22.3
SST13-S-11	89.0	0.2	10.2	0.6	0.1	0.0	1.00	25.0	0.95	22.3
SST13-S-12	82.7	0.3	15.8	1.0	0.2	0.0	1.00	24.9	0.94	22.2
SST13-S-13	86.3	0.2	12.5	0.9	0.1	0.0	1.00	25.0	0.94	22.1
SST13-S-14	84.0	0.2	14.7	1.0	0.2	0.0	1.00	25.0	0.94	22.2
SST13-S-15	84.4	0.0	14.1	1.3	0.1	0.0	1.00	25.1	0.91	21.6
SST13-S-16	68.0	0.3	26.4	5.1	0.1	0.0	1.00	24.9	0.84	19.7
SST13-S-17	49.7	0.1	40.5	9.6	0.1	0.0	1.00	25.0	0.81	19.0
SST13-S-18	10.9	0.1	69.3	19.3	0.2	0.2	0.99	24.8	0.78	18.3
SST13-S-19	13.5	0.0	68.1	17.7	0.3	0.3	1.00	25.1	0.79	18.6
SST13-S-20	11.2	0.1	74.2	14.3	0.2	0.1	1.00	24.9	0.84	19.7
SST13-S-21	9.9	0.1	78.8	10.9	0.2	0.1	0.99	24.8	0.88	20.7

[a] Calculated according to Bauersachs et al., 2015.